

DIGITAL ACCESS TO SCHOLARSHIP AT HARVARD
DASH.HARVARD.EDU

HARVARD LIBRARY


Epigenetic Determinants of CD8+ T Cell Exhaustion

Citation

Sen, Debattama R. 2019. Epigenetic Determinants of CD8+ T Cell Exhaustion. Doctoral dissertation, Harvard University, Graduate School of Arts & Sciences.

Link

http://nrs.harvard.edu/urn-3:HUL.InstRepos:42029661

Terms of use

This article was downloaded from Harvard University's DASH repository, and is made available under the terms and conditions applicable to Other Posted Material (LAA), as set forth at

https://harvardwiki.atlassian.net/wiki/external/NGY5NDE4ZjgzNTc5NDQzMGIzZWZhMGFlOWI2M2EwYTg

Accessibility

https://accessibility.huit.harvard.edu/digital-accessibility-policy

Share Your Story

The Harvard community has made this article openly available.
Please share how this access benefits you. Submit a story

Epigenetic Determinants of CD8$^+$ T Cell Exhaustion

A dissertation presented

by

Debattama R. Sen

to

The Division of Medical Sciences

in partial fulfillment of the requirements

for the degree of

Doctor of Philosophy

in the subject of

Immunology

Harvard University

Cambridge, Massachusetts

March 2019

© 2019 Debattama R. Sen

All rights reserved.

Dissertation Advisor: W. Nicholas Haining Debattama R. Sen

Epigenetic Determinants of CD8$^+$ T Cell Exhaustion

Abstract

T cell exhaustion describes an acquired dysfunction common in settings of chronic viral infection. Despite clinical efforts to rescue exhaustion, the fundamental mechanisms specifying this state, and the potential for reprogramming exhausted T cells, remain poorly understood.

Since the epigenome can govern cell state, we profiled accessible chromatin in exhausted CD8$^+$ T cells. Exhausted cells acquired a state-specific landscape of enhancers that profoundly differed from functional memory. Comparison of mouse cells to those isolated from HCV and HIV infection identified a conserved epigenetic program of exhaustion. Critically, CD8$^+$ tumor infiltrating lymphocytes (TILs) also shared epigenetic and transcriptional features with chronic viral infection, suggesting that T cell exhaustion is a fundamental adaptation to settings of chronic stimulation.

Having established that exhausted T cells acquire distinct regulatory regions, we then asked whether that epigenetic state is fixed or plastic following resolution of chronic infection. Longitudinal analysis of HCV-specific CD8$^+$ T cells after curative therapy showed that canonical features of exhaustion, including super-enhancers near key transcription factors, were fixed and did not resolve long-term. Furthermore, anti-PD-1 therapy, which is thought to reinvigorate exhausted TILs by blocking inhibitory signaling, could not reverse the exhausted epigenetic profile. T cell exhaustion is therefore a stable epigenetic state that is not rescued by common treatment modalities.

We then sought new strategies to modulate T cell exhaustion. First, we used Cas9-mediated genome editing of an exhaustion-specific enhancer to show its requirement for

sustained PD-1 expression. This highlights the potential for tuning regulators of exhaustion through enhancer perturbation. Second, we characterized heterogeneity within exhaustion and found a subpopulation of “progenitor-exhausted” T cells that retained polyfunctionality, were better able to control tumor growth and could uniquely respond to anti-PD-1. Melanoma patients with increased progenitor-exhausted TILs experienced longer responses to checkpoint inhibitors, suggesting that expanding specific subsets of exhausted T cells may improve outcomes.

Our studies delineate the epigenetic determinants of T cell exhaustion, including its shared features across disease contexts and the effects of therapeutic intervention. Together, they suggest that ameliorating T cell exhaustion may require novel approaches to increase epigenetic plasticity and/or expand specific subsets of exhausted T cells.

“So long, and thanks for all the fish”

-Douglas Adams

“কোনো জিনিস চিনব যে রে, প্রথম থেকে শেষ,
নেব যে সব বুঝে প'ড়ে-- নাই সে সময় লেশ।
…
এই যে নেশা লাগল চোখে এইটুকু যেই ছোটে
অমনি যেন সময় আমার বাকি না রয় মোটে।
…
সেই আনন্দে চল্ রে ধেয়ে কালের পিছু পিছু।”

“Knowledge is precious to us,
because we shall never have time to
complete it.

...Keep that in mind and rejoice”

-Rabindranath Tagore

Acknowledgements

This PhD experience has been an incredible journey, encompassing some of the best and worst times of my life, and I am so grateful to the extraordinary friends, colleagues, and mentors who have supported me along the way.

Above all, I would like to thank my thesis advisor Dr. Nicholas Haining. From the very beginning, I have been amazed by his scientific vision and his relentless enthusiasm for the work that we do. Nick has continually pushed me to be a better scientist, from learning how to think big about scientific questions to designing elegant and efficient experiments. I am very much going to miss all of our discussions about science (also life!) and throwing half-baked ideas up on the board until we both agreed we had something good. In Nick's lab, I've had the training opportunities and experiences that every graduate student should receive – freedom to think outside the box, review papers, mentor students, attend conferences…the list could go on. But perhaps what I've appreciated most is that he cares deeply not just about the science, but also the personal and professional future of his trainees. Nick has been an incredible mentor and a devoted advocate – I face the prospect of leaving his lab with mixed emotions.

The Haining lab encompasses an exceptional community of scientists, who are smart, passionate, caring, and collaborative. I came into the lab with less than 6 months of bench experience, but the lab members basically taught me everything I know and laid a foundation that allowed me to fearlessly approach new techniques or concepts. I would also like to thank my lab mates, current and former, for being an invaluable support system with experiments, lab management and listening to my grievances on a regular basis.

My work has been very collaborative, both within the Haining lab and externally. I would like to thank all of my co-authors for making the science not just possible but fun, despite all the

late-nights and long phone calls. I'm looking forward to working closely with all of you on future projects.

I'd like to thank my advisory committee members Arlene Sharpe, Christophe Benoist, and Bradley Bernstein, who have been an invaluable source of feedback. I am grateful for their critical insights and advice that helped to make this research project successful. I would also like to thank the wonderful faculty in the Immunology Program who I have been fortunate to be able to work with.

Perhaps even more than me, finishing this PhD will mean a lot to my parents. They first brought me to the US when I was 13, and since then, they have made many sacrifices to give myself and my sister the opportunities to pursue our dreams. It is because of their sacrifices and their loving, yet tough upbringing that I have been able to pursue the things I am passionate about. Thank you so much, Ma and Baba, for everything. A big shout out also to my baby sister, Tapti, who remains my pride and joy, my guiding light in dark times.

Finally, I would like to acknowledge my amazing partner, Sean McCanty, who has gone above and beyond in every way over the last few years. Every day, I am grateful for his unwavering support and remarkable wisdom, and I truly could not have survived this last few years without him. Thank you for always helping me strive to be the best version of myself.

Table of Contents

Chapter 1. Introduction 1
Section I: T cell exhaustion 3
Section II: Epigenetics and chromatin accessibility 11
Section III: Dissertation objectives 16
Chapter 2. State-specific epigenetic landscape defines CD8⁺ T cell exhaustion in chronic LCMV 17
Introduction 18
Results 19
CD8⁺ T cell exhaustion is associated with extensive changes in accessible chromatin 19
State-specific enhancers form modules that map to functionally distinct classes of genes 23
High-resolution functional mapping of an exhaustion-specific enhancer identifies minimal sequences that regulate PD-1 25
Exhaustion-specific epigenetic profiles in mice are conserved in antigen-specific human T cells in HIV-1 infection 31
Discussion 34
Materials and methods 36
Chapter 3. Epigenetic scarring of exhausted CD8⁺ T cells in chronic Hepatitis C infection after curative therapy 47
Introduction 48
Results 49
Distinct epigenetic changes underlie CD8⁺ T cell responses to chronic HCV infection 49
Epigenetic signature of T cell exhaustion is conserved across chronic viral infections 52
Cure of chronic infection causes antigen-specific partial remodeling of the epigenetic landscape 54
HCV-specific CD8⁺ T cells retain epigenetic scars of exhaustion 57
Scars represent critical epigenetic hallmarks of exhaustion 60
Epigenetic scars of exhaustion are retained long-term after cure of infection 62
Discussion 63
Materials and methods 66
Chapter 4. Functionally specialized subsets of exhausted CD8⁺ T cells differentially mediate tumor control and respond to checkpoint blockade 72
Introduction 73
Results 74
Chronic viral infection and tumors elicit analogous subsets of exhausted CD8⁺ T cells 74
Progenitor and terminally exhausted CD8⁺ TILs have distinct epigenetic and transcriptional features 79
Progenitor exhausted and terminally exhausted CD8⁺ TILs have distinct functional properties 83
Progenitor exhausted CD8⁺ T cells differentiate into terminally exhausted CD8⁺ T cells 85
Progenitor exhausted CD8⁺ T cells persist in the absence of antigen and mediate long-term tumor control in vivo 87
Progenitor exhausted CD8⁺ T cells respond to PD-1 blockade 90
Discussion 92
Materials and methods 95
Chapter 5. Conclusions 107
Bibliography 112
Publications 126

Chapter 1. Introduction

The differentiation of $CD8^+$ cytotoxic T cells (CTLs) from their naïve precursors is a central event in the immune response to viruses. In most viral infections, naïve $CD8^+$ T cells are activated to differentiate into effector cells specialized in infection control, a subset of which can subsequently develop into protective memory. Critically, outcomes after viral infection can vary from full host recovery to lethal immunopathology.

Enhancing T cell effector function while limiting bystander damage in the host has remained a central challenge in the field. In that context, a puzzling observation was made – high dose inoculations with certain strains of Lymphocytic Choriomeningitis Virus (LCMV) unexpectedly led to less immunopathology, not more. Therefore in 1993, Moskophidis et al. compared the T cell response to persistent LCMV infection with an acute LCMV infection in adult mice. They described a novel paradigm of acquired T cell dysfunction and coined the term “T cell exhaustion.”

T cell exhaustion is now known to occur in chronic viral infections such as Hepatitis C (HCV) and HIV, as well as many cancers. Previous work has established that exhausted T cells possess specific functional defects and a distinct gene expression profile. However, the underlying mechanisms specifying this state and the potential for reprogramming T cell exhaustion remain open questions in the field.

In this chapter, we detail foundational literature and motivations pertaining to the study of regulatory changes in T cell exhaustion.

Section I: T cell exhaustion

Characteristics of CD8+ T cell exhaustion

Moskophidis et al. had initially characterized exhaustion as the deletion of transferred LCMV-responsive TCR-transgenic cells[1]. In 1996, technical advances enabled *in vivo* identification of antigen-specific endogenous responses[2]. Seminal work leveraging these new tetramer reagents demonstrated that a polyclonal T cell repertoire could give rise to different cell fates: CTLs recognizing certain viral epitopes were deleted whereas other epitope responses persisted in the host with reduced antiviral effector function[3, 4]. This raised the question, what are the different manifestations of T cell exhaustion?

The LCMV model system provided tractable and well-controlled approaches to this question[5]. Most studies used two strains of the LCMV virus, Armstrong and Clone 13, which cause an acute or chronic infection respectively[5, 6]. Since the two strains differ only by two amino acids[6], CD8+ T cell responses to shared epitopes between acute and chronic infection could be studied. Furthermore, the P14 mouse strain[7], a TCR-transgenic line specific for the shared gp33 epitope of LCMV, could be used for a variety of CD8+ T cell transfer studies. Using these reagents, several groups found that CD4+ T cells were required for maintaining exhausted CD8+ T cell frequencies, as well as for long-term control of chronic, but not acute, LCMV infection[4, 8]. In the same period, the functional capacities of exhausted CD8+ T cells were also dissected.

Compared to effector CTLs in acute infection, exhausted cells had lowered interferon-gamma (IFN-γ) production[3, 4], as well as defects in TNF and IL-2 secretion[9]. They were less cytolytic compared to effector CD8+ T cells isolated from early stages of infection[3, 4]. Exhausted T cells also showed reduced ability to proliferate after *in vitro* stimulation and were more predisposed to apoptosis[4]. Nevertheless, exhausted T cells could persist long-term in chronically infected hosts, independent of homeostatic cytokines such as IL-7 and IL-15[10]. Somewhat

paradoxically, transfer of exhausted T cells from chronically infected mice into uninfected mice or infection-resolved mice led to lower, and not greater, recovery of cells compared to their recovery from Clone 13 infection[10, 11]. Thus, it was suggested that exhausted $CD8^+$ T cells were "antigen-addicted" and that their long-term persistence, despite impaired survival, was driven by continued proliferation[10]. Critically, the development of T cell exhaustion appeared to preclude memory formation[11]. $CD8^+$ T cells responding to LCMV Clone 13 had lowered expression of IL-7 receptor, an important marker of memory precursors[11, 12, 13].

Delineation of these functional defects prompted a new question – do exhausted $CD8^+$ T cells have any impact on disease outcomes? In a landmark 1999 paper, Schmitz et al. showed that transient depletion of exhausted $CD8^+$ T cells led to an increase in viral titers, which could be reversed upon reemergence of $CD8^+$ T cells[14]. Consistent with this, β-2-microglobulin knockout mice, which lack proper $CD8^+$ T cell function, also had higher viral titers[8], confirming that exhausted T cells could still play a key effector role in viral control.

At this point, several competing hypotheses regarding the etiology of T cell exhaustion had been eliminated: T cell exhaustion seemed distinct from T cell anergy or peripheral tolerance. Furthermore, some fundamental qualities of T cell exhaustion had been established in the LCMV model of chronic viral infection: exhausted T cells portrayed a variety of functional defects ranging from impaired survival, proliferative capacity, effector cytokine production and cytotoxicity. Nevertheless, many questions remained, including the extent to which these findings could be generalized to other disease contexts.

T cell exhaustion in human chronic viral infections

Poor functionality within the $CD8^+$ T cell response to chronic viral infections had already been noted. For example, $CD8^+$ T cells responding to human immunodeficiency virus (HIV) were found

to be poorly cytotoxic[15] and had decreased ability to produce IFN-γ[16, 17]. Loss of IFN-γ producing cells correlated with progressive depletion of the $CD4^+$ T cell compartment[18], pointing to the importance of $CD4^+$ T cell help in maintaining HIV-specific $CD8^+$ T cell responses. It also appeared that the functionality of $CD8^+$ T cells, rather than absolute numbers, largely differentiated progressors and controllers of chronic HIV[19, 20]. However, at that point the mechanisms driving this dysfunction remained unknown, with hypotheses including virus-induced immunosuppression and incomplete activation under consideration.

Similarly, T cell impairment in hepatitis C virus (HCV) infection had been demonstrated by multiple groups[21, 22]. Compared to $CD8^+$ T cell responses to Epstein-Barr virus (EBV) and cytomegalovirus (CMV), HCV-specific cells secreted less IFN-γ and TNF, with almost no cytokine co-production[21]. Despite increased frequency of HCV-specific $CD8^+$ T cell responses in chronic infection, they had poor proliferative capacity which correlated with weaker $CD4^+$ T cell responses[22].

Broadly, the observed defects in HIV and HCV – i.e. impaired cytokine production, reduced cytotoxicity and increased apoptosis – recapitulated the canonical description of T cell exhaustion in murine LCMV infection. Indeed, even in their original 1993 study, Moskophidis et al. speculated about the potential role of T cell exhaustion in explaining the inability to control Hepatitis B virus and the disappearance of anti-HIV CTLs late in disease[1]. The challenge lay in how to demonstrate that the etiology of dysfunction in HIV/HCV and the phenomenon of T cell exhaustion were one and the same, without a clear marker of exhausted T cells. Thus, a 2006 paper by Barber et al., showing that exhausted T cells were marked by elevated PD-1 expression[23], represented a huge advance in the study of exhaustion.

PD-1 and T cell exhaustion

By this time, PD-1 had already been characterized as an inhibitory receptor[24, 25, 26] expressed on mouse[27] and human T cells[28]. However, the major work on PD-1 had focused on its role in regulating T cell tolerance and preventing autoimmunity[29, 30, 31, 32]. Through microarray analysis comparing functional and exhausted T cells from LCMV, Barber et al. identified PD-1 as highly upregulated in the exhausted condition. Thus, they were the first to show that even though PD-1 could be transiently upregulated in an acute effector response, it remained elevated in exhausted T cells from chronic LCMV[23].

Once established as a marker of exhausted T cells in LCMV, PD-1 expression was rapidly utilized to identify and dissect the functionality of exhausted T cells in several other models of chronic viral infection including SIV (simian immunodeficiency virus), HIV, HCV and HBV. In particular, PD-1 was found to be upregulated on SIV and HIV-specific but not CMV-specific $CD8^+$ T cells[33, 34]. PD-1 was also elevated in HIV-specific $CD4^+$ T cells, and levels of PD-1 expression correlated with markers of HIV disease progression such as plasma viral load[35, 36]. Corroborating studies in HCV showed that PD-1 was expressed early on most HCV-specific T cell responses[37], and that PD-1 expression dissipated in resolvers but not in settings of chronic HCV. This was true in both the peripheral, as well the intrahepatic $CD8^+$ T cell compartment[38]. Similar results were observed in the context of chronic HBV infection[39]. Together, these studies established PD-1 as a ubiquitous marker of T cell exhaustion and provided key insights into the regulation of PD-1 in several human chronic viral infections.

Remarkably, Barber et al. showed not just that PD-1 was upregulated on exhausted T cells but also provided evidence that reducing PD-1 binding to its ligands PD-L1 and PD-L2 could lead to greater T cell functionality. Specifically, they showed that attenuating PD-1 signaling by antibody blockade of the ligand led to increased T cell proliferation, increased frequency of IFN-γ producing cells as well as enhanced viral control[23].

Several groups subsequently showed that PD-1 blockade could also augment functionality of virus-specific cells from HIV[34, 35], HCV[37, 40, 41] and HBV[42] *in vitro*. This included improvements in $CD8^+$ T cell proliferation, and cytokine secretion[34, 40]. These findings were then extended *in vivo* using the SIV model system, where PD-1 blockade resulted in rapid expansion of SIV-specific $CD8^+$ T cells and lowered serum viremia without widespread immunopathology[43]. Critically, cessation of therapy eventually led to a relapse in viral load[43], suggesting that PD-1 blockade was not sufficient in permanently reversing chronic viral infection. Indeed, whether PD-1 blockade can truly overcome all aspects of exhaustion-associated dysfunction, or be maintained long-term, remains a critical open question.

In the same period, PD-1 blockade was also showing remarkable efficacy in mouse models of cancer. Since then, anti-PD-1 therapy has become a major modality of cancer treatment, having been fast-tracked for FDA approval in the treatment of metastatic melanoma[44] in 2014, and since extended to treatment of non-small cell lung cancer, renal cell carcinoma, Hodgkin's lymphoma, bladder cancer and many others[45]. While additional FDA approvals have come for PD-1 and PD-L1 blocking antibodies at a remarkable pace, commensurate insight into its mechanism of action and its effect on $CD8^+$ T cell populations has lagged. Some have argued that the efficacy of PD-1 blockade is partially related to reversal of T cell exhaustion in cancer. However, the extent to which T cell exhaustion is induced in the tumor microenvironment, and the effect of PD-1, is an active subject of debate.

T cell exhaustion in cancer

The potential importance of PD-1 signaling in modulating immune responses to cancer was investigated early, spurred on by observations in 2002 that its ligand PD-L1 was highly expressed on many human tumor tissues[46]. By 2004, it was shown that PD-1 blockade could reduce metastasis in the murine B16 melanoma and CT26 colon cancer models[47], as well as overcome

tumor cell resistance[48]. While the importance of a robust T cell response for tumor control was beginning to be appreciated, almost nothing was known about the mechanisms by which T cell immunity failed in the tumor microenvironment.

Previous reports of T cell dysfunction in the tumor had largely been attributed to "immunological ignorance" of tumor-associated self-antigens, the induction of tolerance, and/or the immunosuppressive tumor microenvironment (TME)[49]. In a landmark paper, Steve Rosenberg's group reported that melanoma antigen-specific $CD8^+$ T cells from human tumors expressed high levels of PD-1 relative to normal tissue[50]. They also noted impaired IFN-γ production specifically within the PD-1 high compartment of tumor-infiltrating lymphocytes (TILs). Others showed that model antigen-specific responses to chronic myeloid leukemia exhibited high PD-1 levels, limited cytotoxic activity, and defective expansion restimulation[51]. These findings implicated a potential role of T cell exhaustion in limiting anti-tumor efficacy.

Further studies followed, extending these findings to other tumor-reactive populations such as chimeric antigen receptor (CAR) T cells[52, 53], and performing deeper characterization of relative dysfunctionality within TILs in melanoma[54, 55]. However, other groups have provided alternative explanations of observed T cell dysfunction. It was suggested that T cell dysfunction or hypo-responsiveness within TILs is unique, being driven by mechanisms of self-tolerance and/or the distinct milieu of the tumor microenvironment[56]. Some have also proposed that previously observed similarities between tumor-associated dysfunction and T cell exhaustion might be conflated by signatures of T cell activation[57]. Therefore, whether the profile of dysfunctional $CD8^+$ TILs recapitulates the canonical processes of T cell exhaustion remains an important open question.

Ongoing debate about the contexts in which exhaustion may or may not arise are additionally complicated by the focus on PD-1 expression. PD-1 has important roles in other contexts of T cell development and differentiation, including during thymic selection[58], naïve T cell

activation[59, 60] and effector differentiation[60, 61]. Therefore, it was increasingly recognized that PD-1 may not be sufficient to accurately identify exhausted T cells and that a deeper characterization of their functional and transcriptional state was necessary.

Transcriptional profile of T cell exhaustion

In 2007, Wherry et al. published the first systems-level analysis of exhausted T cells in chronic LCMV, directly comparing them to effector and memory T cells arising in acute LCMV infection[62]. Their work provided convincing evidence that exhausted T cells had a unique transcriptional signature that went beyond differences in PD-1 expression. Exhaustion could be clearly distinguished from other signatures of impaired T cell function like anergy[62]. Indeed, exhausted T cells differentially expressed many other inhibitory receptors such as Lag3 and CTLA-4[62, 63], as well as key transcription factors such as Blimp-1 and NFAT[62]. Furthermore, network analysis of exhaustion-associated transcriptional changes pointed towards altered pathways and proposed potential regulators of exhaustion such as the transcription factors T-bet, Eomes, Tox, and Helios[64].

$CD8^+$ T cell responses to HIV were similarly found to be transcriptionally distinct. Quigley et al. from the Haining lab analyzed gene expression profiles within $CD8^+$ T cells from controllers and progressors in HIV[65]. They identified numerous transcriptional changes, including those that could be induced by PD-1 signaling, and revealed that those changes were similar to alterations observed in the LCMV mouse model. Among these, they highlighted a new role for the transcription factor BATF in the context of exhaustion. BATF was upregulated in dysfunctional HIV-specific cells, and could be silenced using shRNAs to increase IFN-γ production and enhance proliferative capacity[65]. Transcriptional changes consistent with exhaustion were also identified by other groups within $CD8^+$ T cell responses to chronic HCV infection[66], as well as within TILs

isolated from human melanoma[55]. Thus, it was now clearly established that exhausted T cells were defined not only by altered functionality, but also by a distinct transcriptional profile.

These findings underscored emerging and intense interest into the potential transcriptional regulators of T cell exhaustion. In a contemporaneous study, it was observed that haploinsufficiency of Blimp-1, which was found to be overexpressed in exhausted cells, could lower vital titers and enhance $CD8^+$ T cell functionality in chronic LCMV[67]. Conversely, loss of T-bet impaired viral control and increased PD-1 expression in chronic infection[68]. Later work by Anjana Rao's group established the critical regulatory role of NFAT in T cell exhaustion[69] and Kai Wucherpfennig's group characterized the inhibitory role of a microRNA miR-31 which was downstream of NFAT[70]. While these studies provided insight into the roles of some individual transcription factors, major questions still remained about how the functional and transcriptional profile of T cell exhaustion was established globally and what regulatory mechanisms involved in its maintenance. In particular, it remained unknown whether T cell exhaustion might be differentially regulated at the epigenetic level.

Section II: Epigenetics and chromatin accessibility

Epigenetics and cell state regulation

Cell behavior is largely determined by gene expression programs, which are themselves governed by transcription factors (TFs) binding to regulatory regions known as enhancers. Differential activity of enhancer elements has been shown to be regulated largely at the level of the epigenome[71, 72, 73].

Almost 30 years before the empirical discovery of enhancers, Conrad Waddington became interested in understanding the heterogeneity of cellular differentiation, particularly in the context of organismal development[74]. Focusing on how cell fate decisions were made, he proposed a new regulatory mechanism called epigenetics that could regulate these decisions and mediate “genetic assimilation” of environmental cues. He developed the concept of an epigenetic landscape of differentiation, where an initially undifferentiated and totipotent cell could “roll downhill” towards terminal differentiation, and its ultimate cell fate would be guided by the grooves of the landscape. Although this remains a compelling model in the field of cellular differentiation and developmental biology, molecular mechanisms that might underlie such regulation were completely unknown at the time. We now know that enhancer function is one mechanism by which such control of cell fate can be achieved[71, 72].

Enhancer activity was first characterized in 1981 by several groups studying the SV40 viral genome [75 76]. These studies identified *cis*-acting sequences of DNA which were required for efficient gene expression and could enhance transcription both proximally and distally to the promoter[75 76]. Eukaryotic enhancers were then identified two years later in back-to-back papers studying the mouse immunoglobulin heavy chain locus[77, 78]. Work over the next 2 decades established that enhancer activity was not uniform, but instead exquisitely spatially and temporally regulated, and that such activity was instrumental in the control of cellular differentiation[71, 72, 79].

Indeed, characterization of state-specific regulatory elements were a critical step towards solving the puzzle of how a myriad of cell states can arise from a pre-specified genome within multicellular organisms[80]. Thus, epigenetic mechanisms can be thought of as a bridge between a shared genotype and context-specific phenotype.

Mechanisms of epigenetic regulation

Currently, the best characterized processes of epigenetic regulation include DNA methylation, histone modifications, and the structure of accessible chromatin[72]. Within these, there is considerable variety in relative stability, heritability and effect on gene regulation[71, 72]. In mammalian cells, DNA methylation involves the addition of methyl groups primarily to CpG dinucleotides by DNA-methyltransferases (DNMTs) [81]. The presence of these methyl groups can directly repress transcription and inhibit the binding of transcription factors[82]. Therefore, DNA methylation is primarily thought to inhibit specific transcriptional programs. In contrast, histone modifications, which constitute another major class of epigenetic changes, are associated with both activation and repression of gene expression[83, 84]. The specific outcome is determined by which chemical modification is made and which histone subunit was affected. Some of the more well-established histone modifications include the mono-methylation (H3K4me1) and tri-methylation (H3K4me3) of Histone 3 (H3) lysine 4, which generally mark enhancer and promoter elements, respectively[85]. Another important histone mark is the acetylation (H3K27Ac) of H3 lysine 27, which is found at both active enhancers and promoters[86]. Conversely, tri-methylation (H3K27me3) of H3 lysine 27 can be associated Polycomb-mediated repression[87] and tri-methylation (H3K9me3) of H3 lysine 9 is generally found on heterochromatin. These marks can co-occur[83, 84] – the combinatorial complexity of histone modifications and associated regulatory impact (often dubbed the “histone code”) is an area of active investigation[88].

Unfortunately, defining DNA methylation and/or histone modifications that may specify T cell exhaustion has been limited in the past by the low numbers of exhausted $CD8^+$ T cells that can be recovered from mouse models or patient samples. Therefore, an alternative approach, such as profiling of chromatin accessibility, was required to query the epigenetic state of T cell exhaustion.

Regulatory role of chromatin accessibility

Regulatory elements such as enhancers, promoters and insulators generally lie in areas of accessible chromatin[89, 90]. Indeed, chromatin accessibility is thought to be partially driven by binding of transcription factors within regulatory regions that ultimately leads to nucleosome exclusion[80, 89, 90]. Traditionally, measurements of chromatin accessibility have relied on the observation that accessible chromatin is less protected from, and thus "hypersensitive" to, enzymes such as DNase I[91, 92]. In the mid 2000s, it became possible to define areas of DNase I hypersensitivity (DHS) genome-wide, first using microarrays[93, 94] and then via high-throughput sequencing[95]. These studies revealed that the over 75% of accessible chromatin lay outside of gene promoters, suggesting that profiling chromatin accessibility could map a new layer of information onto measurements of gene transcription[95]. In 2012, Thurman et al. profiled accessible chromatin in 125 human cell lines and identified thousands of novel putative enhancers, many of which were incredibly cell- and tissue-specific[96]. While these studies profiling accessibility represented significant biological advances, technical requirements for minimum cellular input prevented practical characterization of many cell types derived from primary tissues and disease contexts.

In 2013, Buenrostro et al. developed a novel assay (Assay of Transposase-Accessible Chromatin using Sequencing; ATAC-seq) that allowed mapping of nucleosome-free, open regions of chromatin from very small cell numbers (<10,000)[97]. This was achieved by taking

advantage of the Tn5 transposase enzyme, which enabled simultaneous fragmentation of DNA and ligation of sequencing adapters. Of note, ATAC-seq chromatin accessible regions (ChARs) largely correlated with DHS regions[97]. Since then, the Greenleaf, Chang and Buenrostro labs have made further technological innovations that allow profiling of chromatin accessibility from frozen tissue sections[98], and even down to the level of individual cells[99].

ATAC-seq has been used to globally characterize many important biological processes, including 23 cancer types from TCGA[100] and primary cell types spanning hematopoiesis[101, 102]. In addition to providing new insight into the chromatin landscape of primary cell differentiation and tumorigenesis, these studies highlight the utility of chromatin accessibility in explaining molecular regulation and cell behavior. For example, the binding of non-pioneer transcription factors at any given time is largely restricted to areas of open chromatin[103]. This suggests that chromatin accessibility can be used as a reliable proxy for cumulative TF binding[104]. Chromatin accessibility has also been used to shed light on causal variants from genome-wide association studies[105].

Given the widespread impact of epigenetic changes such as histone modifications and chromatin accessibility, it is no surprise that this framework has proven useful in describing immune cell processes. Several groups have showed that hematopoiesis progresses through extensive gain and loss of lineage-specific enhancers[101, 102]. Others have identified an erythrocyte-specific enhancer of the *BCL11A* gene that is conserved across mice and humans, and is critical for regulating the switch from fetal hemoglobin[106]. *In vivo* editing of the *Bcl11a*-enhancer showed equivalent regulatory potential when compared with targeting the gene itself, without causing undesired bystander changes in non-erythroid lineages[107]. Within T cell populations, Vahedi et al. established that naïve $CD4^+$ T cell differentiation into Th1 and Th2 cell fates involves STAT-mediated activation and suppression of enhancer activity[108]. Emerging work within $CD8^+$ T cells now suggests that $CD8^+$ T cell memory formation is associated with epigenetic changes[109]. Could the same be true for the development of $CD8^+$ T cell exhaustion?

Epigenetics and T cell exhaustion

Several previous observations suggest that T cell exhaustion might represent a distinct epigenetic state of T cell differentiation. First, it was noted that antigen-specific T cells from chronic infection failed to form memory upon transfer to recipient mice at day 15 post-infection, but not at day 8[11]. This highlighted that the development of exhausted cells was associated with varying levels of plasticity and suggested that there might be a threshold after which it could no longer be reversed. Second, it was observed that exhausted cells maintained their phenotype upon removal from their environment, suggesting that cell intrinsic changes were at least partially responsible[110]. Those changes could also be passed on to daughter cells independent of the surrounding milieu[110].

Consistent with this, examination of the gene loci encoding PD-1 showed that the promoter was transiently demethylated in antigen-specific T cells from acute viral infection but remained demethylated in chronic LCMV[111]. A similar pattern of epigenetic de-repression was observed in HIV-specific $CD8^+$ T cells and could not be reversed by loss of TCR signaling[112]. Taken together, these studies suggest that epigenetic changes might be important for the expression of PD-1, but the extent to which they regulate other aspects of T cell exhaustion remains unknown. Therefore, a more systematic analysis of the epigenetic state of T cell exhaustion is required.

Section III: Dissertation objectives

In the 26 years since T cell exhaustion was first described, work from many groups has definitively established its importance in many human disease contexts[113]. Beyond chronic viral infections such as HIV, HCV and HBV, the potential role of T cell exhaustion has been investigated in numerous human cancers, chronic bacterial infections[114] and even autoimmunity[115]. The remarkable success of checkpoint blockade immunotherapies, which target molecules also associated with T cell exhaustion, has sparked intense interest in better understanding of the exhausted state.

In this thesis, we characterize the epigenetic landscape of $CD8^+$ T cell exhaustion. In chapter 2, we map chromatin accessibility during naïve T cell differentiation into functional memory or exhaustion in the LCMV mouse model, and ask whether exhausted $CD8^+$ T cells are epigenetically distinct. In chapter 3, we investigate whether exhaustion-associated epigenetic changes are observed in chronic HCV infection, and can be reversed by recently developed curative therapies. In chapter 4, we compare epigenetic, transcriptional, and functional heterogeneity of dysfunctional $CD8^+$ T cells in cancer to canonical models of T cell exhaustion. Together, these studies delineate the epigenetic determinants of T cell exhaustion, including its shared features across cancer and chronic viral infection and its plasticity following therapeutic perturbation. As such, they provide the basis for novel strategies to reverse exhaustion and to mitigate the deleterious effects of chronic antigen stimulation.

Chapter 2. The epigenetic landscape of $CD8^+$ T cell exhaustion in chronic LCMV

Parts of this chapter are currently accepted for publication as:

Debattama R. Sen*, James Kaminski*, R. Anthony Barnitz, Makoto Kurachi, Ulrike Gerdemann, Kathleen B. Yates, Hsiao-Wei Tsao, Jernej Godec, Martin W. LaFleur, Flavian D. Brown, Pierre Tonnerre, Raymond T. Chung, Damien C. Tully, Todd M. Allen, Nicole Frahm, Georg M. Lauer, E. John Wherry, Nir Yosef†, and W. Nicholas Haining†. The Epigenetic Landscape of T Cell Exhaustion. *Science*. 2016 Dec 2;354(6316):1165-1169.

*These authors contributed equally

†Corresponding authors

Introduction

T cell exhaustion – an acquired state of T cell dysfunction – is a hallmark of chronic viral infection[62, 116], and clinical trials of checkpoint blockade, which aim to reverse T cell exhaustion in cancer, have proven strikingly effective[44, 117]. Chimeric antigen receptor (CAR)-T cell therapy has also proven highly effective for hematologic malignancies[118], but the development of exhaustion in engineered T cells to treat solid tumors remains a significant barrier to its broader use[52]. The identification of mechanisms that regulate exhausted T cells is therefore a major goal in cancer immunotherapy.

Exhaustion is thought to be a distinct state of T cell differentiation with a specific transcriptional profile[62, 64]. Common features of $CD8^+$ T cell exhaustion between humans and mice include progressively decreasing production of effector cytokines such as IL-2, TNF and IFN-γ as well as a reduction in cytotoxicity and proliferative capacity[119]. This state of dysfunction is also marked by increased expression of co-inhibitory T cell receptors such as PD-1, CTLA-4, Lag3, 2B4 and Tim-3[63].

Specific patterns of gene expression and cellular fate are mediated by the coordinated action of hundreds of cis-regulatory modules or enhancers. Enhancers are genomic regions that

contain binding sites for various transcription factors (TFs), leading to changes in promoter activity and gene transcription. While regulation of the epigenome during normal CD8+ T cell maturation (naïve to effector to memory) has been previously described[109, 120], the chromatin dynamics during formation of exhausted T cells have never been functionally assessed.

Defining the TFs and enhancers that specify exhaustion has been limited by low recovery numbers of exhausted CD8+ T-cells from mouse models or patient samples. We have recently applied an Assay of Transposase-Accessible Chromatin using Sequencing (ATAC-seq)[97] to map open regions of chromatin, which strongly correspond to regulatory elements. We have used this approach to show that exhaustion is associated with distinct regulatory regions, and the magnitude of epigenetic changes is far greater than gene expression differences. We have also identified an enhancer near the PD-1 gene that is unique to exhaustion, and may be responsible for the prolonged/excessive expression of PD-1 in dysfunctional T cells. Using CRISPR/Cas9 mediated genome editing and a cell line model, we have edited this candidate PD-1 enhancer and verified its ability to regulate PD-1 expression.

Results

CD8+ T cell exhaustion is associated with extensive changes in accessible chromatin

To identify regulatory regions, such as enhancers and promoters, in exhausted CD8+ T cells, we used ATAC-seq to demarcate areas of accessible chromatin in antigen-specific CD8+ T cells differentiating in response to lymphocytic choriomeningitis virus (LCMV) infection (Fig. 2.1A). Acute LCMV infection elicits highly functional effector CD8+ T cells at day 8 (d8) post-infection (p.i.), which differentiate into protective memory CD8+ T cells at d27 p.i. In contrast chronic LCMV infection gives rise to exhausted CD8+ T cells[62, 64, 116, 117]. Initial analysis of naïve CD8+ T cells and

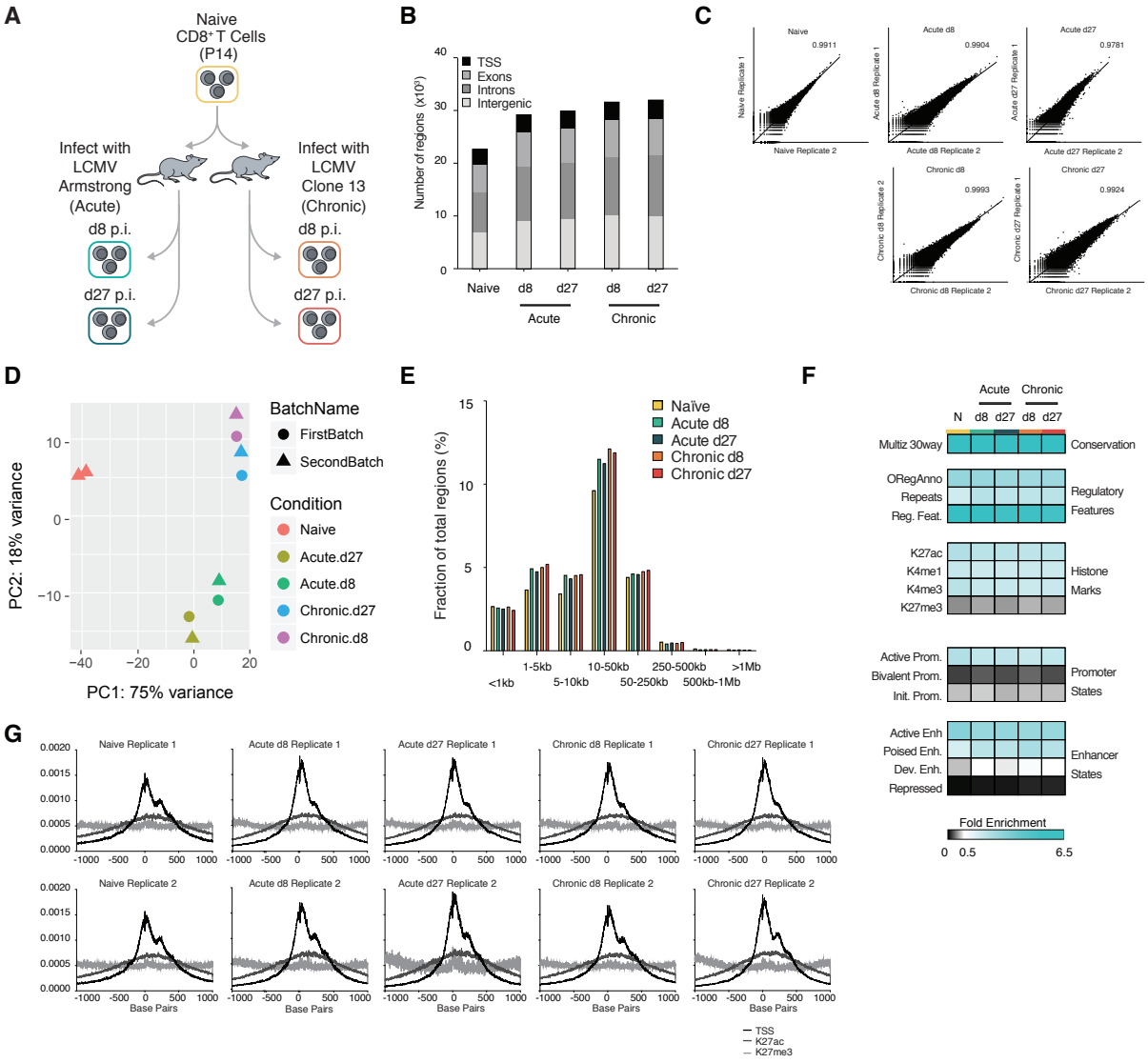


Figure 2.1. Characteristics of chromatin accessible regions from mouse CD8+ T cells. **(A)** Schematic diagram of the experiment. **(B)** Number of chromatin accessible regions per condition, partitioned into those overlapping transcriptional start sites (TSS), exons, introns and intergenic areas as indicated. **(C)** Scatterplot showing correlation in peak intensity between biological replicates for Naïve, Acute d8, Acute d27, Chronic d8 and Chronic d27 states. (**D**) Principal component analysis of biological replicates for Naïve, Acute d8, Acute d27, Chronic d8 and Chronic d27 states across all 43,171 ChARs. **(E)** Distance to nearest TSS for all intergenic chromatin accessible regions (as percentage of total), for all five cell states. **(F)** Fold enrichment of regions annotated for evolutionary conservation, regulatory region status and histone marks within ATAC peaks, for all five cell states. **(G)** Combined ATAC signal across all TSSs (black), H3K27ac peaks (dark grey) and H3K27me3 (light grey).

those at d8 and d27 p.i. identified between 22,646 and 31,969 chromatin accessible regions (ChARs) in each state (*FDR* < 0.001; Fig. 2.1B). High correlation between biological replicates confirmed good data quality[97] (Figs. 2.1C-D). The distribution of ChARs across transcriptional start sites (TSS), exons, introns and intergenic regions was consistent with previous reports[96] (Figs. 2.1B and 2.1E). As expected, ChARs from each state were strongly enriched for regions of high evolutionary conservation, regulatory annotations, activating promoter and enhancer histone marks, but were depleted of Polycomb repressed regions (Figs. 2.1F-G)[84, 96].

We found that the chromatin accessibility of naive CD8$^+$ T cells underwent large-scale remodeling (Figs. 2.2A-B) during differentiation (DEseq2, *FDR* < 0.05). The majority (71%, Fig. 2.2B) of ChARs either emerged (e.g. those at the *Ifng* locus, Fig. 2.2A) or disappeared (e.g. *Ccr7*, Fig. 2.2A) as naive CD8$^+$ T cells underwent differentiation. The gain and loss of ChARs were not balanced; a much larger fraction of regions emerged at d8 p.i. and persisted (Fig. 2.2C, d8 and d27; acute 31.6%, chronic 38.8%), or emerged only at d27 (Fig. 2.2C, d27 only; acute 14.3%, chronic 16.9%), than were either transiently detected at d8 p.i. (Fig. 2.2C, d8 only; acute 14.9%, chronic 19.6%) or lost from naïve cells (Fig. 2.2C, naive only; acute 11.3% of total regions; chronic 12.6%). Thus, differentiation from a naïve CD8$^+$ T cell state is associated with a net increase, rather than decrease, in chromatin accessibility (Fig. 2.2D).

We next compared ChARs from exhausted CD8$^+$ T cells to those found in functional effector or memory CD8$^+$ T cells and found marked, global differences in the pattern of regulatory regions. We identified 7368 ChARs that were present at d8 and/or d27 p.i. in CD8$^+$ T cells responding to chronic infection but were absent in acute infection (Fig. 2.2E), and 4395 regions that were present at d8 and/or d27 p.i. in acute infection, but lacking in exhausted CD8$^+$T cells. Differential regulatory regions between acute and chronic infection showed features of enhancers:

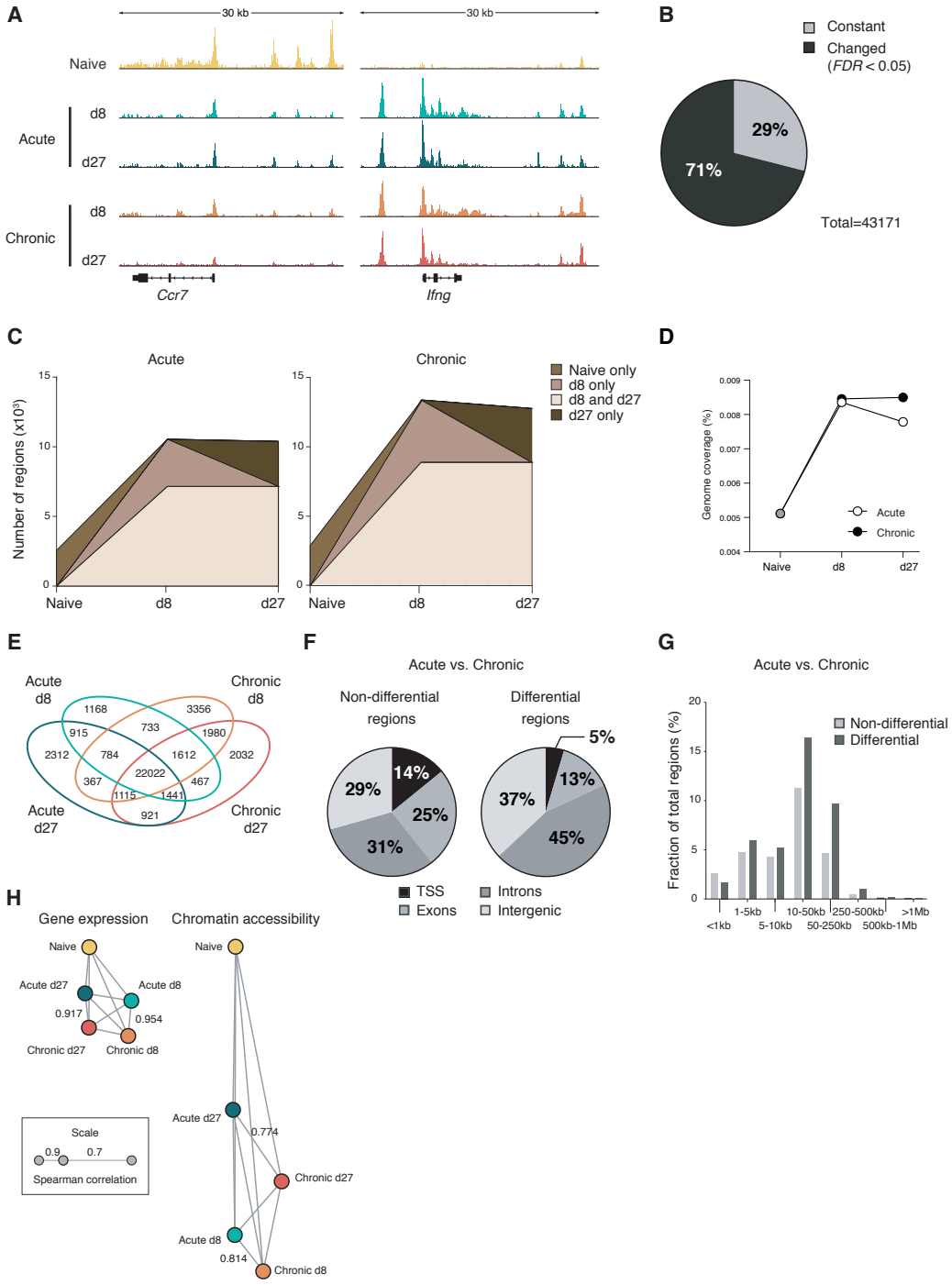


Figure 2.2. CD8⁺ T cell exhaustion is associated with extensive changes in accessible chromatin. **(A)** Representative ATAC-seq tracks at the *Ccr7* and *Ifng* gene loci. **(B)** Fraction of constant and changing chromatin accessible regions. (**C**) Developmental trajectory of new regions at each time point. **(D)** Fraction of the genome covered by chromatin accessible regions over time. **(E)** Overlap in chromatin accessible regions between cell states. **(F)** Distribution of non-differential (left) and differential (right) regions between acute and chronic CD8⁺ T cell states. **(G)** Distance to nearest TSS for all intergenic regions that are non-differential (light grey) and differential (dark grey). **(H)** Correlation network of similarity between states measured by gene expression (left) and chromatin accessibility (right). Edge length corresponds to similarity (1-Spearman coefficient)

they tended to be depleted of TSSs (5% vs. 14% in non-differential regions), enriched for intergenic and intronic areas (37% vs. 29% and 45% vs. 31%; Fig. 2.2F), and were distal to gene promoters (Fig. 2.2G). The magnitude of difference in the profile of regulatory regions between exhausted and functional CD8$^+$ T cells was greater than that seen in gene expression. We found that 44.48% of all ChARs were differentially present between functional and exhausted cells at each time point, compared to only 9.75% of differentially expressed genes (both values estimated at *FDR* < 0.05). Consistent with this, the rank correlation between each T cell state by gene expression was much higher than at the level of regulatory regions (Fig. 2.2H). This suggests that state change during CD8$^+$ T cell differentiation is accompanied by a larger reorganization of accessible chromatin than is apparent by examination of gene expression.

State-specific enhancers form modules that map to functionally distinct classes of genes

Unsupervised clustering identified "modules" of differential ChARs with similar patterns of activity (Fig. 2.3A). We identified seven modules of regulatory regions representing highly state-specific patterns of activity. Modules *a* – *e* corresponded to ChARs primarily active in CD8$^+$ T cells from naïve, acute d8 p.i, acute d27 p.i., chronic d8 p.i. and chronic d27 p.i., respectively. Module *f* identified a shared set of ChARs between naïve T cells and acute d27 p.i., while module *g* contained shared ChARs between naïve and chronic d8 p.i. (Fig. 2.3A). We found a highly significant positive correlation between the average peak-intensity of ChARs within each module and the average gene expression of the adjacent genes ($P < 0.001$) (Figs. 2.3B and 2.3C). This suggests that, on average, the ChARs contained in each module tended to be associated with the activation, rather than repression, of corresponding genes.

Genes in each state-specific module included many with known functions in the corresponding T cell state. For example, module a, most active in naïve T cells, contained ChARs adjacent to *Ccr7* and *Lef1* (Fig. 2.3B). Module d, active in chronic d8 and d27 p.i., contained

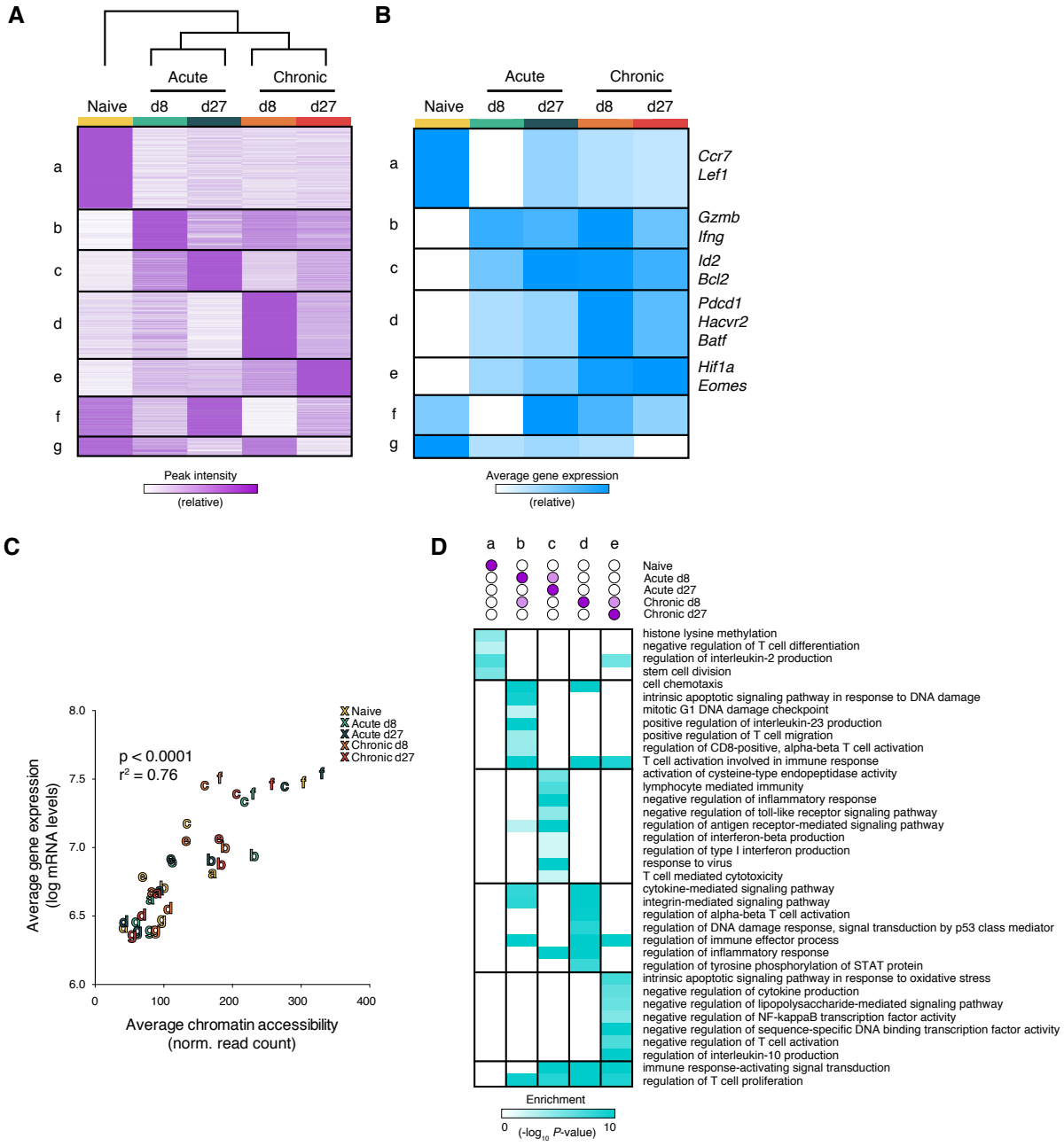


Figure 2.3. State-specific enhancers in CD8+ T cells form modules that map to functionally distinct classes of genes. **(A)** Heatmap of peak intensity for all differentially accessible regions (rows) clustered by similarity across cell states (columns). **(B)** Heatmap showing row-normalized average mRNA expression of neighboring genes within each module in **(A)** in each cell state. Informative genes from each module are shown on right. **(C)** Correlation between average gene expression and average chromatin accessibility for each module in each cell state. Letter symbols correspond to modules as indicated in **(A)** and **(B)**. **(D)** Heatmap showing enrichment of Gene Ontology terms (rows) in each module (columns). *P*-values (binomial test) presented as 1–log10.

ChARs adjacent to the inhibitory receptors *Pdcd1* and *Havcr2* (which encodes Tim3) and the transcription factor *Batf*, all genes that are upregulated in exhausted CD8+ T cells[62, 64]. We hypothesized that the modular structure of active regulatory regions would be associated with distinct regulatory programs, and surveyed the function of genes adjacent to ChARs within each module. Indeed, the functional classes of genes in each module were distinct, as measured by Gene Ontology term enrichment (Fig. 2.3D). For example, naïve-associated module a was associated with genes involved in histone lysine methylation, regulation of IL-2 production, and stem cell division. In contrast, module b, which was primarily active in cells from acute d8 p.i., was associated with genes involved in cell chemotaxis and regulation of CD8+ α-β T cell differentiation. Module e, which was associated with exhaustion, was enriched for genes involved in negative regulation of cytokine production, negative regulation of LPS-mediated signaling, negative regulation of T cell activation, and regulation of IL-10 production. Thus, ChARs that distinguish naïve, effector, memory and exhausted CD8+ T cells are organized into state-specific modules that positively regulate functionally distinct programs of genes.

High-resolution functional mapping of an exhaustion-specific enhancer identifies minimal sequences that regulate PD-1

We next sought to test whether regulatory regions specific to exhausted cells could regulate genes differentially expressed in exhausted CD8+ T cells. Persistent expression of PD-1 is a cardinal feature of exhausted CD8+ T cells, but PD-1 is also transiently expressed by effector CD8+ T cells during acute LCMV infection[64, 117]. Although persistent demethylation at known regulatory regions has been observed in exhausted CD8+ T cells in humans[112] and mouse models[111], it remains unclear whether PD-1 expression in exhausted CD8+ T cells is regulated by exhaustion-specific regulatory regions not present in functional CD8+ cells. We identified nine ChARs within 45 kb of the *Pdcd1* gene locus (Fig. 2.4A), and found several that correspond to

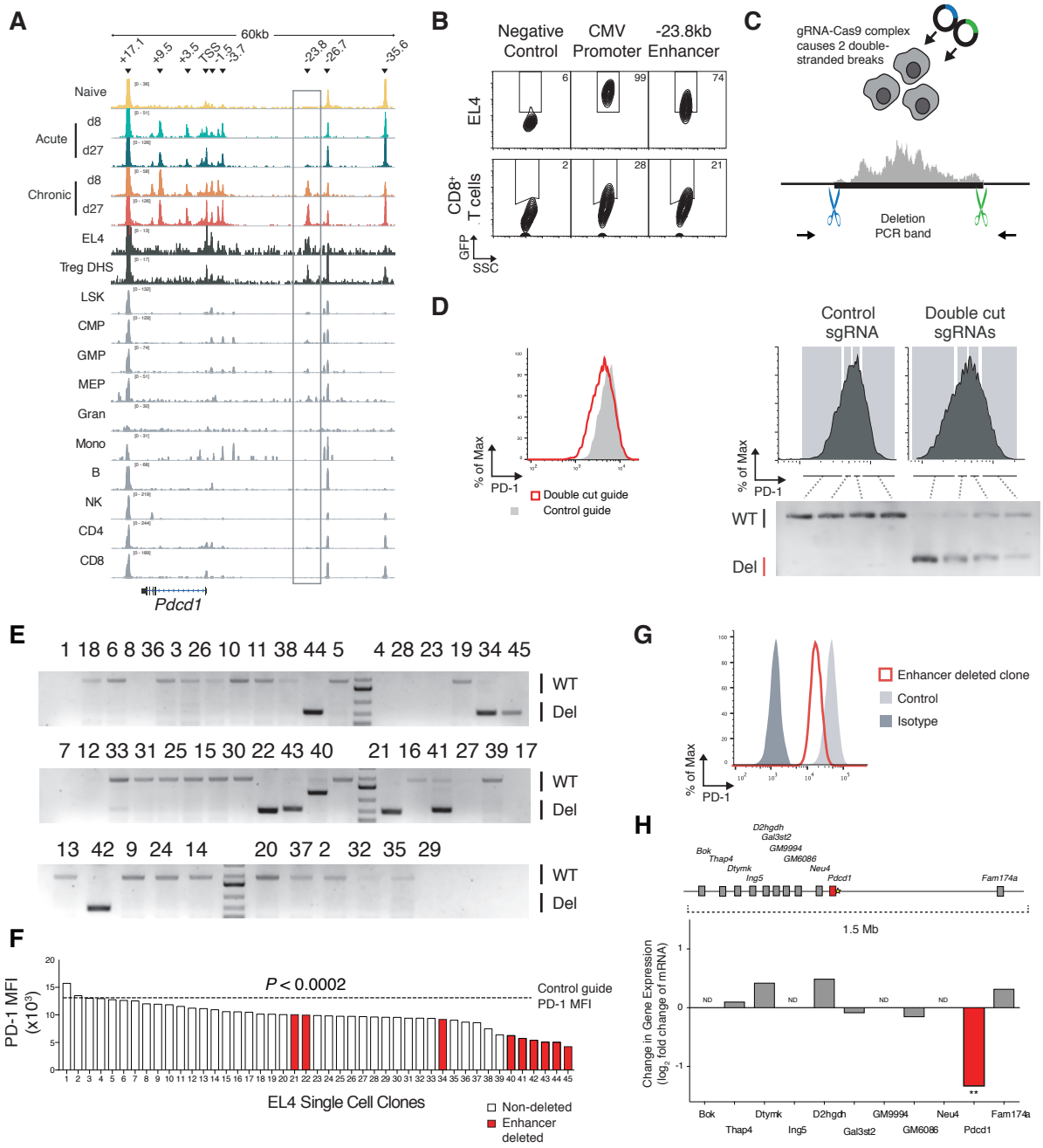


Figure 2.4. PD-1 is regulated by an enhancer found in exhausted but not functional CD8⁺ T cells. **(A)** ATAC-seq tracks from CD8⁺ T cells, EL4 cell line and hematopoietic lineages indicated. Arrows indicate individual ChARs. **(B)** GFP reporter in EL4s (upper) and activated CD8⁺ T cells (lower). **(C)** Schematic diagram of genome editing strategy. **(D)** Left: PD-1 expression in EL4 cells transfected with control (light grey) or double-cut sgRNAs (red) targeting the -23.8kb region. Left: Cell sorting gates (upper panels) and corresponding genomic PCR for the PD-1 enhancer region (lower panels) showing proportion of wild-type (WT) or deleted (Del) alleles in EL4 cells. **(E)** Gel showing PCR screening results using genomic DNA from 45 EL4 single cell clones receiving double enhancer targeting sgRNAs. **(F)** Expression of PD-1 in EL4 single-cell clones that are WT (white bars) or Del (red) for the -23.8kb enhancer ($P < 0.0002$, Mann-Whitney rank-sum test for PD-1 expression). **(G)** PD-1 expression of EL4 wild-type (light grey) or enhancer deleted (red) single cell clone. **(H)** Relative mRNA expression in WT or Del clones ($P < 0.005$, T-test).

previously-described regions with enhancer activity (-1.5kb and -3.7kb, Fig. 2.4A)[121]; these were present in both acute and chronic infection. We also identified an additional region approximately -23.8kb upstream of the *Pdcd1* TSS that only showed appreciable chromatin accessibility in exhausted CD8$^+$ T cells at d8 and at d27 p.i. from chronic infection and not in naïve, effector, or memory CD8$^+$ T cells from acute infection (Fig. 2.4A).

We hypothesized that this ChAR might function as an enhancer of PD-1 that is required for persistent, high levels of expression in exhausted CD8$^+$ T cells. This led us to survey chromatin accessibility at this region in the murine EL4 T cell line, and in previously published DHS[122] or ATAC-seq data[101]. We found that chromatin accessibility was not detected at any significant level throughout hematopoietic cell differentiation from Lin$^-$ Sca$^+$ Kit$^+$ cells, including terminally differentiated cell types such as granulocytes, monocytes, B cells, and NK cells (Fig. 2.4A). However, we identified a ChAR at the same region in EL4 cells and regulatory T cells, both of which can constitutively express high levels of PD-1[121, 123]. To test the function of the -23.8kb ChAR as a T cell enhancer, we cloned a 781bp fragment corresponding to this region into a reporter construct. This fragment was sufficient to induce a 10-12 fold increase in reporter gene expression in EL4 cells and *in vitro* activated CD8$^+$ T cells (Fig. 2.4B) relative to a vector encoding a minimal promoter only. This suggests that the ChAR at -23.8kb can function as an enhancer.

We then tested whether the -23.8kb enhancer was necessary for high-level PD-1 expression. We used the CRISPR/Cas9 nuclease to delete a 1.2kb fragment at that position in EL4 cells, which have both sustained high-level PD-1 expression and open chromatin at that enhancer site[106, 124] (Figs. 2.4C). We tested whether loss of the -23.8kb region affected PD-1 expression using several approaches. First, we showed the regions to be required for high-level PD-1 expression. We transfected Cas9-expressing EL4 cells with a pair of sgRNAs flanking the enhancer or with control guides, sorted the cells into sub-populations that differed in PD-1 expression and tested for the relative abundance of enhancer-deleted or wild-type alleles by

genomic PCR (Fig. 2.4D) in each sub-population. In EL4 cells transfected with the -23.8kb targeting pair of sgRNAs, the cells with the lowest PD-1 expression had the highest abundance of the enhancer-deleted band, and lowest abundance of the wild-type band (Fig. 2.4D).

Second, we generated a large number of single-cell clones from PD-1^{lo} EL4 cells transfected with the -23.8kb sgRNA pair. We identified nine clones out of 45 screened, (20%; Figs. 2.4E-F) with deletion of the -23.8kb region and found that the geometric mean fluorescence intensity (MFI) of the deleted clones was significantly lower than the non-deleted clones (Mann-Whitney test $P < 0.002$) (Fig. 2.4F). We confirmed deletion of the -23.8kb ChAR using Sanger sequencing and found that deletion of this region resulted in a 63.2% decrease in PD-1 expression but not total loss of expression, suggesting additional regulatory regions in EL4 cells were also involved in regulating PD-1 expression (Fig. 2.4G).

Third, we assessed whether deletion of the -23.8kb ChAR specifically decreased PD-1 expression by quantifying the expression of all genes with detectable expression that are within 1.5Mb of the *Pdcd1* locus. Only PD-1 mRNA expression was significantly decreased by deletion of the -23.8kb ChAR (Fig. 2.4H). This suggests that the -23.8kb ChAR present in exhausted CD8^{+} T cells serves as an enhancer that is required to maintain high-level PD-1 expression.

We next sought to identify the functional contribution of specific sequences within the -23.8kb enhancer to the regulation of PD-1 expression. We used Cas9-mediated *in situ* saturation mutagenesis and designed all possible sgRNAs within the enhancer as constrained by the protospacer adjacent motif (PAM)[106,125]. In order to compare the effect of mutagenizing the -23.8kb enhancer with other regulatory elements adjacent to the *Pdcd1* locus, we also designed a similar tiled set of sgRNAs to target the other eight PD-1 regulatory sequences defined by our ATAC-seq analysis (Fig. 2.5A). We transduced Cas9-expressing EL4 cells with a pool of 1754 enhancer-targeting sgRNAs, 117 sgRNAs targeting the *Pdcd1* exons as positive controls, and 200 non-targeting sgRNAs as negative controls (Fig. 2.5A). The median distance between

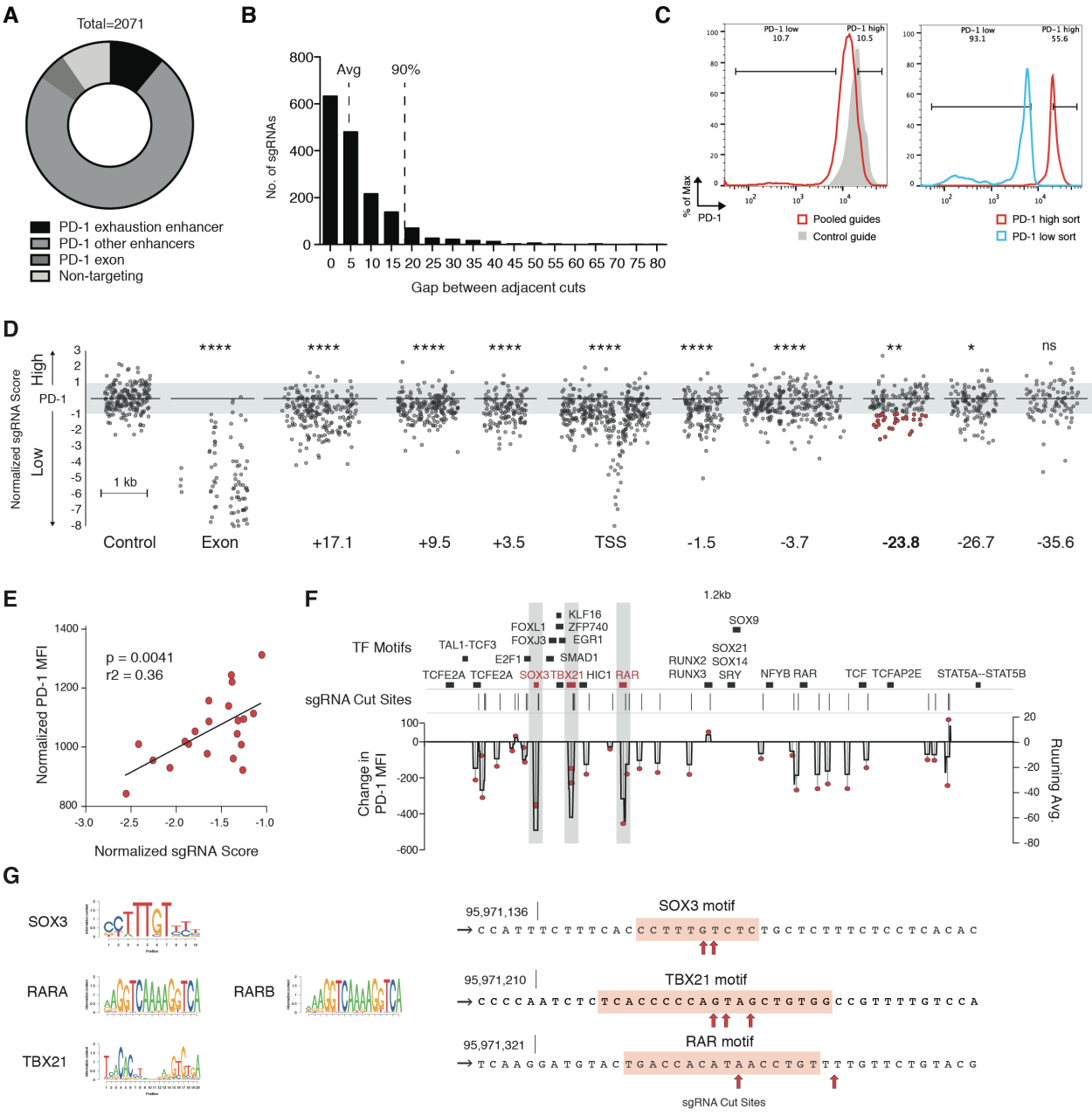


Figure 2.5. High resolution functional mapping of exh-specific enhancer identifies minimal sequences that regulate PD-1. (A) Composition of sgRNAs within pooled screening library. **(B)** Distribution of gaps between adjacent sgRNA cut sites. **(C)** PD-1 distribution (left) in pooled sgRNA transduced EL4s (red) compared to control-transduced EL4s (grey). Gates indicate PD-1 high and low sorted fractions. Post-sort distribution of PD-1 in high and low sorted populations (right). **(D)** Normalized enrichment of sgRNAs (grey symbols) within PD-1 high and low populations. Control non-targeting sgRNAs are pseudo-mapped with 5bp spacing. Red symbols correspond to the 21 sgRNAs with the largest effect within the -23.8kb enhancer, for which isogenic lines were later produced. **(E)** Correlation between normalized enrichment score in (E) and PD-1 MFI of individually transfected EL4 cells, for 21 top-scoring sgRNAs in the -23.8kb enhancer. average of PD-1 MFI changes caused by sgRNA activity shown in black (right axis). **(G)** Motifs for Sox3, RAR and TBX21 (left) with locations of scoring sgRNA cut sites falling in/near motif shown on the right.

(Figure 2.5 continued) (F) Overlap of TF motifs and sgRNA activity within the -23.8kb enhancer. Lines represent cut sites of top-scoring sgRNAs. Change in PD-1 MFI relative control guide transfected populations for each sgRNA (red symbol, left axis); 10bp running average of PD-1 MFI changes caused by sgRNA activity shown in black (right axis). **(G)** Motifs for Sox3, RAR and TBX21 (left) with locations of scoring sgRNA cut sites falling in/near motif shown on the right.

adjacent sgRNAs was 5bp, with 90% of sgRNAs falling within 18bp of each other, allowing us to identify genomic cleavage sites that disrupt PD-1 expression with high resolution (Fig. 2.5B).

We sorted transduced EL4s into populations based on high vs. low PD-1 expression, and quantified the abundance of individual sgRNAs within the two fractions using sequencing of extracted genomic DNA (Fig. 2.5C). In comparison to non-targeting sgRNAs, which were equivalently distributed between PD-1 high and low fractions, sgRNAs targeting *Pdcd1* exons were highly enriched in the PD-1 low fraction as expected (Fig. 2.5D). We found that sgRNAs targeting eight of the nine regulatory regions were also significantly enriched in the PD-1 low fraction to varying degrees, ($P < 0.00001$ to $P < 0.01$), suggesting a dense representation of critical sequences affecting PD-1 expression in each of the eight regulatory regions. However, sgRNAs in the -35.6kb ChAR had no significant effect on PD-1 expression, consistent with prior observations that this region falls outside the CTCF-mediated boundaries of the *Pdcd1* locus[121].

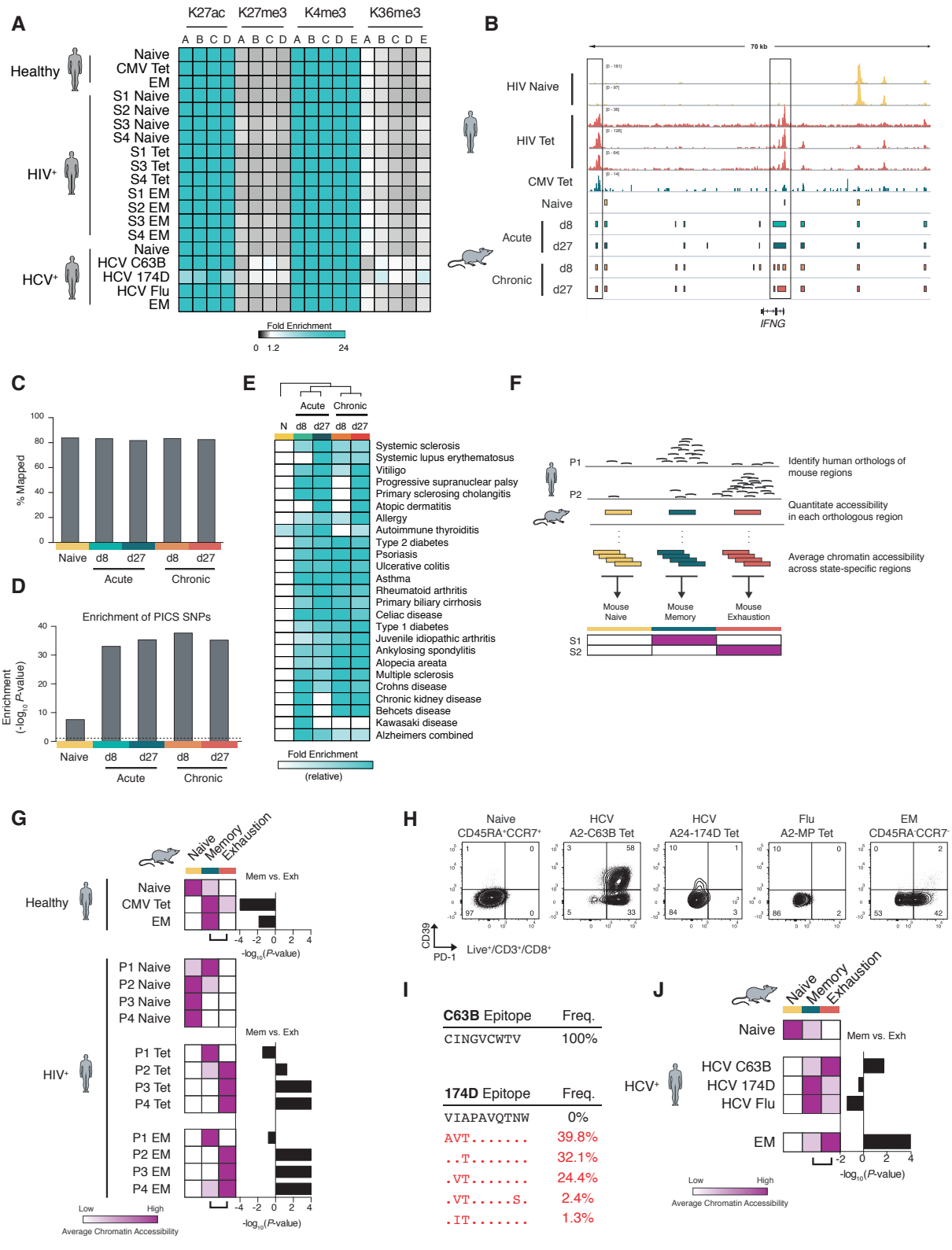
We focused on sgRNAs within the -23.8kb enhancer and generated 32 isogenic lines of Cas9-expressing EL4 cells, each transfected with one of the sgRNAs within the enhancer that was enriched in the PD-1 low fraction. We found a strong correlation between the predicted activity in a pooled setting of the sgRNAs most strongly enriched in the PD-1 negative fraction (PD-1 high:low ratio >1SD below mean) and their effect on PD-1 MFI in individual cell lines ($P = 0.0041$, Fig. 2.5E). This suggests that the pooled screen identified sgRNAs disrupting critical sequences of the enhancer with high specificity. Inspection of the predicted cleavage site locations revealed three critical regions of the enhancer in which cleavage markedly affected PD-1 expression (Fig. 2.5F, grey shading). These three locations with greatest sensitivity to disruption corresponded to motifs for Sox3, T-bet (encoded by *Tbx21*) and retinoic acid receptor (RAR) in

exhausted CD8$^+$ T cells *in vivo* (Fig. 2.5G). These data suggest that TF binding to these motifs in the -23.8kb enhancer may play a critical role in regulating PD-1 in exhausted CD8$^+$ T cells.

Exhaustion-specific epigenetic profiles in mice are conserved in antigen-specific human T cells in HIV-1 infection

Analysis of mouse models of LCMV infection suggests that T cell exhaustion is associated with a distinct epigenetic state. To test if the exhaustion-specific enhancer profile in mouse models was also a feature of human exhausted CD8$^+$ T cells, we analyzed global patterns of chromatin accessibility in tetramer$^+$ CD8$^+$ T cells specific for HIV from four subjects with chronic progressive HIV who were not on therapy. We compared these patterns to those found in cytomegalovirus (CMV)-specific CD8$^+$ T cells from a healthy donor. Bulk populations of naive (CCR7$^+$CD45RA$^+$) and effector memory (CCR7$^-$CD45RA$^-$) from each donor served as controls. We found that ChARs from each donor were highly enriched for activating chromatin marks, and depleted of regions containing repressive marks, confirming good data quality (Fig. 2.6A).

Figure 2.6. Exhaustion-specific epigenetic profiles in the mouse are conserved in antigen-specific exhausted human T cells in HIV and HCV infection. (A) Fold enrichment of regions annotated for published histone marks in human primary T cells, within ATAC peaks for all human samples. **B)** Representative ATAC-seq tracks from Naïve, HIV tetramer$^+$ and CMV tetramer$^+$ samples (top). Orthologous regions from 5 mouse cell states at *IFNG* locus (colored blocks, bottom). **(C)** Percentage of all peaks entirely/partially mapped to human genome (hg19). **(D)** Enrichment of PICS SNPs in mouse orthologous ChARs. Dotted line illustrates $P = 0.05$ (hypergeometric test). **(E)** Fold enrichment of autoimmune diseases SNPs in orthologous regulatory regions relative to randomly selected regions. **(F)** Schematic diagram of mouse and human comparative analysis. **(G)** Average chromatin accessibility at regions orthologous to mouse naïve, memory and exhaustion enhancers in human samples indicated. **(H)** PD-1 and CD39 expression in naïve, HCV C63B tetramer$^+$, HCV 174D tetramer$^+$, Flu MP tetramer$^+$, and effector memory CD8$^+$ T cell populations from a single HCV-infected donor. **(I)** Viral sequences encoding C63B and 174D epitopes. **(J)** Average chromatin accessibility at regions orthologous to mouse naïve, memory and exhaustion enhancers in human samples indicated from a single HCV-infected donor.


A
K27ac
K27me3
K4me3
K36me3
A B C D A B C D A B C D E A B C D E
Healthy
HIV+
HCV+
Naive
CMV Tet
EM
S1 Naive
S2 Naive
S3 Naive
S4 Naive
S1 Tet
S3 Tet
S4 Tet
S1 EM
S2 EM
S3 EM
S4 EM
Naive
HCV C63B
HCV 174D
HCV Flu
EM
Fold Enrichment
0 1.2 24
B
70 kb
HIV Naive
HIV Tet
CMV Tet
Naive
Acute
Chronic
d8
d27
IFNG
C
% Mapped
Naive d8 d27 d8 d27
Acute
Chronic
D
Enrichment of PICS SNPs
Enrichment (-log10 P-value)
Naive d8 d27 d8 d27
Acute
Chronic
E
Acute
Chronic
N d8 d27 d8 d27
Systemic sclerosis
Systemic lupus erythematosus
Vitiligo
Progressive supranuclear palsy
Primary sclerosing cholangitis
Atopic dermatitis
Allergy
Autoimmune thyroiditis
Type 2 diabetes
Psoriasis
Ulcerative colitis
Asthma
Rheumatoid arthritis
Primary biliary cirrhosis
Celiac disease
Type 1 diabetes
Juvenile idiopathic arthritis
Ankylosing spondylitis
Alopecia areata
Multiple sclerosis
Crohns disease
Chronic kidney disease
Behcets disease
Kawasaki disease
Alzheimers combined
Fold Enrichment
(relative)
F
P1
P2
Identify human orthologs of mouse regions
Quantitate accessibility in each orthologous region
Average chromatin accessibility across state-specific regions
Mouse Naive
Mouse Memory
Mouse Exhaustion
S1
S2
G
Naive
Memory
Exhaustion
Healthy
Naive
CMV Tet
EM
Mem vs. Exh
-log10(P-value)
HIV+
P1 Naive
P2 Naive
P3 Naive
P4 Naive
P1 Tet
P2 Tet
P3 Tet
P4 Tet
P1 EM
P2 EM
P3 EM
P4 EM
Low
High
Average Chromatin Accessibility
H
Naive CD45RA+CCR7+
HCV A2-C63B Tet
HCV A24-174D Tet
Flu A2-MP Tet
EM CD45RA-CCR7-
CD39
PD-1
Live+/CD3+/CD8+
I
C63B Epitope Freq.
CINGVCWTV 100%
174D Epitope Freq.
VIAPAVQTNW 0%
AVT..... 39.8%
..T..... 32.1%
.VT..... 24.4%
.VT.....S. 2.4%
.IT..... 1.3%
J
Naive
Memory
Exhaustion
Naive
HCV+
HCV C63B
HCV 174D
HCV Flu
EM
Mem vs. Exh
-log10(P-value)
Low
High
Average Chromatin Accessibility

We mapped ChARs identified in the mouse model to their human orthologous regions and successfully aligned 80-85% of all mouse ChARs (Fig. 2.6B-C)[126, 127]. Regions mapped from all five mouse CD8$^+$ T cell states were significantly enriched for disease-associated SNPs (PICS SNPs, $P < 2.77 \times 10^{-8}$; hypergeometric test; Fig. 2.6D-E)[105], suggesting mapped regions corresponded to important regulatory regions within the immune system. However, regions at the *PDCD1* locus were not among those mapped from the mouse model, as previously observed[121], limiting our ability to detect an ortholog to the -23.8kb enhancer observed in the mouse model.

We identified non-overlapping sets of ChARs unique to naïve, memory (acute d27) or exhausted cells (chronic d27) in the mouse and tested for chromatin accessibility within orthologous regions in each human sample (Fig. 2.6F). Human naïve CD8$^+$ T cells from the majority of donors showed significantly greater chromatin accessibility in naïve-specific regions defined in the mouse than in memory- or exhaustion-specific regions. In the healthy donor, CMV-specific tetramer$^+$ CD8$^+$ T cells, and effector memory cells were enriched for memory-specific regions (MW test, $P = 0.01$ to $P < 0.0001$) (Fig. 2.6G). In contrast, HIV-specific tetramer$^+$ cells from 3 out of the 4 subjects showed significantly greater chromatin accessibility in exhaustion-specific regions (MW test, $P = 0.05$ to $P < 0.001$) than in memory-specific regions. Interestingly, effector memory CD8$^+$ T cells in HIV-infected subjects also showed greater chromatin accessibility in exhaustion-specific regions, possibly as a result of unmeasured exhausted HIV-specific T cells within that compartment or from bystander T cells with aberrant differentiation[128].

We confirmed these findings in a subject with chronic HCV infection by surveying exhaustion-specific epigenetic patterns in multiple tetramer$^+$ populations from the same donor. We isolated tetramer$^+$ CD8$^+$ T cells specific for two different epitopes from HCV and one specific for influenza (Flu), as well as bulk naïve and effector memory cells. Flow cytometry demonstrated that naïve CD8$^+$ T cells were uniformly negative for the exhaustion markers PD-1 and CD39, as expected. The majority of tetramer$^+$ CD8$^+$ T cells specific for the HCV C63B epitope expressed

high levels of PD-1[129, 130] and CD39[131], as previously described for HCV-specific CD8+ T cells in chronic infection (Fig. 2.6H). However, HCV tetramer+ cells specific for the 174D epitope were PD-1 and CD39 low, closely resembling the staining pattern of functional Flu tetramer+ cells. Sequencing of the HCV genome in this subject revealed that unlike the C63B epitope, the 174D epitope had undergone extensive viral escape and no wild-type viral sequence could be detected. This suggests that the 174D tetramer+ T cells were no longer encountering cognate antigen (Fig. 2.6I). Consistent with this observation, we found that the C63B Tet+ cells showed significantly greater chromatin accessibility at exhaustion-specific regions MW test, $P = 0.01$) than memory regions. In contrast, 174D tetramer+ cells showed greater chromatin accessibility in memory-specific regions, as did influenza-specific CD8+ T cells (MW test, $P = 0.04$) (Fig. 2.6I). Thus, the state-specific pattern of chromatin accessibility found in mouse exhausted CD8+ T cells is conserved in human exhausted CD8+ T cells.

Discussion

Exhausted T cells in cancer and chronic viral infection express distinctive patterns of genes, including sustained expression of programmed cell death protein-1 (PD-1). However, the regulation of gene expression in exhausted T cells is poorly understood. Here we define the accessible chromatin landscape in exhausted CD8+ T cells and show that it is distinct from functional memory CD8+ T cells. Exhausted CD8+ T cells in humans and a mouse model of chronic viral infection acquire a state-specific epigenetic landscape organized into functional modules of enhancers. Genome editing shows that PD-1 expression is regulated in part by an exhaustion-specific enhancer that contains essential RAR, T-bet and Sox3 motifs. These data have three important implications for our understanding of T cell exhaustion.

First, our data show that exhaustion occurs with a combination of remodeled enhancer accessibility and new TF binding, and supports a model in which exhausted CD8+ T cells are not

simply “persistent effectors” but rather a differentiation state distinct from their functional counterparts. Identifying the plasticity of this state and whether or how it could be reverted becomes a critical question. The absence of an exhaustion-specific epigenetic profile in HCV-specific CD8+ T cells that no longer recognize an escaped epitope suggests that reducing antigen burden may be an important factor in rescuing exhaustion but awaits confirmation in longitudinal studies.

Second, we show that *in situ* mutagenesis of enhancers *in vitro* may be a useful approach for fine mapping of enhancer function. The feasibility of TF ChIP studies is limited in situations where few relevant cells can be isolated. As an alternative, we identified motifs at state-specific enhancers in exhausted CD8+ T cells and probed the function of these TF motifs using Cas9-mediated saturation mutagenesis *in vitro*. While this approach is limited by the degeneracy of TF motifs (e.g. a T-bet motif may in fact be bound by other T-box factors such as Eomesodermin), it highlights the ability to uncover a role for novel potential regulators of T cell exhaustion such as the RAR family of TFs.

Third, we speculate that mapping state-specific enhancers in exhausted T cells may provide an opportunity to improve the therapeutic efficacy of adoptive T cell therapy. Infusion of T cells engineered to express chimeric antigen receptors directed at cancer have had less success in solid tumors in part because of the development of T cell exhaustion in the engineered T cell product[52, 132]. Genome editing of therapeutic T cells to make them resistant to exhaustion is an appealing concept and has led to recent studies investigating the deletion of the PD-1 gene locus[133, 134]. Editing exhaustion-specific enhancers[106] that regulate genes which impair the function of exhausted CD8+ T cells may provide an additional approach to modulate T cell function that is more “tunable” and state-specific than targeting exons. Creating detailed functional maps of enhancers specific to exhausted CD8+ T cells in humans may therefore provide a crucial step towards the rational engineering of T cells for therapeutic use.

Materials and methods

Mice

Wild type C57/BL/6N (CD45.2+) and congenic B6.SJL-Ptprca Pepcb/BoyJ (CD45.1+) mice were obtained from the US National Cancer Institute. C57BL/6N P14 mice (LCMV-specific T cell receptor transgenic) were bred in-house. Male mice were used at between 6 and 10 weeks of age. All animal experiments were done in accordance with the Animal Care and Use Committee for the University of Pennsylvania.

Infection and isolation of mouse lymphocytes

LCMV strains were produced and titred as described[135, 136]. Two cohorts of mice were infected by intraperitoneal injection of LCMV Armstrong (2×10^5 plaque-forming units) or intravenous injection of LCMV Clone 13 (4×10^6 plaque-forming units). All donor P14 cells were prepared from naive spleen using $CD8^+$ negative selection (Miltenyi Biotec). To generate effector, memory and exhausted $CD8^+$ T cells, approximately 1-2 x 10^3 P14 cells were transferred into recipient mice, followed by LCMV infection one day later. Target effector/memory/exhausted P14 cells were harvested from recipient spleens at d8 or d27 p.i. After enrichment using CD45.2 FITC Ab and anti-FITC microbes (Miltenyi), cells were sorted by Aria II (BD). Naïve and effector/memory/exhausted $CD8^+$ T (P14) cells were sorted by gating on $CD8^+$ $TCRVa2^+$ $CD62L^+$ $CD44^{lo}$ and $CD8^+$ $TCRVa2^+$ $CD45.2^+$ $CD45.1^-$ population, respectively. The following antibodies from Biolegend were used for flow-cytometry: anti–TCR Vα2 (B20.1), anti-CD8α (53-6.7), anti-CD44 (IM7), anti-CD45.1 (A20), anti-CD45.2 (104), and anti-CD62L (MEL14).

ATAC-seq

We sorted 40-50,000 cells per biological replicate (Naïve, Acute d8, Acute d27, Chronic d8, Chronic d27 and EL4), which were then washed once in cold PBS and lysed in 50µL cold lysis

buffer (10 mM Tris-HCl, pH 7.4, 10 mM NaCl, 3 mM MgCl2, 0.1% IGEPAL CA-630). Lysed nuclei were incubated in Tn5 transposition reaction mix as described[97] and purified using MinElute Reaction Cleanup kit (Qiagen). ATAC-seq fragments from one set of replicates for Acute d8, Acute d27, Chronic d8 and Chronic d27, as well as both biological replicates for Naïve cells and EL4 cells, were size selected for fragments between 115 and 600 bp using Pippin Prep 2% Agarose Gel Cassettes and the Pippin Prep DNA Size Selection System (Sage Science). Post size-selection, ATAC libraries were amplified and Nextera sequencing primers ligated using Polymerase Chain Reaction (PCR). Finally, PCR primers were removed using Agencourt AMPure XP bead cleanup (Beckman Coulter/Agencourt) and library quality was verified using a Tapestation machine. High quality DNA libraries were sequenced on the Illumina HiSeq2000.

Quality control of ATAC-seq data and alignment to the genome

We used the FASTQC pipeline (Babraham Bioinformatics) on our reads, and aligned them to the reference genome (mm9) with bowtie version 1.1.1[137], retaining only reads that mapped to a unique position in the genome ["–m 1"]. We marked duplicate reads in the bam files using PICARD and checked for contamination of primer sequences.

Identification of peaks in ATAC-seq data

After alignment of the reads to the reference genome, reads aligned to the positive strand were moved +4 bp, and reads aligning the negative strand were moved -5bp[97]. For each of our five replicate pairs, we merged the two replicates using samtools, and then called peaks using MACS2 version 2.1.0, setting the FDR to 0.001 with the "nomodel" option and default mouse genome size. To generate our final universe of peaks, we took the union of all of these peaks while merging overlapping regions. We extracted the shifted ATAC-Seq cut sites from our data and counted the number that fell into each peak region. We then used DESeq2 to identify the differential

abundance of cut sites between the peaks and performed all pairwise comparisons of the five conditions and considered those with an FDR below 0.05 to be differential.

Enrichment of genomic features in ATAC-seq peaks

For each sample, we investigated the set of peaks calculated by MACS2 for enrichment of genomic features relative to their coverage in the mouse genome. For each genomic feature, we calculated the fold enrichment as [Overlap of Genomic Feature with ATAC-Seq Peak Regions / Total Size of Peak Regions] / [Overlap of Genomic Feature with Mouse Genome / Effective Size of Mouse Genome], with all sizes expressed in base pairs.

We set the effective size of the mouse genome to be 2,716,965,481 bp. *P*-values were calculated using a binomial test where n= Number of Peaks, x = Number of Peaks Overlapped by Annotation, p = (Overlap with Mouse Genome / Effective Size of the Mouse Genome).

The genomic features we used include: (i) regulatory features annotations from the Ensemble database[138], (ii) regulatory features found by the ORegAnno database[139], (iii) conserved regions annotated by the multiz30way algorithm, here we consider regions with multiz30way score>0.7, (iv) repeat regions annotated by RepeatMasker (http://www.repeatmasker.org), (v) putative promoter regions - taking 10 kb upstream and 1 kb downstream of transcripts annotated in RefSeq[140], (vi) gene body annotations in RefSeq; (vii) 3' proximal regions (taking 1kb upstream and 5kb upstream to 3' end); (viii) regions enriched in binding of BATF, IRF4, c-Jun, JunD, and JunB, along with histone marks H3K4me1, H3K4me3, H3K27ac, H3K36me3, and H3K27me3 (Polycomb-repression), and additional annotations Poised Enhancer, Active Enhancer, Bivalent Promoter, Developmental Enhancer, and Init. Promoter in CD8+ T Cells[135]. We also added the peaks we obtained in this study for two replicates of EL4 cells.

Cluster and gene ontology analysis

K-means clustering was applied using GENE-E (Broad Institute) to differential ChAR signal intensity across all five cell states. Optimum number of clusters was determined using the gap statistic in MATLAB. Association of ChARs to neighboring genes and enrichment of Gene Ontology (GO) terms within modules (using the entire genome as a background set) was determined using GREAT with default settings (http://bejerano.stanford.edu/great/public/html/). Selected GO terms are presented as a heatmap in Fig. 2.3D.

CRISPR design

SgRNA-specifying oligo sequences were chosen to maximize on-target efficiency based on publicly available on-line tools (Broad Institute). Single stranded sgRNA oligos (Integrated DNA Technologies) were annealed and ligated into PXPR003 as previously described[124]. SgRNA plasmids were introduced into cell lines using lentiviral packaging or nucleofection. For lentivirus production, 293T cells were seeded in DMEM with 10% (vol/vol) FBS. Cells were transfected with sgRNA plasmids and the packaging plasmids Δ8.9 and VSV-g using TurboFect (ThermoFisher). Viral supernatants were collected 72 hours later. For nucleofection, EL4 cells were mixed with 100ul of Nucleofector solution and 2ug of sgRNA plasmid. Cells were then transfected using Nucleofector Kit L (Lonza) and the C-09 program on the Amaxa Nucleofector I machine.

Cell culture

EL4 cells (ATCC) were cultured in RPMI with 10% (vol/vol) FBS, HEPES, Penicillin/Streptomycin and β-mercaptoethanol (R10 media). Cas9 expressing cell lines were produced using PLX304 plasmid lentivirally packaged as described above. Cas9 expressing cells were then transduced or transfected with sgRNA plasmids, selected for plasmid presence using puromycin, and used

for all subsequent experiments 3-5 days post-selection. Single cell clones of bulk EL4s were made using limiting dilution.

Reporter assays

DNA sequences corresponding to the 781 bp core of the -23.8kb PD-1 enhancer (chr1: 95971119 - 95971900, mm9), and the CMV promoter were cloned upstream of a TATA box minimal promoter driving GFP expression within a lentiviral construct. Plasmids were lentivirally packaged as described above. Viral supernatant was concentrated 100x by ultracentrifugation for 2 hours at 20,000xg.

$CD8^+$ T cells were isolated from naive spleens using CD8 negative selection MACS kit (Miltenyi Biotec) and cultured in R10 medium. Naive cells were stimulated for 24 hrs with plate-bound anti-CD3 (4 μg/ml; 2C11; BD Pharmingen) and anti-CD28 (4 μg/ml; 37.51; BD Pharmingen) in the presence of recombinant human IL-2 (100 U/ml, R&D Systems) for *in vitro* activation prior to transduction. *In vitro* activated T cells and EL4 cells were transduced with concentrated virus by incubation with polybrene (5ug/ml) and spin infection (2000 RPM for 45 min at 37 °C). GFP expression was measured by flow cytometry 48-72 hours post transduction.

Enhancer deletion

The region -23.8kb from the *Pdcd1* TSS was deleted using a pair of sgRNA targeting sequences flanking the region. EL4 cells transfected with -23.8kb-targeting sgRNAs or negative control sgRNAs were sorted on the basis of differing levels of PD-1 expression and genomic PCR was used to detect deletion in sorted EL4s. Genomic DNA was isolated from bulk and clonal cell lines using 50ul QuickExtract DNA solution and incubated according to manufacturer instructions. PCR was performed on genomic DNA from each sample using the deletion screening primer pairs and run on a 1% agarose gel with EtBr. For clonal lines, biallelic deletion clones were defined as

having PCR amplification of only the deletion band, while non-deleter clones amplified only the WT band. Deletion was verified by submitting the PCR amplification products for Sanger sequencing.

RT-qPCR

Clonal cells lines as well as control sgRNA receiving bulk populations were lysed IN RLT and RNA was extracted using RNeasy Plus Mini kit (Qiagen). cDNA was generated using ImProm-II Reverse Transcriptase (Promega), and analyzed on a Viia 7 Quantitative PCR instrument using Taqman probes.

***In situ* saturation mutagenesis**

All possible tiling sgRNAs as constrained by Cas9 –NGG protospacer adjacent motif presence within all nine PD-1 enhancers and all PD-1 exons were designed using publicly available online tools (http://portals.broadinstitute.org/gpp/public/analysis-tools/sgrna-design). Non-targeting sgRNAs were designed by the Genomics Perturbation Platform at the Broad Institute. All sgRNA oligos were synthesized and cloned into the lentiGuide-Puro vector backbone as previously described (16, 17). Plasmid libraries were lentivirally packaged as described above, and Cas9-expressing EL4s were transduced by incubation with polybrene (5ug/ml) and spin infection (2000 RPM for 45 min at 37 °C). Control transductions were done to ensure 1000x library coverage with a multiplicity of infection of approximately 0.3. Transduced cells were selected with puromycin for 72 hours, and a sample was taken post-selection as the starting d0 representation of the library. Cells were cultured throughout the experiment to ensure 1000x coverage of the library at all times.

Library-transduced cells were stained with anti-PD-1 fluorescent antibodies and sorted into PD-1 high and PD-low populations (Fig. 2.5C). Replicate sorts were done between d20-d50 post-selection, and genomic DNA was isolated from sorted populations using the Dneasy Blood

and Tissue Kit (Qiagen). Bulk cells from d0 post-selection, input plasmid pools as well as sorted populations were sequenced as previously described (16, 17). SgRNA abundance was quantified within each sample by normalizing reads to library sequencing depth. SgRNA enrichment in PD-1 high vs. PD-1 low populations were calculated as follows: 1) sgRNA abundance in each sample was log-transformed; 2) sgRNA abundance at d0 was subtracted from its abundance in each sample to account for initial variation in sgRNA representation; 3) any sgRNA that was not detected in at least one sorted sample was excluded from further analysis as a cellular dropout; 4) for each sorted sample (high and low analyzed separately), the abundance of enhancer- and exon-targeting sgRNAs were normalized calculating z-scores relative to the distribution of the control guides; 5) the normalized score for each sgRNA in the PD-1 low compartment was subtracted from the score in the PD-high compartment, to generate a normalized enrichment score for each sgRNA for each replicate; and 6) the enrichment score for each sgRNA was averaged across replicates. Enhancer- and exon-targeting sgRNA cleavage sites were mapped to the mouse genome (mm9), while control non-targeting sgRNAs were pseudomapped with 5 bp spacing.

Validation of individual sgRNAs

32 sgRNAs that were enriched in the PD-1 low fraction within the -23.8kb enhancer were chosen for individual validation. Oligos representing each sgRNA (IDT) were cloned individually into Cas9 and sgRNA dual delivery construct. Plasmids were then nucleofected into EL4 cells as previously described to produce 32 isogenic cell lines. Each cell line was selected 18-36 hours post-nucleofection in puromycin, and cultured in R10 medium. Cells were stained for PD-1 expression or the corresponding isotype control. Geometric mean fluorescence intensity (MFI) of PD-1 expression in each cell line was normalized to the MFI of staining with isotype control.

Identifying motifs in genome

We used the PWM databases from Jolma 2013 , Chen 2008[141], UniPROBE (mouse)[142], and JASPAR 2014 (core vertebrates)[143] available in the list of databases at http://meme-suite.org/db/motifs. We then called motifs in version 9 of the mouse genome using FIMO[144] and a threshold of $1x10^{-5}$. We began with a total of 1,446 motifs and removed any that had zero hits, or more than 1.5 million hits.

Subjects

Four HIV-infected participants in the Seattle Natural Progression cohort were selected for this study (46). Progressors were defined as having median viral loads >10,000 RNA copies/ml in the last year. All subjects were studied in chronic infection and were antiretroviral therapy naïve. 40-60 million PBMCs were obtained from each subject. The relevant institutional review boards approved all human subject protocols, and all subjects provided written informed consent before enrollment.

A baseline sample was obtained for a single HCV-infected patient enrolled on a trial to evaluate the effect of successful antiviral therapy on innate and adaptive immune responses for genotype 1a hepatitis C virus infection (NCT02476617). The HCV subject was chronically infected with an HCV viral load of 828,000 IU/ml. Based on the expressed HLA class I alleles, we screened for virus-specific $CD8^+$ T cell responses using HLA class I multimers. We identified responses targeting HCV A*02:01 C63B CINGVCWTV, HCV A*24:01 174D VIAPAVQTNW and influenza A*02:01 MP GILGFVFTL. Multimer-binding $CD8^+$ T cells were isolated by FACS from PBMCs obtained through leukapheresis. The patient had consented to this Institutional Review Board approved study.

PBMCs were obtained via density centrifugation from a normal volunteer and screened for a CMV tetramer$^+$ T cell response. The relevant institutional review board approved the human subject protocol, and all subjects provided written informed consent before enrollment.

Isolation of human lymphocyte populations for ATAC-seq

PBMCs were thawed rapidly in warm RPMI supplemented in 10% FBS. CD8$^+$ T cells were enriched using MACS CD8 negative selection kit (Miltenyi Biotec). After enrichment, cells were stained and sorted on a FACSAria cell sorter (BD Biosciences). The following fluorochrome-conjugated antibodies from Biolegend were used for flow-cytometry: anti–CD45RA (HI100), anti-CCR7 (G043H7), anti-2B4 (C1.7), anti-CD3 (OKT3), anti-CD39 (A1), anti-PD-1 (EH12.2H7), and anti-CD8a (SK1). The following fluorochrome-conjugated multimers were used for flow-cytometry: HIV A*03:01 RLRPGGKKK, HIV A*02:01 SLYNTVATL, HIV B*08:01 GEIYKRWII, CMV A*02:01 pp65-NLV NLVPMVATV, HCV A*02:01 C63B CINGVCWTV, HCV A*24:01 174D VIAPAVQTNW, and influenza A*02:01 MP GILGFVFTL. A maximum of 70,000 cells were sorted PBS supplemented with 10% FBS and ATAC-seq libraries were generated as previously described. Due to limiting starting material, ATAC libraries were not size-selected prior to multiplexed sequencing on the Illumina HiSeq2000. Post-sequencing quality control, alignment of human ATAC reads to the human genome (hg19), MACS2 peak calling, and DESeq2 peak normalization was done as previously described.

Mapping peaks to human genome and SNP analysis

Orthologous mouse ChARs (mm10) were mapped to the human genome (hg19) as described[126]. Since the mapping algorithm requires input regions in mm10, the UCSC liftover tool was applied to ChARs to transfer them onto mm10 from mm9. GWAS SNPs in the NHGRI catalog (https://www.ebi.ac.uk/gwas/) annotated as “immune system disease” was defined as being

immune-related. Hypergeometric tests were performed to quantify overlap of enhancers with all GWAS SNPS, immune-related SNPS as well as PICS SNPs.

Comparative analysis of mouse and human data

All mouse peaks identified across the 5 cell states (Naïve, Acute d8, Acute d27, Chronic d8, Chronic d27) were partitioned into 3 categories based on MACS2-called peaks: peaks identified uniquely in Naïve cells relative to Acute and Chronic d27 (mouse Naïve only), peaks identified uniquely in Acute d27 cells relative to Naive and Chronic d27 (mouse Memory only), and peaks identified uniquely in Chronic d27 cells relative to Naive and Acute d27 (mouse Exhaustion only). Orthologous mouse peaks within the three categories (Naïve, Memory, Exhaustion) were mapped to the human genome and filtered for overlap with at least one MACS2 human peak called independently across all human samples. Then, for each human sample, average chromatin accessibility was calculated separately for the 3 categories of mouse orthologous peaks (Naïve, Memory, Exhaustion). Average chromatin accessibility within each category was normalized to account for inherent differences in chromatin accessibility across the 3 classes of peaks.

Amplification and deep sequencing of HCV epitopes

For HCV epitopes 174D and C63B, amplicons surrounding these epitopes were generated using the following conditions. The reaction consisted of 2x First Strand Buffer, sense (A2F: AAC GTT GCG ATC TGG AAG AC or A3F: GCT CTC ATG ACC GGC TTT AC) and antisense primers (A2R: GGA AGC GTG GTT GTC TCA AT or A3R: AGA GAT CTC CCG CTC ATC CT) at 0.4μM, and a Superscript III RT/Platinum *Taq* Mix (Invitrogen), with the following conditions: cDNA synthesis for 30 minutes at 50°C, followed by heat denaturation at 94°C for 2 minutes, the PCR amplification conditions were 40 x (94°C, 15 s; 55°C, 30 s; 68°C 180 s), with a final extension at 68°C for 5 minutes. PCR amplicons were fragmented and barcoded using NexteraXT DNA Library

Prep Kit, as per manufacturer's protocol. Samples were pooled and sequenced on an Illumina MiSeq platform, using a 2 x 250 bp V2 reagent kit. Paired-end reads obtained from Illumina MiSeq were assembled into an HCV consensus sequence using the VICUNA *de novo* assembler software (47) and finished with V-FAT v1.0. Reads were mapped back to this consensus using Mosaik v2.1.73, and intra-host variants called by V-Phaser v2.0 (48, 49). All reads have been deposited to the NCBI Sequence Read Archive under accession number SRR3951347.

Chapter 3. Epigenetic scarring of exhausted $CD8^+$ T cells in chronic Hepatitis C infection after curative therapy

Parts of this chapter are currently in preparation for publication as:

Debattama R. Sen, Kathleen B. Yates, Ulrike Gerdemann, Pierre Tonnerre, David Wolski, Genevieve E. Martin, Rose Al Abosy, Dawn E. Comstock, Sarah A. Weiss, John Frater, Georg M. Lauer, W. Nicholas Haining. Epigenetic scarring of exhausted $CD8^+$ T cells in chronic Hepatitis C infection after curative therapy. (Manuscript in preparation)

Introduction

The development of $CD8^+$ T cell exhaustion, characterized by a range of functional deficits, is a hallmark of chronic viral infections[113]. In mouse models of chronic viral infection, exhausted T cells acquire a distinct transcriptional and epigenetic state[62, 64, 145]. However, whether similar epigenetic changes underlie the functional impairment of human $CD8^+$ T cells in chronic Hepatitis C infection, as well as the ultimate fate of these T cells after curative therapy, remains unknown.

T cell exhaustion has been extensively studied in mice using strains of the Lymphocytic Chorimeningitis Virus (LCMV)[5], and is characterized by expression of multiple co-inhibitory receptors, low effector cytokine production, and poor control of virus[3, 4, 9, 63]. Similar functional deficits can be observed within human T cells responding to chronic viral infections such as Human Immunodeficiency Virus (HIV) and Hepatitis C Virus (HCV)[15, 21, 22, 35]. Notably, only 30% of all HCV infections are spontaneously resolved in humans, in part due to the rapid induction of T cell exhaustion within the HCV-specific T cell compartment[146]. Exhausted T cells in HCV show high expression of inhibitory receptors such as PD-1, Tim-3 and CD39 and decreased expression of cytokines such as IFN-γ and TNF[37, 38, 66, 131, 147].

Checkpoint blockade immunotherapy aims to relieve T cell exhaustion by reducing inhibitory T cell signaling through the PD-1/PD-L1 axis[148, 149]. While immune checkpoint blockade therapies in the setting of HCV can transiently lead to greater effector T cell function[37, 40, 41],

emerging evidence in mouse models suggests that anti-PD-1 therapy does not fundamentally reverse the epigenetic state of exhaustion[150]. As a result, new strategies for therapeutic intervention are needed to relieve the clinical presentation of T cell exhaustion.

Recently developed direct-acting antiviral (DAA) therapies have been strikingly effective in curing HCV-associated viremia and may represent an alternative strategy to reverse T cell dysfunction in HCV[151, 152, 153]. Previous work has demonstrated that a subset of exhausted T cells can be maintained long-term after cure of infection[154]. However, whether DAA therapy can fundamentally reprogram exhausted $CD8^+$ T cells has not been investigated.

Here we show that exhausted $CD8^+$ T cells in HCV establish a distinct epigenetic program that is shared across chronic viral infections, and that cannot be reversed by DAA therapy. Evaluation of HCV-specific $CD8^+$ T cells within the same individual before and after cure of infection suggested that establishment of an exhaustion-associated epigenetic signature is dependent largely on chronic Ag stimulation, and not the inflammatory milieu. Epigenetic "scars" of exhaustion involved distinct transcriptional regulators, including the transcription factors Tox and HIF-1α. These scars were retained within HCV-specific cells upon long-term follow-up post-DAA therapy. New insight into the epigenetic inflexibility of $CD8^+$ T cell responses in HCV has crucial implications for clinical efforts to reverse T cell exhaustion.

Results

Distinct epigenetic changes underlie $CD8^+$ T cell responses to chronic HCV infection

To characterize the epigenetic state induced by chronic HCV infection, we used ATAC-seq to profile chromatin accessibility of antigen-specific $CD8^+$ T cells responding to HCV and influenza (flu) virus, as well as control naive $CD8^+$ T cells, in 6 chronically-infected donors (Fig. 3.1A). We recovered 128,355 chromatin-accessible regions (ChARs) across our entire dataset, with a range of 47,000 to 78,000 peaks that were identified within each cell subset. Strong enrichment of

chromatin accessibility at transcriptional start sites (TSSs) genome-wide relative to background suggested high data quality (Fig. 3.1B).

We also observed expected epigenetic changes between various T cell states, supporting our ability to distinguish biologically meaningful differences. These changes included increased accessibility in naive T cells near *Ccr7*, a gene that enables naive T cell trafficking to secondary lymphoid organs (Fig. 3.1C). Conversely, antigen experienced cells showed a gain of ChARs in the *IFNG* gene locus, consistent with its role as an effector cytokine (Fig. 3.1C). We further validated our epigenetic profiles by asking how these changes in chromatin accessibility related to transcriptional differences between the cell populations. All ChARs were ranked by differential accessibility and binned into 8 groups ranging from most to least accessible in naive T cells relative to HCV tet$^+$ T cells. We then plotted the average mRNA expression of neighboring genes and observed a concordant shift in transcription levels (Fig. 3.1D). Therefore, the vast majority of differential ChARs acted as positive regulators of gene expression.

Principal component analysis of all differential regions separated not just naive T cells from non-naive T cells, but also influenza-specific T cells from HCV-specific responses (Fig. 3.1E). To further characterize features that distinguished the Flu-specific and HCV-specific responses, we performed supervised differential accessibility analysis between Flu tet$^+$ and HCV tet$^+$ CD8$^+$ T cells. 20,043 regions had higher accessibility in HCV tet$^+$ relative to Flu tet$^+$ cells (FDR < 0.05, DESeq2), suggesting that the HCV-specific population had a markedly different chromatin accessibility landscape (Fig. 3.1F). Differentially-accessible ChARs were found near key genes such as Eomes and NFAT1, suggesting that observed changes might play a functional role.

We then looked for evidence that these large-scale epigenetic changes were relevant in disease processes. We reasoned that if differential ChARs represented important regulatory units, natural human variation within these areas might be correlated with varying disease outcomes. Thus, we compared the enrichment of single nucleotide polymorphisms (SNPs) derived from

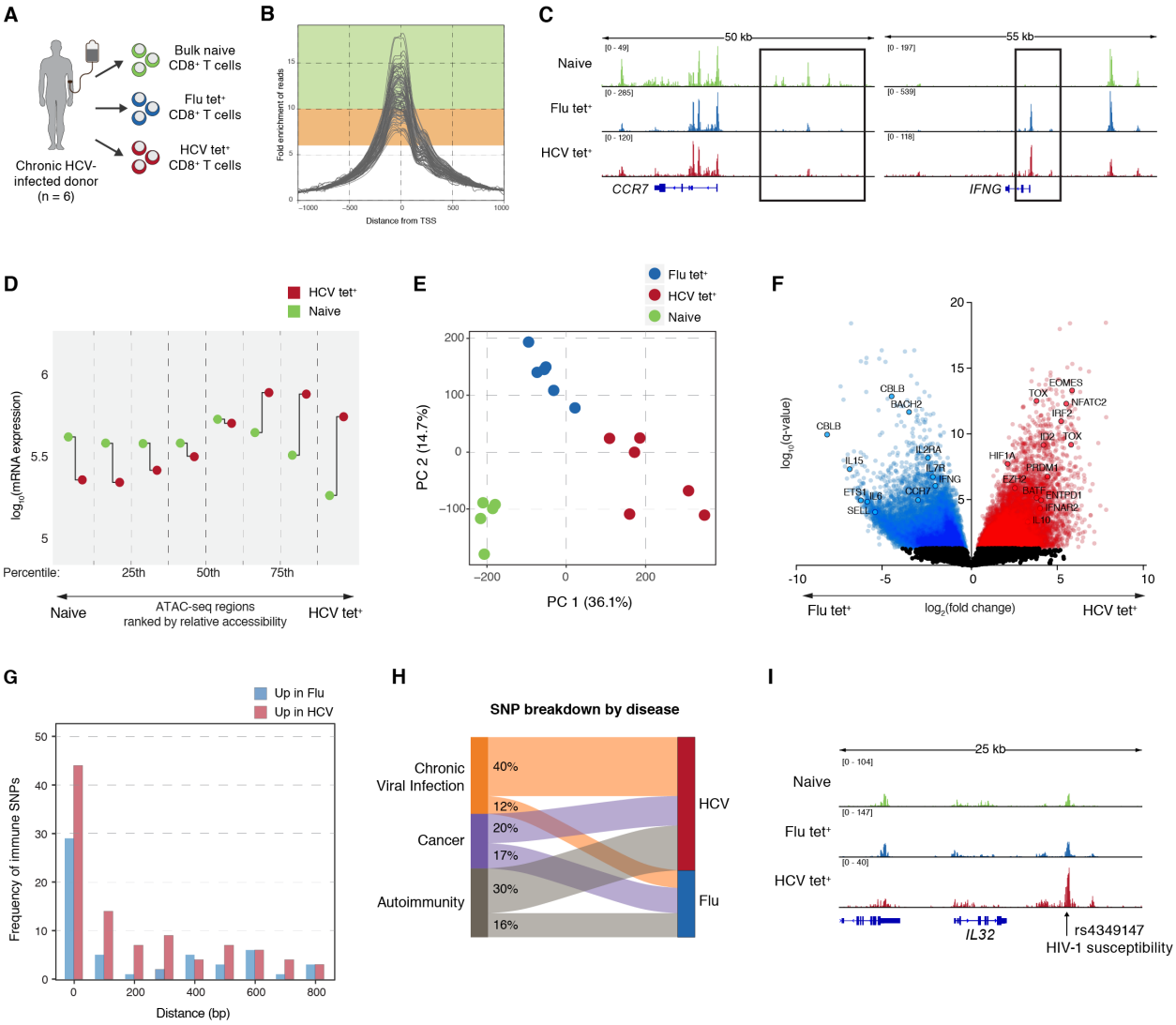


Figure 3.1. Distinct epigenetic changes underlie CD8⁺ T cell responses to chronic HCV infection. **(A)** Schematic diagram of the experiment. **(B)** TSS enrichment of all samples. **(C)** Representative ATAC-seq tracks at the *CCR7* and *IFNG* gene loci. **(D)** Median mRNA expression of genes neighboring chromatin accessibility regions, which were partitioned into 8 bins based on relative accessibility in naïve vs. HCV tet⁺ CD8⁺ T cells. Gene expression from naïve T cells is denoted in green, and that from HCV tet⁺ cells in red. **(E)** Principal component analysis of naïve, HCV tet⁺ and Flu tet⁺ CD8⁺ T cell populations across 6 patients. **(F)** Volcano plot highlighting differential transcripts present in Flu tet⁺ CD8⁺ T cells versus HCV tet⁺ CD8⁺ T cells (colored dots, FDR < 0.05). **(G)** Frequency distribution of immune SNP distances to the closest Flu-specific (blue) or HCV-specific(red) ChAR. SNPs lying within ChARs are denoted by a distance value of 0. **(H)** Classification of SNPs falling within HCV-specific (red) and Flu-specific (blue) ChARs. SNPs were subcategorized into those associated with chronic viral infection, cancer or autoimmune disease. (**I)** Representative ATAC-seq tracks at the *IL32* gene locus, showing the location of a SNP associated with HIV-1 susceptibility.

genome-wide association studies (GWAS) between Flu tet$^+$ and HCV tet$^+$ specific ChARs. ChARs unique to HCV tet$^+$ cells vs. those unique to Flu tet$^+$ cells had a stronger enrichment of SNPs derived from immune-related studies relative to all GWAS studies (2.1-fold vs. 1.7 fold). Indeed, this was true not just for overlapping SNPs but also SNPs located within 400 bps of HCV-specific ChARs (Fig. 3.1G). Enriched SNPs preferentially located within HCV-specific ChARs included those related to immune-mediated processes such as multiple sclerosis and HIV-1 control. Furthermore, when those SNPs were subcategorized by etiology, those related to chronic viral infections were specifically overrepresented in HCV tet$^+$ specific ChARs vs. Flu tet$^+$ specific ones (40% vs. 12%) (Fig. 3.1H). For example, a GWAS SNP for HIV-1 susceptibility was found within an HCV tet$^+$ specific region near the *IL32* gene, encoding a pro-inflammatory cytokine (Fig. 3.1I). In contrast, SNPs relating to autoimmune diseases or cancer were more evenly distributed (20% and 30% vs. 17% and 16% in HCV and Flu, respectively) (Fig. 3.1H). Overall, these data suggest that the CD8$^+$ T cell response to HCV involves large-scale epigenetic changes which are associated with functional significance.

Epigenetic signature of T cell exhaustion is conserved across chronic viral infections

Our previous work has shown that the development of T cell exhaustion in chronic viral infections such as LCMV induces characteristic epigenetic changes[145]. We reasoned that the changes that observed in HCV tet+ cells could be exhaustion-related, or could be driven by the specific immunobiology of the Hepatitis C virus. We therefore asked whether observed changes in chromatin accessibility were recovered in another paradigm of chronic viral infection caused by human immunodeficiency virus (HIV). Comparison of ATAC-seq profiles isolated from chronically infected HIV donors identified 20,625 and 21,740 ChARs that were more accessible in naive and HIV tet$^+$ cells, respectively (Fig. 3.2A). As expected, naive-specific ChARs in HIV had higher chromatin accessibility in naive T cells from HCV infection compared to other cells (Fig. 3.2B).

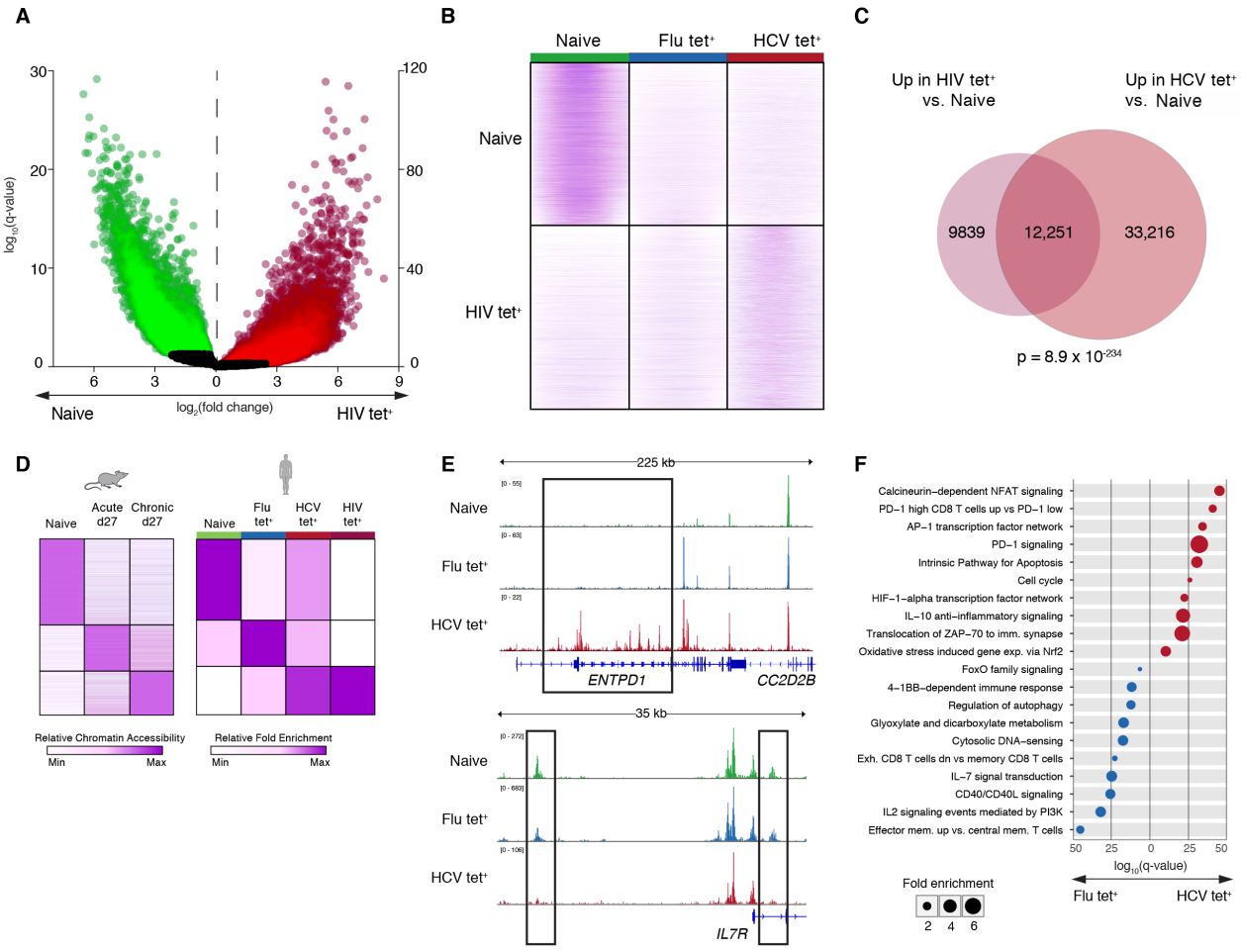


Figure 3.2. Epigenetic signature of T cell exhaustion is conserved across chronic viral infections. **(A)** Volcano plot highlighting differential transcripts present in HIV tet+ CD8+ T cells versus naive CD8+ T cells from HIV patients (colored dots, FDR < 0.05). **(B)** Chromatin accessibility at naïve-specific and HIV-specific ChARs within the indicated conditions from the HCV cohort. **(C)** Venn diagram of overlap between ChARs with increased in accessibility in HIV and HCV tet+ T cells relative to naïve T cells. **(D)** Heatmap of peak intensity within modules of ChARs (rows) from mouse naïve CD8+ T cells, and CD8+ T cells responding to acute and chronic LCMV (left). Fold enrichment of regions orthologous to mouse naïve, memory and exhaustion enhancers in human samples indicated (right). **(E)** Representative ATAC-seq tracks at the *ENTPD1* and *IL7R* gene loci. **(F)** Gene ontology and gene set enrichment (rows) in Flu-specific (blue) or HCV-specific (red) ChARs. FDR values (hypergeometric test) presented as 1–log10.

In contrast, HIV-specific ChARs showed greater chromatin accessibility in HCV tet+ cells compared to naive and Flu tet+ cells (Fig. 3.2B). Indeed, 12,251 ChARs showed greater accessibility in both HIV and HCV tet+ CD8+ T cells relative to their naïve T cell counterparts,

representing marked similarity ($p = 8.9 \times 10^{-234}$; hypergeometric test) (Fig. 3.2C). Thus, similar epigenetic states can be induced by different chronic viral infections such as HIV and HCV.

We next analyzed how the HCV-specific epigenetic state related to that induced by the gold-standard LCMV mouse model of T cell exhaustion. Flu tet$^+$ cells had higher accessibility in orthologous memory-specific regions defined in LCMV Armstrong. Conversely, ChARs specific to HCV tet$^+$ and HIV tet$^+$ cells strongly enriched for exhaustion-specific regions that were identified in LCMV Clone 13 (Fig. 3.2D). This suggests that epigenetic changes driven by HCV infection are conserved across other human viral infections such as HIV as well as mouse models of T cell exhaustion. These changes included differential ChARs near key exhaustion-specific inhibitory receptor genes such as *ENTPD1* (encoding CD39) (Fig. 3.2E). Furthermore, HCV-specific cells lacked memory-associated ChARs that were recovered near *CD127* (IL-7R) in Flu tet$^+$ populations (Fig. 3.2E). Consistent with this, Flu-specific ChARs enriched for pathways associated with IL-7 signaling and effector memory formation, while HCV-specific ChARs were found near genes from pathways related to the biology of T cell exhaustion such as NFAT signaling and PD-1 upregulation (Fig. 3.2F).

Cure of chronic infection causes antigen-specific partial remodeling of the epigenetic landscape

Recently developed direct-acting antiviral therapies have enabled cure of chronic HCV infection without use of interferon. We asked whether removal of chronic antigen and inflammation could lead to remodeling of the epigenetic state of exhaustion, by profiling antigen-specific CD8$^+$ T cells from the same donors 12 weeks after DAA therapy (Fig. 3.3A). Importantly, we were able to detect multiple HCV tet$^+$ responses within each patient - ones where the virus mutated away from the T cell epitope, thus abrogating recognition early during infection[155] (denoted “HCV esc”), and ones where the T cell response to virus was maintained through the course of chronic infection

(denoted “HCV”). First, we examined inhibitory receptor expression on tetramer$^+$ populations by flow cytometry. The Flu tet$^+$ response remained PD-1 and CD39 low before and after therapy (Fig. 3.3B). In contrast, the HCV tet$^+$ response showed high PD-1 and CD39 expression before therapy that decreased after treatment. Thus, cure of infection can induce changes in inhibitory receptor expression (Fig. 3.3B).

We then examined the degree of epigenetic changes induced by DAA therapy. 22,865 ChARs were differentially accessible between HCV tet$^+$ cells pre and post-therapy (FDR < 0.05; DESeq2) (Fig. 3.3C). Notably, almost no changes (<5 differential ChARs, FDR < 0.05) were detected within naive and Flu tet$^+$ compartment (Fig. 3.3C). This finding can be explained in two ways: either TCR- independent chronic inflammation does not mediate significant epigenetic changes, or those changes are permanent and thus unaffected by cure of infection. We reasoned that comparison to naive and memory populations from healthy donors could pinpoint changes driven by the inflammatory microenvironment in bystander populations. Therefore, we generated chromatin accessibility profiles from bulk naive and effector memory populations from 4 healthy donors and compared them to naive and Flu tet$^+$ populations in HCV. Strikingly, less than 0.05% of all ChARs were differentially accessible between the respective naive populations, and only 4% of all ChARs were altered between Flu tet$^+$ cells and bulk effector memory populations (Fig. 3.3D). These data suggest that the resolution of an inflammatory milieu imprints minimal epigenetic changes in bystander populations.

In addition to a persistent inflammatory microenvironment, chronic TCR stimulation is thought to be the other major contributor to the development of T cell exhaustion. Since observed epigenetic changes could not be attributed solely to the presence of inflammation, given the lack of changes in naïve and Flu tet$^+$ T cells, we hypothesized that chronic TCR stimulation might instead be the major driver. We reasoned that comparison of the HCV tet$^+$ response to the HCV esc response, which experiences little to no TCR stimulation in the presence of chronic infection,

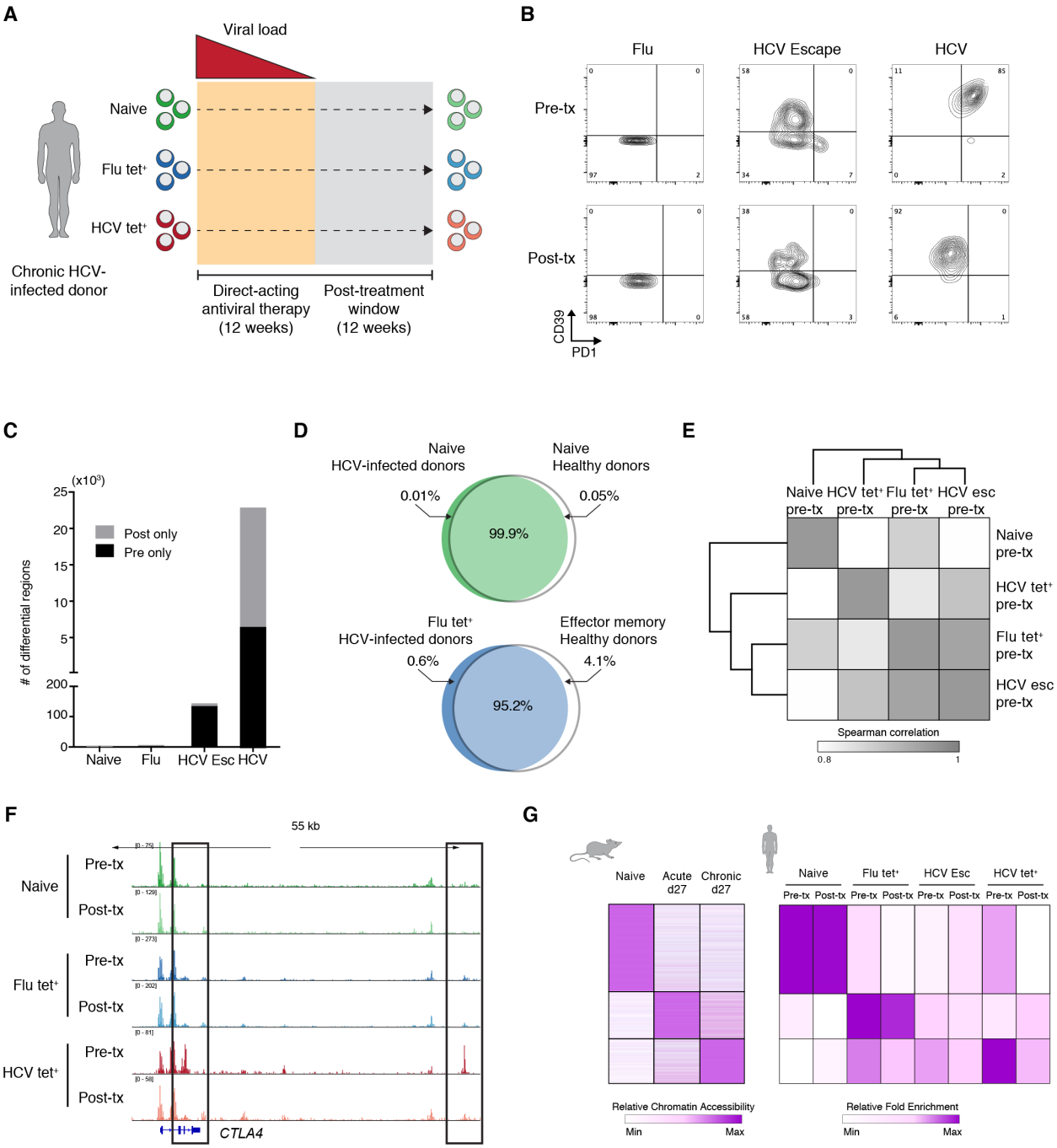


Figure 3.3. Cure of chronic infection causes antigen-specific remodeling of the epigenetic landscape. (A) Schematic diagram of the treatment regimen. **(B)** PD-1 and CD39 staining on tetramer populations before (top) and after (bottom) DAA therapy. **(C)** Quantification of differential ChARs within indicated conditions, before and after DAA therapy. **(D)** Venn diagram of ChAR overlap in naïve T cells (top) and Flu tet⁺ cells (bottom) from HCV-infected donors and healthy donors. **(E)** Clustered similarity matrix between the indicated biological conditions at the pre-treatment timepoint. **(F)** Representative ATAC-seq tracks at the *CTLA4* gene locus. **(G)** Heatmap of peak intensity within modules of ChARs (rows) from mouse naïve CD8⁺ T cells, and CD8⁺ T cells responding to acute and chronic LCMV (left). Fold enrichment of regions orthologous to mouse naïve, memory and exhaustion enhancers in human samples indicated (right).

would allow us to dissect the role of TCR signaling while controlling for the inflammatory milieu. First, we noted that the HCV esc population had lower PD-1 expression than HCV tet$^+$ cells even before initiation of DAA-therapy (7% vs. 87%) (Fig. 3.3A), suggesting that loss of TCR signaling might reverse some aspects of T cell exhaustion. Indeed, hierarchical clustering of samples before DAA-therapy showed that the HCV esc response was epigenetically more similar to the functional Flu tet$^+$ response rather than the exhausted HCV tet$^+$ response (Fig. 3.3E). This was supported by the fact that resolution of viral infection led to only minor differences within the HCV esc response (Fig. 3.3C). Together, these data are consistent with a model where chronic TCR signaling, rather than the inflammatory microenvironment, is largely responsible for maintaining the epigenetic profile of exhaustion.

We next sought to understand the pattern of differences initiated by cure of infection within the HCV tet$^+$ population. HCV tet$^+$ specific ChARs near key exhaustion-associated genes such as CTLA4 were lost post-therapy (Fig. 3.3F). Comparison to the LCMV mouse model revealed that these changes were related to a larger remodeling of exhaustion-specific epigenetic changes within HCV tet$^+$ cells pre and post therapy (Fig. 3.3G). Overall, these data suggest that exhaustion-associated epigenetic changes are largely driven by TCR signaling, some of which can be reversed upon loss of chronic antigen.

HCV-specific CD8$^+$ T cells retain epigenetic scars of exhaustion

Despite changes initiated by DAA therapy, we identified T cell exhaustion-specific regions near key genes such as *BATF* and *ENTPD1* (encoding CD39) that were not reversed (Fig. 3.4A). This is consistent with the fact that DAA cure of infection did not reverse high levels of CD39 in the HCV tet$^+$ population at the protein level (Fig. 3.3B). We then analyzed ChARs genome-wide and found that ChARs specific to HCV tet$^+$ cells pre-treatment could be broadly separated into two classes: those that were retained or “scarred” and those that were “reversed” by DAA-therapy

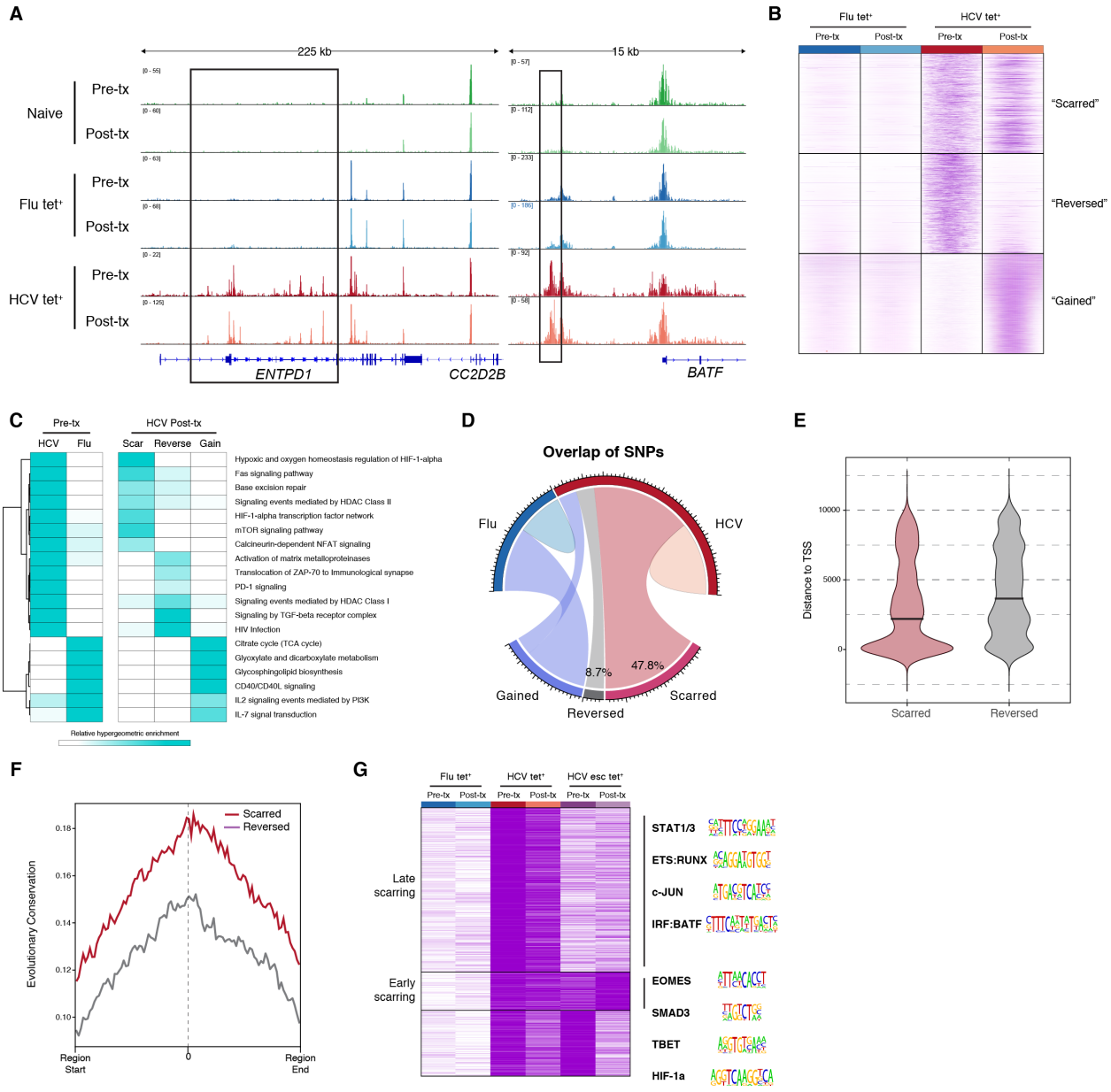


Figure 3.4. HCV-specific CD8⁺ T cells retain epigenetic scars of exhaustion. (A) Representative ATAC-seq tracks at the *ENTPD1* and *BATF* gene loci. **(B)** Chromatin accessibility at "scarred", "reversed" and "gained" ChARs within the indicated conditions from the HCV cohort. **(C)** Heatmap showing pathway enrichment (rows) within HCV-specific and Flu-specific ChARs pre-treatment, and within scarred, reversed and gained ChARs post-treatment (columns). **(D)** Chord diagram showing shared SNPs between HCV-specific and Flu-specific ChARs pre-treatment and scarred, reversed and gained ChARs post-treatment. **(E)** Violin plot of distances to the closest annotated transcriptional start site within the scarred and reversed ChAR set. **(F)** Average evolutionary conservation across the length of all ChARs within the scarred and reversed set. **(G)** Heatmap of chromatin accessibility within scarred ChARs (rows), clustered across the indicated cell states (columns). Sequence logos for transcription factor motifs enriched within the indicated clusters (right).

(Fig. 3.4B). We also studied ChARs that became accessible in HCV tet+ cells only after cure of infection or “gained” regions (Fig. 3.4B). Pathway enrichment suggested that scarred, reversed, and gained ChARs represented distinct modules that regulated functionally distinct programs of genes (Fig. 3.4C). Scarred regions enriched for genes related to hypoxia and HIF-1α signaling while reversed regions enriched for pathways such as translocation of ZAP70 and PD-1 signaling.

We then asked whether scarred vs. reversed ChARs might have different regulatory roles, by assessing several associated features. First, we examined differential genomic localization and found that scarred regions were more proximal to gene promoters (Fig. 3.4D), which may indicate increased regulatory potential. Epigenetic scars of exhaustion also had higher sequence conservation across mammals compared to reversed ChARs (Fig. 3.4E), highlighting their potential importance across species. Consistent with this, scarred regions were 5.5-fold more likely to contain immune related GWAS SNPs (Fig. 3.4F).

We next asked how the establishment of epigenetic scars might be affected by early loss of TCR signaling in the context of chronic viral infection. Comparison of scars between the HCV tet+ and HCV esc tet+ responses revealed distinct regulatory modules (Fig. 3.4G). A portion of scars which were shared between HCV tet+ and HCV esc cells were presumably acquired early in the course of infection. Accordingly, these ChARs were enriched for motifs of canonical transcription factors in exhaustion such as T-bet and Eomes. In contrast, ChARs that were specific to HCV tet+ cells and presumably related to the chronicity of viral exposure were enriched for motifs related to STATs and AP-1 family members.

The retention of epigenetic scars may help explain recent findings about the functionality of HCV tet+ cells after DAA therapy. It was observed that a subset of exhausted T cells could be maintained long-term after cure of infection, and showed increased proliferation upon restimulation[154]. However, HCV-specific cells isolated post-cure remained dysfunctional and produced less IFN-γ and TNF relative to functional influenza-specific memory cells as well as

HCV-specific responses in spontaneous resolvers[154, 156]. Our data suggests that this continued dysfunction of CD8+ T cells post-therapy might be mediated by inflexibility at the epigenetic level.

Scars represent critical epigenetic hallmarks of exhaustion

The preceding data suggested that the process of scarring was not stochastic but instead associated with distinct biological pathways. Therefore, we sought to understand the regulatory impact of this scarring at a deeper level. Characterization of super-enhancers (SEs) and their associated genes has become a leading strategy to define important regulatory nodes in many cell types[157, 158, 159, 160, 161]. Unfortunately, assaying SE activity within HCV-specific exhausted T cells using the gold-standard method of H3K27ac ChIP-seq has been limited by low cell numbers. Therefore, we developed an alternative strategy that would allow inference of super-enhancer activity solely from chromatin accessibility profiles generated using ATAC-seq. As expected, we saw concordant enrichment of H3K27ac signal and presence of open chromatin at the *ETS1* SE locus in CD4+ T cells (Fig. 3.5A)[159]. Indeed, across 8 immune and non-immune cell types, chromatin accessibility data could largely predict H3K27ac-based SE identities, with AUC values ranging from 0.76 to 0.86 (Fig. 3.5B). SE-associated genes as identified via ATAC-seq were transcribed at higher levels than non-SE-associated genes in each respective cell type (Fig. 3.5C), further supporting our ability to accurately recapitulate the results of previous algorithms.

Having validated the method for identifying super-enhancers, we then applied it to the set of epigenetic scars in HCV tet+ cells. The gene encoding the transcription factor TOX was ranked as the top SE-associated gene within exhausted scars (Fig. 3.5D-E). Intriguingly, TOX has been previously implicated in mouse models of T cell exhaustion[64], but its role and mechanism of action remains unknown. Other SE-associated transcriptional regulators included HIF1A, ID2, and NFAT (Fig. 3.5D), all of which have been previously implicated in the context of T cell exhaustion. These data suggest that failure to reverse CD8+ T cell exhaustion after curative therapy may be mediated

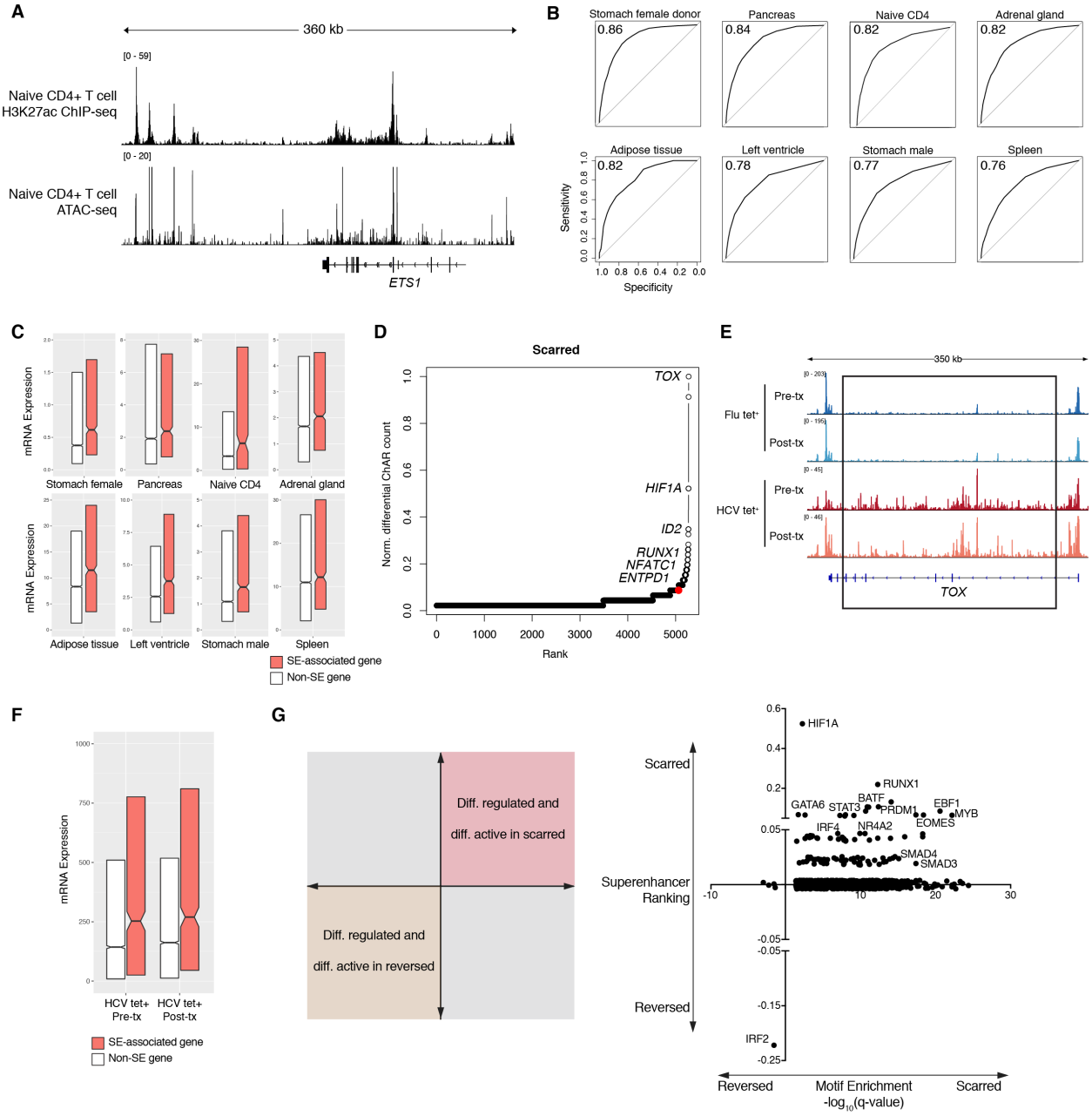


Figure 3.5. Scarred regions identify critical regulators of exhaustion. (A) H3K27ac ChIP-seq signal (top) and ATAC-seq signal (bottom) at the *ETS1* gene locus. **(B)** ROC plots of varying cutoff for ATAC-based ranking of super-enhancer to predict bona fide super-enhancers defined using matched tissue-specific H3K27ac ChIP-seq. **(C)** Boxplots of tissue-specific mRNA expression, partitioned by genes with or without an associated super-enhancer. **(D)** Super-enhancer elbow plots based on ChARs within the scarred set of regions. Each dot represents a different gene. **(E)** Representative ATAC-seq tracks at the *TOX* gene locus. **(F)** Boxplots of mRNA expression from HCV tet+ cells before and after treatment, partitioned by genes with or without an associated super-enhancer. **(G)** Plot of transcription factors based on their super-enhancer ranking (y-axis) and differential motif enrichment between scarred and reversed ChARs (x-axis).

by the activity of distinct transcriptional regulators within epigenetic scars.

As expected, SE-associated genes had higher mRNA expression than non-SE genes (Fig. 3.5F). To further validate the critical regulatory role of SE-associated TFs, we performed differential motif enrichment between ChARs that were scarred and those that were reversed. Strikingly, a significant fraction of SE-associated TFs had motifs that were overrepresented in scarred vs. reversed regions (Fig. 3.5G). This included not just HIF-1α but also other exhaustion-associated TFs such as EOMES, RUNX1, and BATF. Importantly, these transcription factors themselves are differentially regulated by epigenetic scars. Therefore, the overrepresentation of their downstream binding sites in those same scars points to the existence of a greater positive feedback loop that may cement the epigenetic state of T cell exhaustion.

Epigenetic scars of exhaustion are retained long-term after cure of infection

Our results suggested that cure of infection through DAA therapy leaves epigenetic scars that may be important for regulating T cell function. However, the possibility remained that these regions simply represent those that are slower to be reverted compared to others. To account for this, we profiled 4 of the 6 patients 60-80 weeks after cessation of therapy (Fig. 3.6A). The chromatin accessibility profiles of HCV tet$^+$ cells at the late time-point clustered with those generated immediately post-therapy as opposed to with HCV tet$^+$ cells pre-treatment or Flu tet$^+$ memory T cells (Fig. 3.6B). We then compared reversed ChARs at the late time-point to the post-therapy measurement and found that about half were unchanged while the rest continued to decrease in accessibility over time (Fig. 3.6C). In contrast, 79% of scarred ChARs remained unchanged and only 17% diminished in accessibility upon long-term follow-up (Fig. 3.6C). Regions that remained accessible at this time-point included the *TOX* super-enhancer (Fig. 3.6D). Overall, these data suggest that the epigenetic scars of exhaustion are retained long-term after cure of infection.

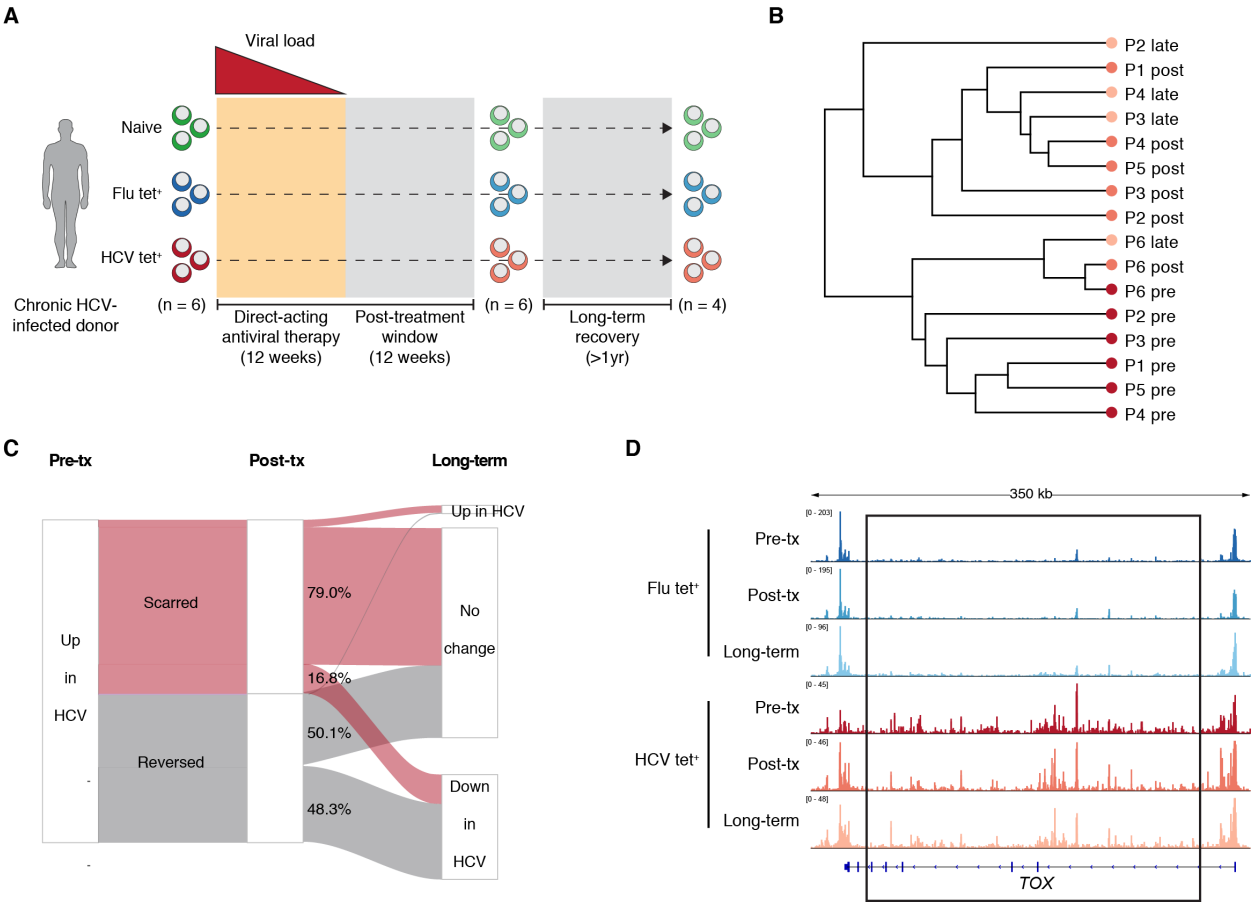


Figure 3.6. Epigenetic scars of exhaustion are retained long-term after cure of infection. **(A)** Schematic diagram of experimental time-points before and after DAA therapy. **(B)** Clustering of individual HCV tet+ profiles from patients across 3 time-points (pre-treatment, post-treatment and long-term). **(C)** Longitudinal trajectory of scarred and reversed ChARs at each time point. **(D)** Representative ATAC-seq tracks at the *TOX* gene locus.

Discussion

T cell responses to chronic Hepatitis C infection are characterized by a range of functional defects[21, 22, 37, 38, 147], but the epigenetic mechanisms that specify this state and the potential for reprogramming T cell exhaustion after curative therapy remains an open question. Here we show that the landscape of regulatory regions in HCV-specific exhausted CD8+ T cells is markedly different from memory responses, that it is established in a TCR-dependent fashion, and that it becomes fixed despite cure of infection. HCV-specific epigenetic changes are conserved across other chronic viral infection settings where T cell exhaustion is observed, including in HIV and the

LCMV mouse model. Cure of viremia through direct-acting antiviral therapy leads to partial remodeling of the epigenetic state, however, a significant subset of exhaustion associated changes are irreversible. Inference of super-enhancers within epigenetic scars prioritizes key transcriptional regulators of exhaustion. Finally, long-term follow up of patients suggests that epigenetic scars are maintained more than 1 year after cessation of therapy. These findings have three important implications for understanding the regulation of exhausted T cells at the epigenetic level.

First, T cell exhaustion represents a distinct epigenetic program that is conserved across chronic viral infection paradigms, including HIV and the LCMV mouse model. Thus, the exhausted state represents a fundamental adaptation in response to chronic stimulation. While this has been previously established in mouse models of chronic viral infection[145], this study is the first to provide evidence for this in human disease at the level of epigenomics. The importance of this epigenetic program is highlighted by the differential enrichment for disease-associated genetic variants within exhaustion-specific regulatory regions.

Second, we dissect the relative contribution of chronic TCR signaling vs. the inflammatory milieu in driving epigenetic changes. Previous studies in both mice and humans have highlighted the potential role of chronic type I IFN signaling as well as immunosuppressive cytokines such as IL-10 and TGF-b in the development of T cell exhaustion[162, 163, 164, 165, 166]. Nevertheless, separating direct cell-intrinsic effects in $CD8^+$ T cells from indirect effects mediated by other populations remains a challenge in these studies. We help resolve this by studying antigen-specific responses to acute and chronic viral infections within the same patient, thus controlling for microenvironment effects. We show that the epigenetic profile of influenza-specific memory T cells is largely indistinguishable from that of effector memory cells from healthy donors. These data suggest that chronic TCR signaling, rather than the inflammatory microenvironment, is largely responsible for inducing epigenetic changes associated with T cell exhaustion. This is supported by the partial

epigenetic remodeling observed within HCV-specific responses where viral epitope escape has abrogated specific TCR recognition despite continued exposure to the inflammatory milieu.

Third, despite partial remodeling after cure of infection, the epigenetic state of T cell exhaustion cannot be fully reversed with DAA treatment. Indeed, epigenetic scars are preserved for over a year after curative therapy. Scarred regions are more promoter-proximal and are enriched for disease-associated SNPs relative to changes reversed by DAA therapy, suggesting they may have greater functional importance. Epigenetic scars include super-enhancer elements near critical exhaustion-associated transcription factors such as TOX and HIF-1α. These findings may explain the lack of effector functionality exhibited by HCV tet$^+$ T cells despite cure of infection. Furthermore, the epigenetic inflexibility of exhausted T cells observed herein is consistent with previous studies showing that checkpoint blockade immunotherapy does not fundamentally reverse exhaustion-associated epigenetic changes[150]. Interestingly, the degree of scarring may be driven by the timing and magnitude of TCR stimulation, given the intermediate phenotype observed within HCV tet$^+$ cells responding to viral epitopes that had escaped.

In this study, we show that the distinct epigenetic landscape of T cell exhaustion cannot be reversed by cure of chronic viral infection and is maintained long-term. Given the failure of immune checkpoint blockade as well as curative therapy in reversing exhaustion-associated epigenetic changes, ameliorating T cell exhaustion may require targeted approaches to increase the epigenetic plasticity of exhausted T cells. Ultimately, early intervention during the development of T cell exhaustion may be the most viable strategy to prevent the establishment of an irreversible epigenetic program that mediates dysfunction.

Materials and methods

HCV cohort subjects and samples

For the HCV cohort, all patients were enrolled in an open label Phase 3 clinical trial of paritaprevir/ritonavir, ombitasvir, dasabuvir and ribavirin for genotype 1a hepatitis C virus infection designed to evaluate the effect of successful antiviral therapy on innate and adaptive immune responses (NCT02476617). The trial was approved by the Massachusetts General Hospital Institutional Review Board.

Trial subjects were confirmed to be chronically infected with HCV genotype (GT) 1a infection based on viral load and were screened for specific HLA alleles. To reduce the impact of sources of variability or bias, subjects that had tested positive for co-infections such as HIV or HBV, or resolved a previous infection on their own were excluded.

Trial participants were treated for 12 weeks with a combination of paritaprevir/ritonavir, ombitasvir, dasabuvir and ribavirin. Only patients with hepatitis C virus RNA levels less than the lower limit of quantification (<LLOQ) 12 weeks after the last dose of study drug were included for further analysis. All included patients were followed for at least 1 year post treatment. Informed consent was given by all subjects under protocols approved by the Massachusetts General Hospital IRB.

Blood samples via leukapheresis were collected from 6 patients at 2-3 time points representing pre-treatment, 12 weeks post-treatment, and long-term followup (60-80 weeks post treatment). Peripheral blood mononuclear cells (PBMCs) were extracted by Ficoll-Paque (GE Healthcare Life Sciences) density gradient centrifugation and frozen down for further processing. A small aliquot of sample was reserved and analyzed by flow cytometry to identify virus-specific $CD8^+$ T cell responses using appropriate HLA class I multimers.

Cell isolation and cell sorting

PBMCs from HCV patients were thawed rapidly in warm T cell culture medium (RPMI supplemented with 10% FBS), and counted. $CD8^+$ T cells were enriched using MACS CD8 negative selection kit (Miltenyi). After enrichment, cells were stained for 15 minutes at 4°C using fluorochrome-conjugated multimers for HCV A*02:01 NS3 1073 CINGVCWTV (Immudex), influenza A*02:01 MP GILGFVFTL (Immudex), and other appropriate HCV multimers representing escaped viral epitopes (ProImmune). When required, unlabeled multimers were conjugated to APC by staining with Pro5 Fluorotags (ProImmune) per manufacturer's protocol.

Multimer-positive cells were enriched using MACS anti-PE, anti-APC and anti-Fitc positive selection kits (Miltenyi). Cells were then stained for other following cell surface markers from Biolegend and sorted on a FACSAria cell sorter (BD Biosciences): anti–CD45RA (HI100), anti-CCR7 (G043H7), anti-CD3 (OKT3), anti-CD39 (A1), anti-PD-1 (EH12.2H7), anti-CD8a (SK1), anti-CD95 (DX2) and Near-IR Live/Dead (Invitrogen). Cell sorting strategy has been summarized in Fig. S1. A maximum of 80,000 cells were sorted into PBS supplemented with 10% FBS for subsequent ATAC-seq library generation.

For the HIV cohort, the following fluorochrome-conjugated multimers from ImmunAware were used: HIV A*02:01 RLRPGGKKK, HIV B*07:02 GPGHKARVL, HIV B*57:01 KAFSPEVIPMF, HIV B*57:01 TSTLQEQIAW, HIV B*53:01 YPLTFGWCF. Cell isolation and processing was performed as previously described.

ATAC-seq library generation

ATAC-seq libraries were generated as previously described. Briefly, cell counts from the sorter were adjusted by assuming 65-70% cell loss. Sorted cells were pelleted for 10 minutes at 400 r.c.f and incubated in 5-50ul of Tn5 reaction mix (2x TD buffer, Tn5 enzyme, 2% digitonin in nuclease-free water) for 30 mins at 37°C. DNA was purified using a QIAgen MinElute Reaction

Cleanup kit, and polymerase chain reaction (PCR) was used to add dual-indexed barcodes (Illumina). Post-PCR cleanup was done using Agencourt AMPure XP beads (Beckman Coulter/Agencourt) and ATAC library quality was verified using Tapestation analysis. Patient samples across multiple time-points were pooled for sequencing whenever possible to minimize batch effects. Samples were sequenced on an Illumina NextSeq500 sequencer using paired-end 37bp reads.

Data processing and quality control

Sequencing reads were demultiplexed into fastq files using bcl2fastq (v2.19.1.403). Quality trimming and primer removal within raw fastq files were done with Trimmomatic (v0.36) using the following parameters: LEADING:15 TRAILING:15 SLIDINGWINDOW:4:15 MINLEN:36. Sequencing read QC was run before and after quality trimming using the FastQC software (Babraham Bioinformatics). Trimmed reads were aligned to hg19 with Bowtie2 (v2.2.9) using a maximum insert size of 1000. Aligned bams were sorted, duplicates marked, and reads mapping to the hg19 genome "blacklist" regions removed using PICARD. Aligned reads were shifted +4bp or -5bp as appropriate.

All samples were assessed for library quality according to ENCODE guidelines (https://www.encodeproject.org/atac-seq/). Briefly, the fraction of reads in called peak regions (FRiP score) as well as TSS enrichment was calculated as previously described. Additionally, concordance of each biological condition was assessed by the average Pearson correlation across all pairwise combinations.

Peak universe generation and differential accessibility analysis

For consensus peak generation, biological replicate samples (n = 6 patients) were downsampled to the lowest read count among the replicates separately for each of 12 biological conditions

(Naive, Flu tet$^+$, HCV tet$^+$, HCV esc tet$^+$ x 3 time-points). Downsampled bams for each biological replicate were then merged using Samtools v1.3.1. Peak-calling was done for each biological condition using MACS (v2.1.1) on merged bam files with a *q*-value threshold of 0.001. Consensus peaks from all biological conditions were then merged to create a single HCV peak universe of 128,355 regions. Cut sites were extracted from each biological replicate and the number of cuts within each peak region was quantified (BEDtools v2.26.0) to generate a raw counts matrix.

DESeq2 (v1.18.1) was used to normalize the counts matrix and perform differential accessibility analysis between all relevant comparisons. For a given comparison, an FDR cutoff of 0.05 was used to determine differential ChARs.

Comparative analysis of chromatin accessibility from LCMV mouse model

Orthologous mouse ChARs (mm10) were mapped to the human genome (hg19) as described[33]. Since the mapping algorithm requires input regions in mm10, the UCSC liftover tool was applied to ChARs to transfer them onto mm10 from mm9. All mouse peaks partitioned into 3 categories based on previously published clustering: peaks found in the Naïve cluster a (mouse Naïve), peaks found in the Acute d27 cluster c (mouse Memory), and peaks found in the Chronic d27 cluster e (mouse Exhausted). Then, for each set of consensus peaks in the HCV dataset, the hypergeometric fold enrichment was calculated separately for the 3 categories of mouse orthologous peaks (Naïve, Memory, Exhaustion).

Enhancer classification

For identification of “scarred”, “reversed” and “gained” regions, first we identified all ChARs that were significantly more accessible in HCV tet$^+$ cells compared to Flu tet$^+$ cells pre-treatment (n = 20,043; FDR < 0.05). Of these, all ChARs that became significantly less accessible in HCV tet$^+$ cells post-treatment compared to HCV tet$^+$ cells pre-treatment were denoted as “reversed” (n =

4399; FDR < 0.05). In contrast, all ChARs that were unchanged in HCV tet+ cells before and after treatment (FDR > 0.05 and log2FC < 1.5) were termed “scarred” (n = 5132). Finally, ChARs that became significantly more accessible in HCV tet+ cells post-treatment compared to HCV tet+ cells pre-treatment were denoted as “gained” (n = 16,416; FDR < 0.05).

Pathway and motif enrichment

Gene to peak associations were determined using the GREAT software package (v3.0.0, http://bejerano.stanford.edu/great/public/html/) with default settings. GREAT was also used to determine gene set enrichment, with default settings and the binomial test to measure significance. Motif enrichment analysis was performed using HOMER (v3.0) with default settings.

SNP overlap analysis

GWAS SNPs in the NHGRI catalog (https://www.ebi.ac.uk/gwas/) annotated as “immune system disease” was defined as being immune-related. Hypergeometric tests were performed to quantify overlap of enhancers with all GWAS SNPS, and immune-related SNPS. Immune-related SNPs were further subcategorized as relating to autoimmunity, cancer or chronic viral infections.

Gene-centric inference of super-enhancer activity

Super-enhancers are generally considered to be composed of many smaller regulatory units, or constituent enhancers[167, 168]. Based on this principle, SEs were identified by counting individual putative enhancers per gene within each sample. Specifically, the online tool GREAT (see above) was used to assign each ChAR to nearby gene(s). Afterwards, the number of regions was calculated per gene and the resultant list was ranked from highest to lowest. The list of ranked genes could then be plotted against the total number of regions to generate a characteristic elbow plot. As observed in the original definition of SEs[167], this gene-centric approach also revealed a

clear point in the distribution where the number of enhancers per gene increased rapidly. The x- and y-axes were then scaled from 0-1 and the inflection point in the curve was determined by using the findElbow tool within the ChemoSpecMarkeR package (Bryan A. Hanson). All genes with a higher number of regions than the inflection point were defined as SE-associated. This method can be used to call SE-associated genes from any set of ChARs, ranging from the whole universe to subsets of regions such as "scarred" or "reversed".

The analysis directly identifies a set of genes associated with SE-like loci rather than identifying chromatin regions themselves, allowing for less ambiguity in assigning SEs to genes. However, the constituent enhancers of a putative super-enhancer can still be identified by inspecting the regions that are assigned to a SE-associated gene. The performance of this method was tested by its ability to predict SE-associated genes as defined by the H3K27ac standard. For consistency, H3K27ac-based SEs were assigned to genes using the GREAT tool.

Data visualization

ATAC-seq tracks were visualized using Integrative Genomics Viewer (v2.3.77). GENE-E (v3.0.215) was used for heatmap visualization and similarity matrix calculations (Pearson). Principal component analysis (PCA) was done using R (v3.3.1) in RStudio (v1.1.453). Volcano plots were generated using Graphpad Prism 7.

Chapter 4. Functionally specialized subsets of exhausted CD8$^+$ T cells differentially mediate tumor control and respond to checkpoint blockade

Parts of this chapter are currently accepted for publication as:

Brian C. Miller*, **Debattama R. Sen***, Rose Al Abosy, Kevin Bi, Yamini V. Virkud, Martin W. LaFleur, Kathleen B. Yates, Ana Lako, Kristen Felt, Girish S. Naik, Michael Manos, Evisa Gjini, Juhi R. Kuchroo, Jeffrey J. Ishizuka, Jenna L. Collier, Gabriel K. Griffin, Seth Maleri, Dawn E. Comstock, Sarah A. Weiss, Flavian D. Brown, Arpit Panda, Margaret D. Zimmer, Robert T. Manguso, F. Stephen Hodi, Scott J. Rodig, Arlene H. Sharpe, W. Nicholas Haining. Subsets of exhausted CD8+ T cells differentially mediate tumor control and respond to checkpoint blockade. *Nature Immunology*. 2019; 20:326–336.

*These authors contributed equally

Introduction

The functional impairment of T cell-mediated immunity within the tumor microenvironment (TME) is a defining feature of many cancers[169]. Checkpoint blockade therapy seeks to reinvigorate T cell responses by targeting inhibitory receptors such as PD-1, which are upregulated by dysfunctional tumor-infiltrating lymphocytes (TILs)[50]. However, the fundamental mechanisms underlying T cell dysfunction in the TME remain poorly understood, as are the mechanisms by which checkpoint blockade overcomes this dysfunction.

Insight into T cell dysfunction has come from studying the T cell response to chronic viral infections such as lymphocytic choriomeningitis virus (LCMV) that induce a specific state termed exhaustion[1, 116, 117, 119, 170]. Transcriptional and epigenetic studies have demonstrated that exhaustion is not simply a transient inhibition of otherwise functional cells, but instead represents a distinct and stable state of T cell differentiation[62, 64, 145, 171].

Exhausted $CD8^+$ T cells responding to chronic LCMV infection are phenotypically and functionally heterogeneous[172, 173, 174, 175, 176, 177]. “Progenitor”[172] or “stem-like”[174] exhausted $CD8^+$ T cells can be defined by intermediate expression of PD-1 and expression of CXCR5. In contrast,

"terminally exhausted" cells co-express high levels of PD-1, Tim-3, and other co-inhibitory receptors[64, 172, 175]. The two subpopulations have important functional differences, and only progenitor exhausted cells proliferate upon anti-PD-1 therapy in chronic viral infection[173, 174, 175, 178].

Initial studies of dysfunctional CD8$^+$ T cells in tumors suggested they share features of T cell exhaustion[50, 55, 148, 169]. However, more recent studies have suggested that TIL dysfunction is distinct from T cell exhaustion[56, 57, 179]. Thus, it remains unknown whether the cell state of dysfunctional CD8$^+$ TILs recapitulates the canonical state of T cell exhaustion. Moreover, it is not clear whether PD-1 checkpoint blockade affects all heterogeneous CD8$^+$ TIL populations[57, 149] equivalently to mediate tumor control or whether specific subsets preferentially mediate response.

Here we show that CD8$^+$ TILs acquire an analogous state of exhaustion to that elicited by chronic viral infection. Within exhausted CD8$^+$ TILs, a small population of progenitor exhausted cells can differentiate into the majority population of highly cytotoxic terminally exhausted TILs, mediate long-term tumor control, and respond to anti-PD-1 therapy. Our data suggest that the efficacy of PD-1 checkpoint blockade is in part due to its selective activity on a functionally distinct subpopulation of exhausted CD8$^+$ TILs.

Results

Chronic viral infection and tumors elicit analogous subsets of exhausted CD8$^+$ T cells

To define the basis for T cell dysfunction in TILs, we compared single cell expression profiles of exhausted CD8$^+$ T cells in chronic viral infection to CD8$^+$ T cells in tumors. We analyzed single-cell RNA-seq (scRNA-seq) profiles of 9,194 GP33 tetramer$^+$ CD8$^+$ T cells in mice infected with LCMV Clone 13 (Cl13) on day 28 post-infection (p.i.) (Fig. 4.1A).

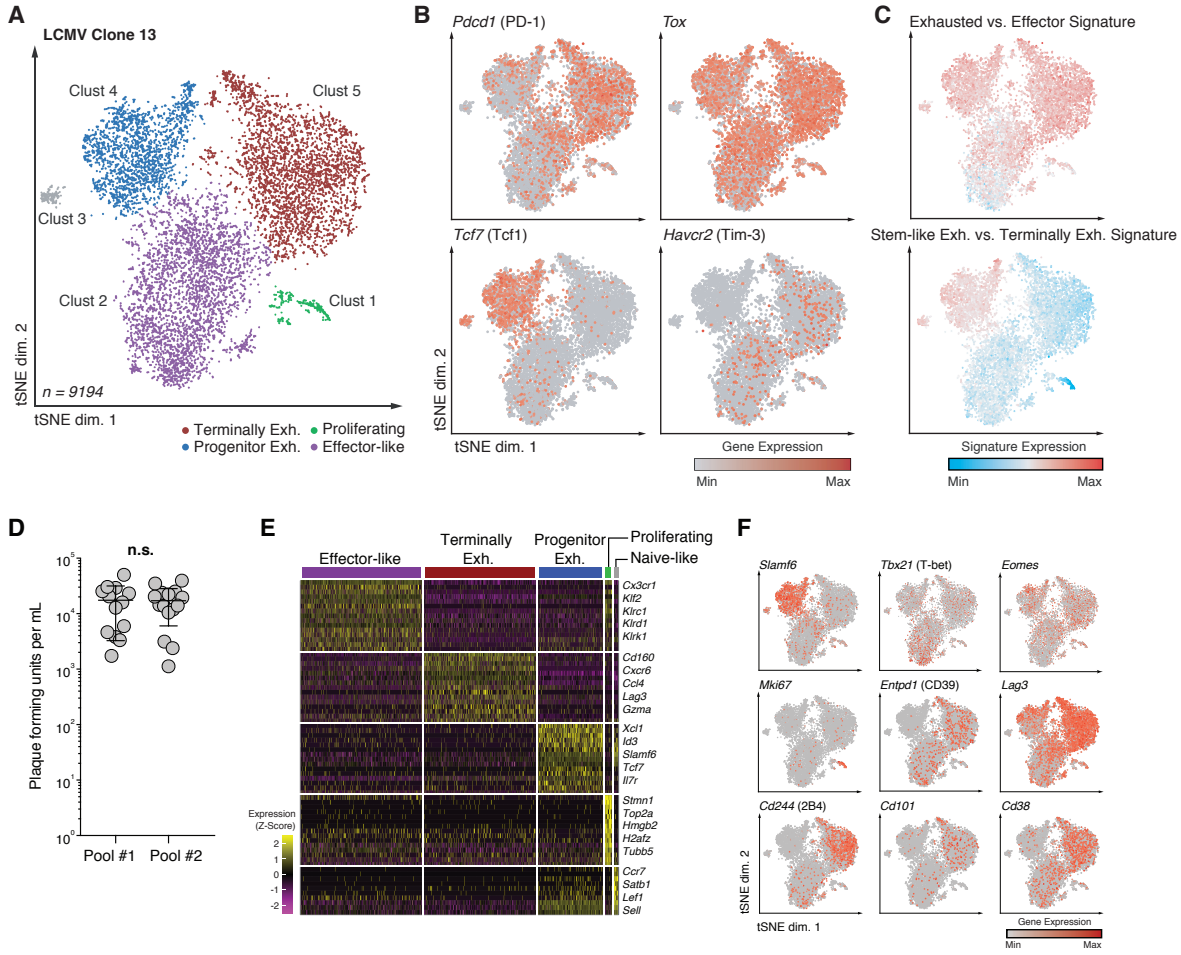


Figure 4.1. Single-cell RNA-seq identifies subsets of exhausted CD8⁺ T cells in chronic viral infection. (A) tSNE projection of single-cell RNA-seq profiles from 9,194 GP33 tetramer⁺ CD8⁺ T cells responding to chronic LCMV (d28 p.i.) colored by cluster. **(B)** Expression of indicated genes in individual cells from (A). (**C**) Enrichment of a signature of genes upregulated in exhausted vs. effector CD8⁺ T cells (GSE9650) or stem-like exhausted vs. terminally exhausted CD8⁺ T cells (GSE84105), $p < 1x10^{-6}$ by two-sided Kolmogorov-Smirnov (KS) test for each comparison. **(D)** Serum viral titers of LCMV Clone 13 infected mice pooled to generate single-cell RNA-seq data, n = 13 (pool 1) or 15 (pool 2) mice. **(E)** Top differentially expressed genes in each cluster, with key transcripts highlighted on the right. Groups colored according to clustering (Fig. 4.1a). **(F)** Expression of indicated genes overlaid on LCMV CD8⁺ T cell tSNE projection.

Unsupervised clustering analysis identified four major populations of cells; each of which expressed genes characteristic of exhausted cells including PD-1 and Tox, an exhaustion-specific transcription factor (TF) (Fig. 4.1B)[64]. The majority of T cells enriched for a signature of T cell exhaustion (Fig. 4.1C)[62], consistent with high viral titers in Clone 13 infection (Fig. 4.1D).

Cluster 1 expressed markers of actively dividing cells (*Mki67*, *Top2a*), while cluster 2 was distinguished by transcripts associated with effector CD8$^+$ T cells (*Cx3cr1*, *Klrc1*, and *Klrd1*) (Fig. 4.1E and F). A small cluster (cluster 3, 1.3% of total cells) expressed markers of naive cells (*Ccr7, Lef1, Sell*), likely representing contaminating naive T cells. Several transcripts upregulated in cluster 4 (*Tcf7*, *Id3*) were associated with a stem-like or progenitor population of exhausted CD8$^+$ T cells in LCMV (Fig. 4.1B and Fig. 4.1F)[172, 173, 174, 175, 176, 177]. Consistent with this, cluster 4 was significantly enriched for a signature of stem-like exhausted vs. terminally exhausted CD8$^+$ T cells (Fig. 4.1C)[174]. Conversely, Tim-3$^+$ T cells, previously defined as terminally exhausted cells, were found predominantly in clusters 2 and 5 and expressed multiple inhibitory receptors (*Entpd1, Cd244)* (Fig. 4.1F)[63]. The heterogeneity within T cells in LCMV was not captured solely by T-bet and Eomes expression, two markers previously used to define progenitor exhausted and terminally exhausted populations (Fig. 4.1F)[64].

We next asked whether CD8$^+$ T cells isolated from B16-OVA mouse melanoma tumors[180] contained analogous subpopulations. We derived signatures defining the progenitor exhausted and terminally exhausted populations from the LCMV dataset, and projected scRNA-seq profiles from B16-OVA CD8$^+$ TILs in the space of these signatures (Fig. 4.2A). Tetramer-sorted CD8$^+$ T cells from day 20 tumors demonstrated near uniform PD-1 and Tox expression and enriched strongly for the signature of exhausted CD8$^+$ T cells (Fig. 4.2B-D). We identified a subpopulation of CD8$^+$ T cells with marked transcriptional similarity to progenitor exhausted CD8$^+$ T cells that expressed *Tcf7* (Tcf1), in contrast to the majority populations which expressed *Havcr2* (Tim-3) (Fig. 4.2A and Fig. 4.2D-E).

We confirmed the presence of these two populations by flow cytometry. We identified TILs with progenitor (Tcf1$^+$Tim-3$^-$) and terminally exhausted (Tcf1$^-$Tim-3$^+$) phenotypes in both tumor-specific (tetramer$^+$) and total antigen-experienced (PD-1$^+$CD44$^+$) CD8$^+$ TILs (Fig. 4.3A-B). The

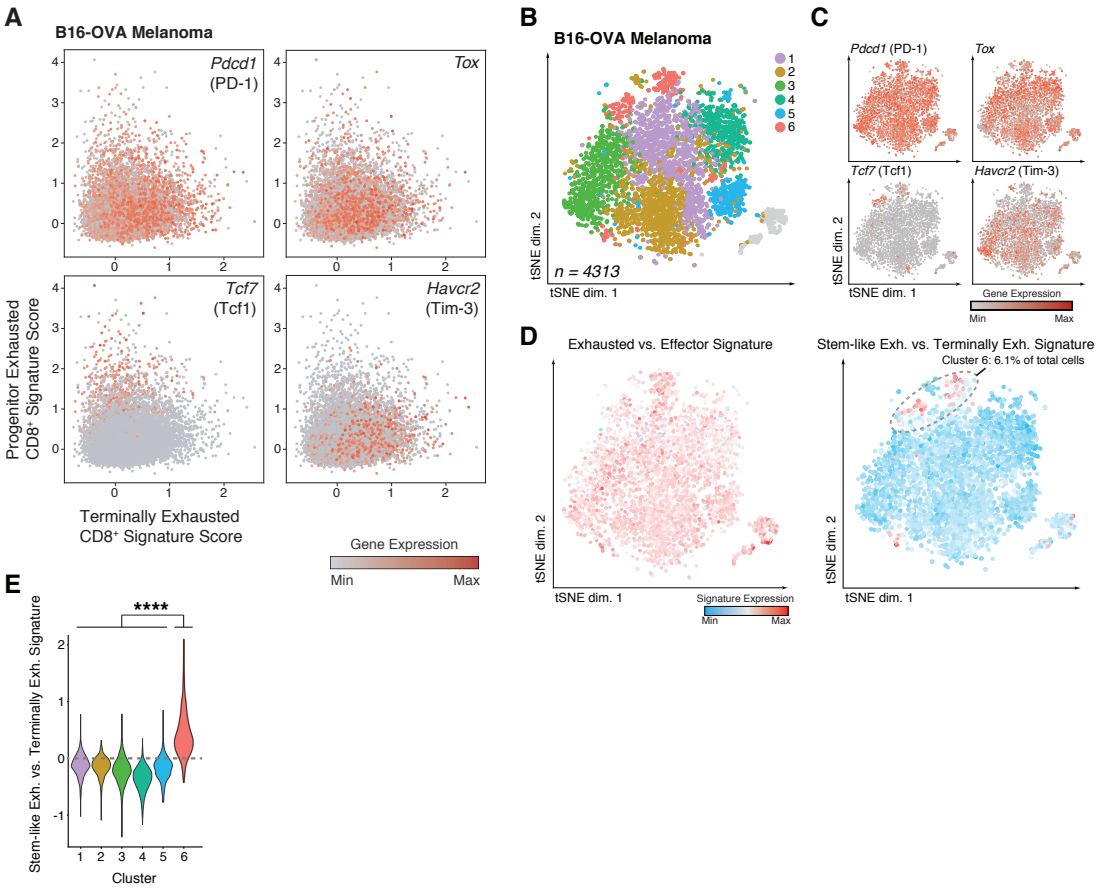


Figure 4.2. Chronic viral infection and tumors elicit analogous subsets of exhausted CD8⁺ T cells. (**A**) scRNA-seq profiles of 11,212 PD-1⁺CD44⁺CD8⁺ T cells isolated from d10 and d20 B16-OVA tumors. Cells were scored for expression of the progenitor exhausted CD8⁺ signature and terminally exhausted CD8⁺ signature from LCMV dataset in 4.1A. Cells were projected in a 2D scatterplot based on their scores. **(B)** tSNE projection of single-cell RNA-seq profiles from 4,313 SIINFEKL tetramer⁺ CD8⁺ T cells from day 20 B16-OVA tumors colored by cluster. Unlabeled cluster in grey represents cell doublets. **(C)** Expression of indicated genes overlaid on tSNE projection from (B). **(D)** Enrichment of a signature of genes upregulated in exhausted vs. effector CD8⁺ T cells (GSE9650) or stem-like exh. vs. terminally exh. CD8⁺ T cells (GSE84105). **(E)** Violin plots of the enrichment score of the gene signature derived from stem-like exhausted vs. terminally exhausted CD8⁺ T cells (GSE84105) for each cell cluster.

two populations could also be identified in B16.F10 tumors without a model antigen (Fig. 4.3C) and in a second mouse melanoma model, D4M.3A-OVA[181](Fig. 4.3D).

To isolate live progenitor exhausted cells for further characterization, we identified *Slamf6* (Ly108) as a cell surface marker that distinguished progenitor exhausted from terminally exhausted CD8⁺ T cells (Fig. 4.1F). Tcf1 and Slamf6 were highly co-expressed in progenitor

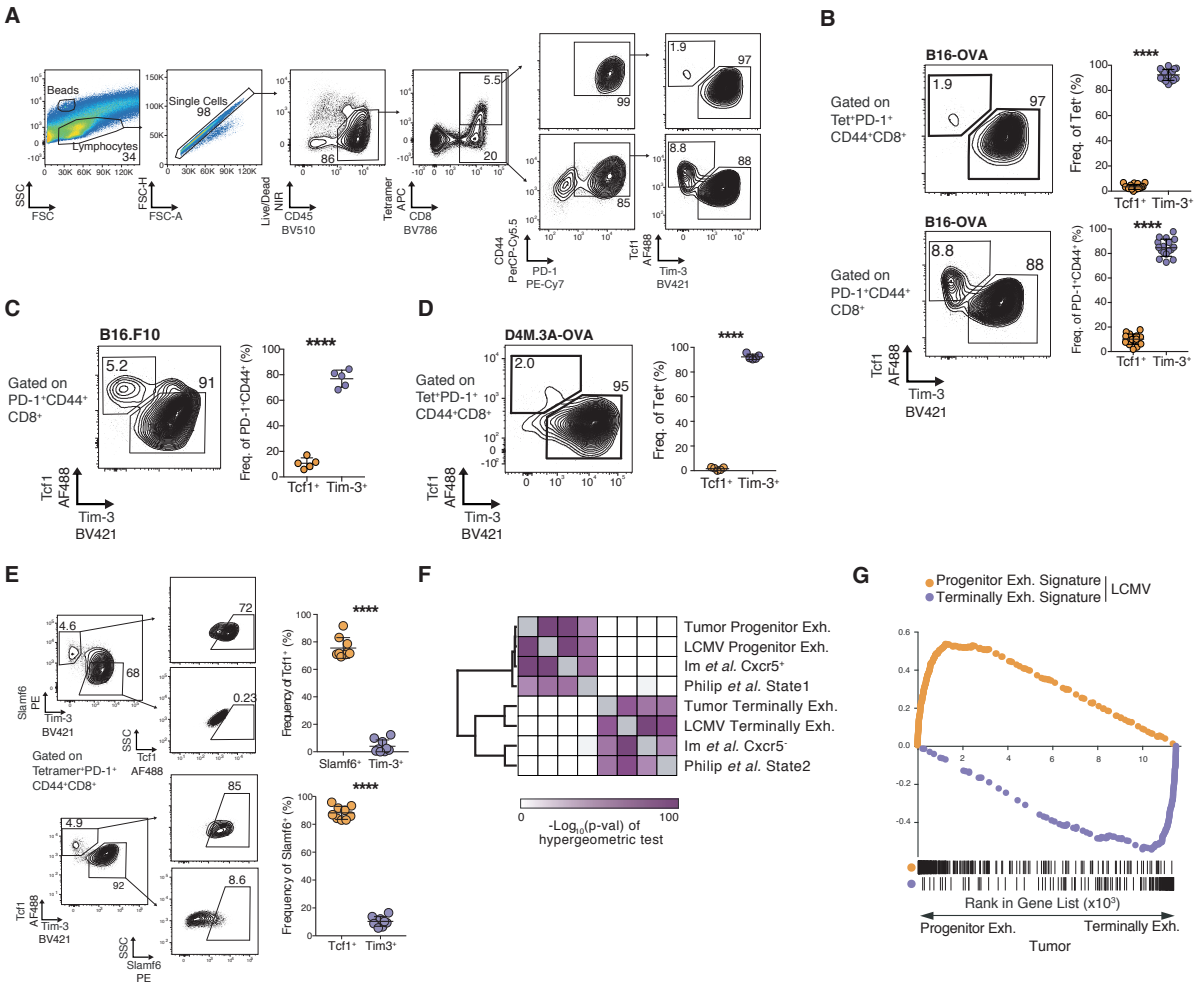


Figure 4.3. Progenitor exhausted and terminally exhausted CD8⁺ T cell populations can be found multiple mouse tumor models. (A) Representative flow cytometry gating strategy for progenitor and terminally exhausted cells. **(B-D)** Frequency of progenitor exhausted (Tcf1⁺Tim-3⁻) and terminally exhausted (Tcf1⁻Tim-3⁺) CD8⁺ T cells from B16-OVA tumors **(B)**, B16.F10 tumors **(C)** or D4M.3A-OVA tumors **(D)**. **(E)** Frequency of Tcf1⁺ cells within Slamf6⁺Tim-3⁻ or Slamf6⁻Tim-3⁺ cells (top) or frequency of Slamf6⁺ cells within Tcf1⁺Tim-3⁻ or Tcf1⁻Tim-3⁺ cells (bottom) from B16-OVA tumors. **(F)** Hypergeometric overlap of gene expression profiles from progenitor exhausted or terminally exhausted gene signatures from LCMV or TILs with expression data from indicated cell states from the literature, top 150 differentially expressed transcripts used for comparison. (**G**) GSEA of a signature of LCMV progenitor exhausted vs. terminally exhausted CD8⁺ T cells (orange) or the inverse (purple) in the ranked list of genes differentially expressed by progenitor exh. vs. terminally exh. CD8⁺ TILs from B16-OVA tumors.

exhausted cells (76% of Slamf6⁺Tim-3⁻ cells expressed Tcf1; 88% of Tcf1⁺Tim-3⁻ cells expressed Slamf6) and very few terminally exhausted (Slamf6⁻Tim-3⁺) cells expressed Tcf1 (4%; Fig. 4.3E).

We next compared the bulk gene expression profiles of Slamf6^{+}Tim-3^{-} (progenitor exhausted) and Slamf6^{-}Tim-3^{+} (terminally exhausted) tetramer^{+} cells in LCMV Cl13 infection and B16-OVA tumors (Fig. 4.3F-G). Gene set enrichment analysis (GSEA) demonstrated significant transcriptional similarity between the corresponding populations (Fig. 4.3G). We also found clear overlap with expression profiles previously defined from similar subpopulations in other studies (Fig. 4.3F). Thus, the same two phenotypically and transcriptionally distinct subpopulations of exhausted CD8^{+} T cells arise in chronic viral infection and in tumors.

Progenitor exhausted and terminally exhausted CD8^{+} TILs have distinct epigenetic and transcriptional states

To determine whether subpopulations of exhausted CD8^{+} T cells in tumors shared the same epigenetic state as those in chronic infection, we defined chromatin accessibility in CD8^{+} T cell subsets from B16-OVA and LCMV Cl13 and compared with functional memory CD8^{+} T cells isolated from LCMV Armstrong infection. Both exhausted subpopulations showed canonical epigenetic features of exhausted cells including chromatin accessible regions (ChARs) around *Tox* and an exhaustion-specific PD-1 enhancer (Fig. 4.4A)[145, 171]. Indeed, epigenetic profiles from both tumors and LCMV Cl13 were more correlated with each other than with memory CD8^{+} T cells (Fig. 4.4B). We identified 8,909 ChARs with increased accessibility in exhausted CD8^{+} cells relative to memory T cells. Pathway enrichment of the genes near these ChARs highlighted signatures of interferon signaling, PD-1 signaling and IL-10 response, whereas memory T cells enriched for memory signatures and fatty acid metabolism (Fig. 4.4C).

Next, we examined regions that varied in accessibility between the two subsets in both tumors and chronic infection. We found differential ChARs adjacent to *Slamf6* specifically in

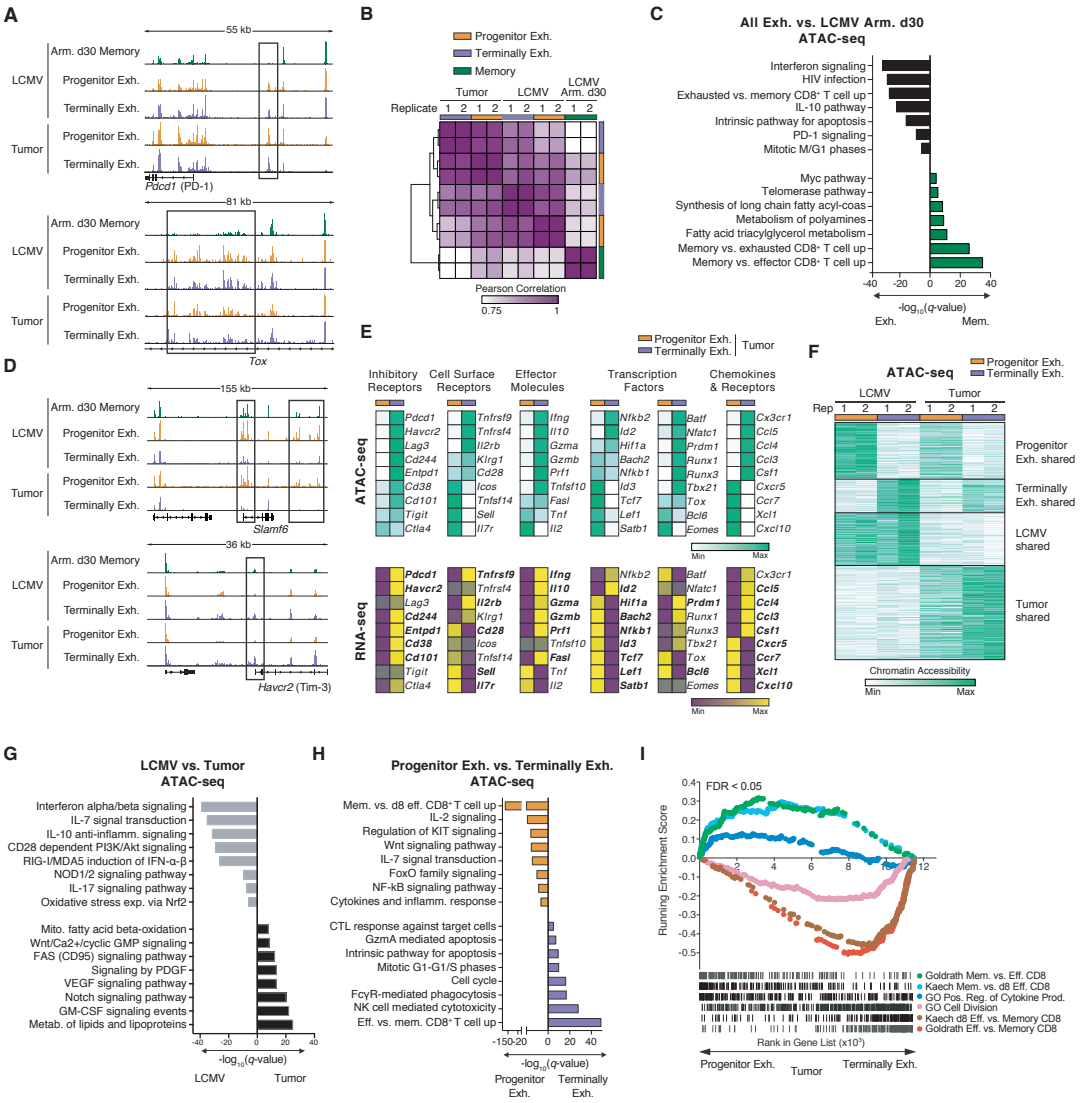


Figure 4.4. Progenitor and terminally exhausted CD8⁺ TILs have distinct epigenetic and transcriptional features. (A) Representative ATAC-seq tracks at the *Pdcd1* (top) and *Tox* (bottom) loci from CD8⁺ T cells sorted from d30 p.i. LCMV-Armstrong (Arm.) infected mice, d30 p.i. LCMV Cl13 infected mice or d22 B16-OVA tumors. **(B)** Pearson correlation of ATAC-seq profiles from progenitor exhausted cells, terminally exhausted cells, and memory cells. **(C)** Enrichment of gene signatures from MSigDB (rows) from regions in shared exhaustion program. Q-values (hypergeometric test) presented as $-\log_{10}$. **(D)** Representative ATAC-seq tracks at the *Slamf6* (top) and *Havcr2* (bottom) loci. **(E)** Heat map illustrating the average ATAC-seq peak intensity (top) or transcript expression (bottom) of the indicated genes. Rows represent averaged z-scores. Bolded names in RNA-seq represent transcripts with significant differential expression by DESeq2 ($q < 0.05$). **(F)** K-means clustering of open chromatin regions from LCMV Cl13 and tumor CD8⁺ T cells ($k = 4$). Universe of all differential peaks (n=56,404). **(G)** Enrichment of gene signatures from MSigDB (rows) from cluster of regions in LCMV Cl13 or tumor. Q-values (hypergeometric test) presented as $-\log_{10}$. **(H)** Enrichment of gene signatures from MSigDB (rows) from the cluster of ChARs specific to progenitor exhausted or terminally exhausted cells in **e**. Q-values (hypergeometric test) presented as $-\log_{10}$. **(I)** GSEA of signatures in the ranked list of genes differentially expressed by progenitor exhausted vs. terminally exhausted CD8⁺ T cells from B16-OVA tumors.the cluster of ChARs specific to progenitor exhausted or terminally exhausted cells in **e**. Q-values (hypergeometric test) presented as $-\log_{10}$.

progenitor exhausted cells and *Havcr2* (Tim-3) in terminally exhausted cells, consistent with their phenotype (Fig. 4.4D). Progenitor exhausted cells had greater chromatin accessibility and higher transcript levels in genes associated with cytokine production (*Tnf*, *Il2*), costimulatory molecules (*Icos*, *Tnfsf14*), and survival/memory (*Il7r, Id3*, *Satb1*) (Fig. 4.4E). Conversely, terminally exhausted cells had more accessibility and expression of co-inhibitory cell surface receptors (*Entpd1*, *Cd244*), effector molecules (*Gzmb*, *Prf1*, *Ifng*), and TFs associated with effector and exhausted cells (*Id2*, *Runx1*, *Prdm1*).

Unsupervised clustering of differential regions identified four clusters: two that differentiated progenitor exhausted from terminally exhausted cells in both model systems, and two that distinguished exhausted T cells arising in tumors from those in chronic viral infection (Fig. 4.4F). Enhancers specific to chronic infection were adjacent to genes involved in type I interferon signaling, while tumor-specific regions were associated with signatures related to growth factor signaling (Fig. 4.4G). Thus, in addition to a shared epigenetic program of exhaustion, different microenvironment signals in infection and tumors imprint distinct epigenetic features.

We next identified 13,430 and 8,085 ChARs unique to progenitor exhausted and terminally exhausted cells respectively that were independent of the microenvironment. This suggests that the two subpopulations represent distinct cell states. Pathway enrichment of genes associated with state-specific ChARs suggested unique biological properties of each population: progenitor exhausted cells were enriched for signatures of cytokine production, survival, and memory, whereas terminally exhausted cells were marked by programs of cell division, apoptosis, and cytotoxicity (Fig. 4.4H). GSEA of transcriptional differences identified similar changes (Fig. 4.4I). Therefore, progenitor and terminally exhausted $CD8^+$ T cells represent two transcriptionally distinct sub-states within T cell exhaustion that are maintained by state-specific epigenetic regulation.

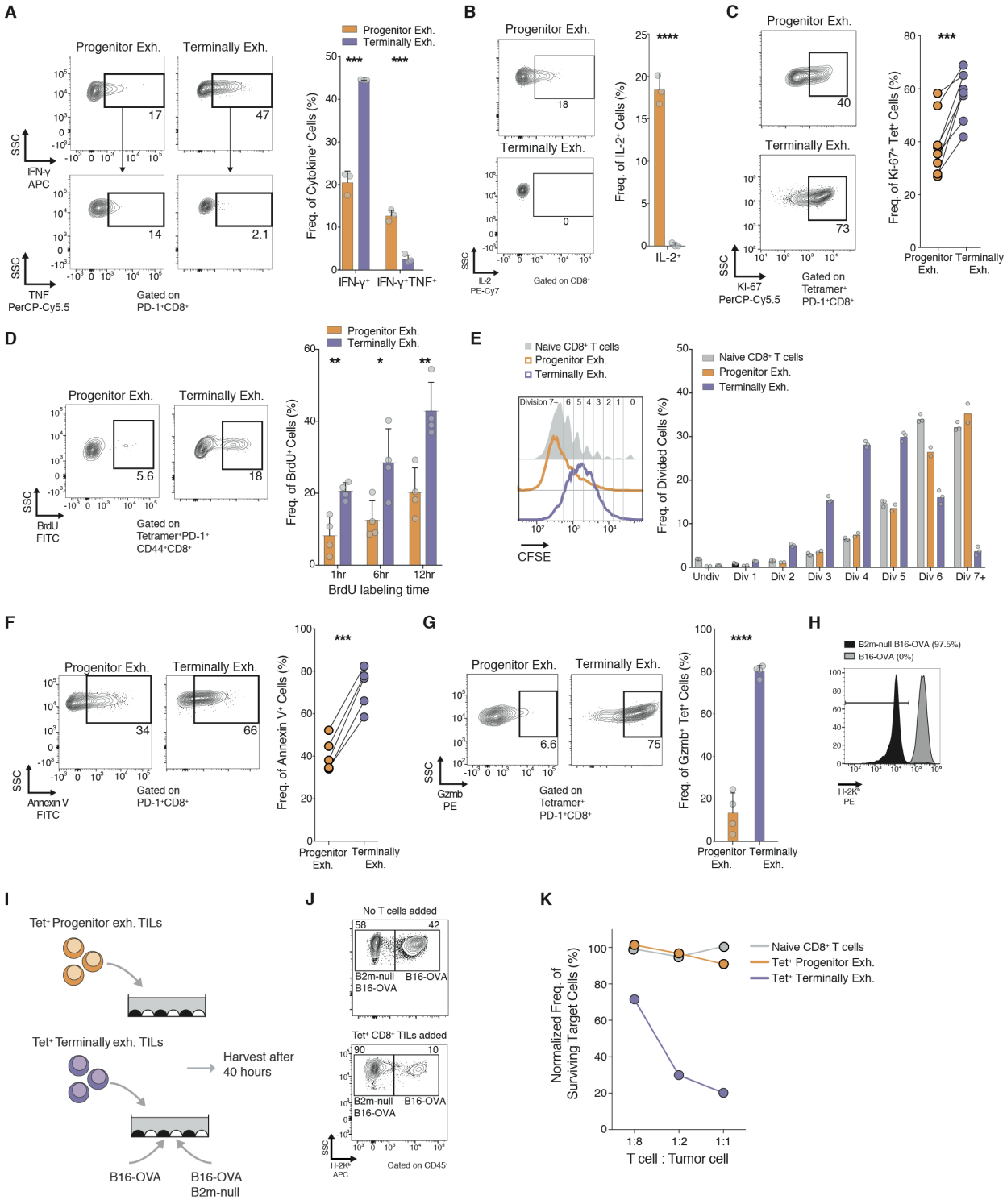


Figure 4.5. Progenitor exhausted and terminally exhausted CD8⁺ TILs have distinct functional properties. (A) Frequency of IFN-γ⁺ and IFN-γ⁺TNF⁺ progenitor exhausted or terminally exhausted TILs stimulated for 6 hours *ex vivo* with SIINFEKL peptide. **(B)** Frequency of IL-2⁺ progenitor or terminally exhausted TILs stimulated for 6 hours *ex vivo* with PMA + ionomycin. **(C)** Frequency of Ki-67⁺ progenitor exhausted or terminally exhausted TILs *ex vivo*. **(D)** Frequency of BrdU⁺ progenitor exhausted or terminally exhausted TILs after indicated times of *in vivo* labeling. **(E)** CFSE dilution of naive, progenitor exhausted, or terminally exhausted CD8⁺ T cells stimulated *ex vivo* with anti-CD3 + anti-CD28.

(Figure 4.5 continued) **(F)** Frequency of Annexin-V$^+$ progenitor exhausted or terminally exhausted TILs *ex vivo*. **(G)** Frequency of granzyme B$^+$ progenitor exhausted or terminally exhausted TILs *ex vivo*. **H)** Representative histograms of H-2K^b expression on B16-OVA and B2m-null B16-OVA cells after 24 hours *in vitro* IFN-γ stimulation. **(I)** Schema of experimental design for *in vitro* killing assay. **(J)** Representative flow plots of tumor cells after 40 hour co-culture with no T cells (top) or tetramer$^+$ CD8$^+$ TILs (bottom) stained against H-2K^b. **(K)** Frequency of surviving target cells (B16-OVA) to control cells (B2m-null B16-OVA) normalized to wells with no T cells added.

Progenitor exhausted and terminally exhausted CD8$^+$ TILs are functionally distinct

Based on differences in the transcriptional and epigenetic states, we hypothesized that CD8$^+$ TIL subsets would have different functions. We found that a higher proportion of terminally exhausted T cells produced interferon-γ (IFN-γ) after *in vitro* stimulation compared with progenitor exhausted cells (44% vs. 21%; Fig. 4.5A). Conversely, progenitor exhausted CD8$^+$ T cells were more polyfunctional, as measured by IFN-γ and TNF co-production (13% vs. 2%) or IL-2 production (18% vs. 0%; Fig. 4.5B).

Terminally exhausted cells expressed higher levels of Ki-67 (58% vs. 39%; Fig. 4.5C), and incorporated more BrdU than did progenitor exhausted T cells (43% vs. 20% after 12-hours; Fig. 4.5D). Despite reduced proliferation *in vivo*, we found that progenitor exhausted cells underwent more rounds of division than terminally exhausted CD8$^+$ T cells upon *in vitro* restimulation (Fig. 4.5E). A higher fraction of terminally exhausted CD8$^+$ T cells stained with the apoptosis marker Annexin-V (72% vs. 41%) (Fig. 4.5F). Thus while terminally exhausted CD8$^+$ T cells proliferated more in the TME, they had reduced proliferative capacity – i.e. the ability to further divide upon restimulation – and higher cell death compared with progenitor exhausted CD8$^+$ T cells[63, 172].

Terminally exhausted CD8$^+$ T cells expressed more granzyme B than progenitor exhausted cells (80% vs. 12%; Fig. 4.5G), and were more cytotoxic in direct cytotoxicity assays with tumor cell targets (Fig. 4.5H-K). Indeed, progenitor exhausted cells killed target cells no more efficiently than naive CD8$^+$ T cells, suggesting that they contribute little or no direct cytotoxicity in the tumor microenvironment.

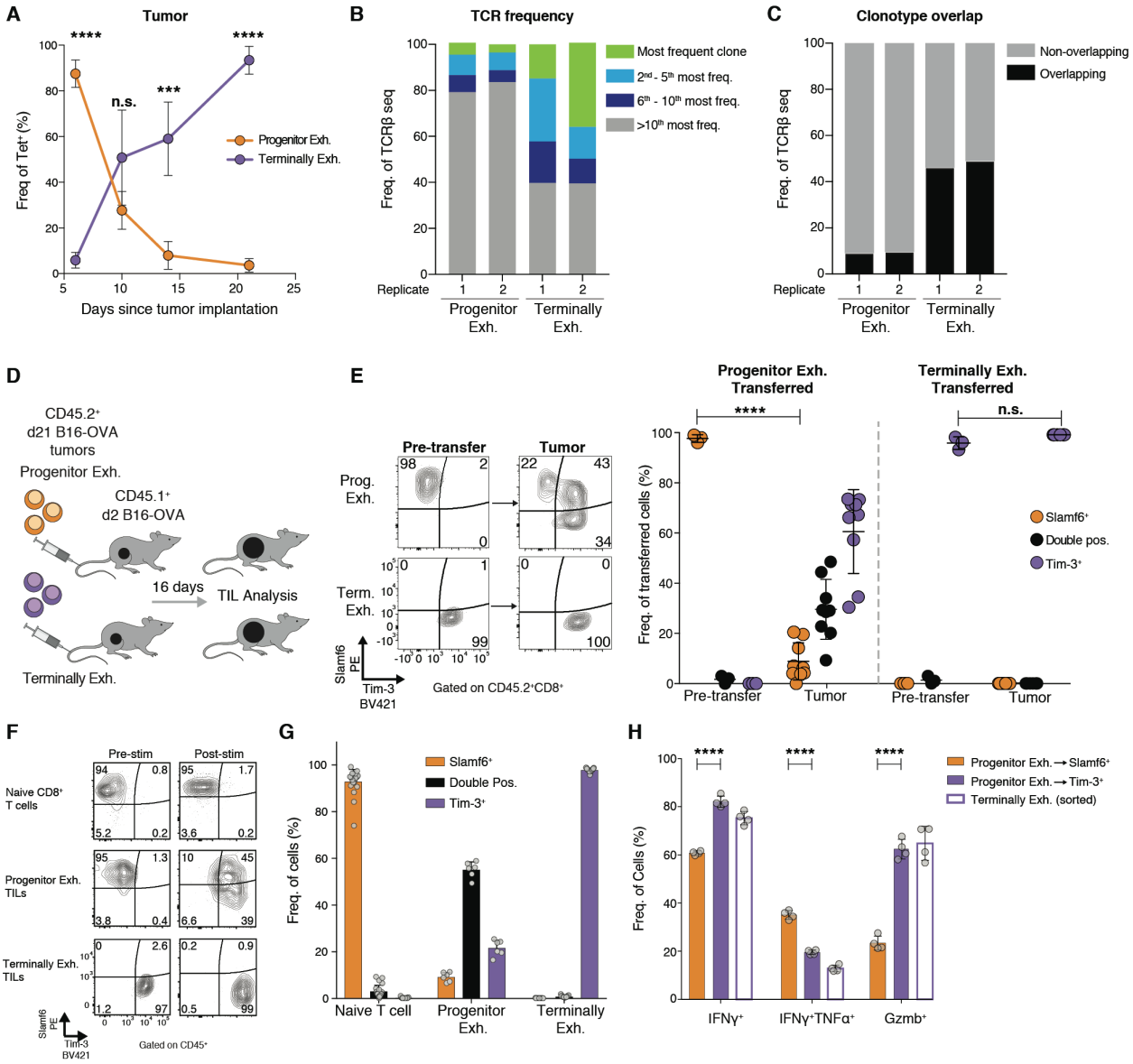


Figure 4.6. Progenitor exhausted CD8⁺ T cells differentiate into terminally exhausted CD8⁺ T cells. (A) Longitudinal analysis of the frequency of progenitor exhausted and terminally exhausted tetramer⁺ CD8⁺ TILs in B16-OVA tumors. **(B)** Frequency of the most common TCRβ clonotypes in progenitor exh. or terminally exh. tetramer⁻PD-1⁺CD44⁺ CD8⁺ TILs from B16-OVA tumors. **(C)** Frequency of TCRβ clonotypes shared between progenitor exhausted and terminally exhausted TILs. **(D)** Schema of experimental design for *in vivo* transfer assay. **(E)** Cell surface phenotype of progenitor exh. or terminally exh. sorted cells pre-transfer and in recipient mouse tumors 16 days post-transfer. **(F)** Representative flow plots of the cell surface phenotype of naive CD8⁺ splenocytes, progenitor exhausted TILs, or terminally exhausted TILs pre-stim (left) or after 40 hours co-culture with tumor cells (right). **(G)** Summary of the phenotype of tetramer⁺ sorted T cells after 40 hours co-culture with tumor cells. **(H)** Frequency of IFN-γ⁺, IFN-γ⁺TNF⁺ or granzyme B⁺ cells from sorted terminally exh. or progenitor exh. cells after 42 hour anti-CD3 + anti-CD28 stimulation *in vitro.* Sorted progenitor exh. cells gated on Slamf6⁺Tim-3⁻ or Slamf6⁻Tim-3⁺ expression after culture.

Progenitor exhausted CD8⁺ T cells differentiate into terminally exhausted CD8⁺ T cells

Previous studies in chronic viral infection have shown that progenitor exhausted cells can give rise to terminally exhausted cells[172, 174, 175]. To understand their lineage relationship in tumors, we analyzed CD8⁺ TILs over a time-course of tumor growth and observed an increasing ratio of terminally exhausted to progenitor exhausted cells (Fig. 4.6A). Progenitor exhausted cells had a more diverse T cell repertoire (TCR) repertoire than terminally exhausted cells (Fig. 4.6B). Less than 10% of clonotypes in progenitor exhausted cells overlapped with those in terminally exhausted cells, whereas nearly 50% of the clonotypes in terminally exhausted cells were shared (Fig. 4.6C). These data are consistent with a model in which progenitor exhausted cells differentiate to give rise to terminally exhausted cells.

To formally test a lineage relationship, we transferred each population into congenically-marked, tumor-bearing mice and assessed the phenotype of the transferred population 16 days later (Fig. 4.6D). After transferring progenitor exhausted cells (Slamf6⁺Tim-3⁻) we recovered both Slamf6⁺ and Tim-3⁺ cells in the TME (Fig. 4.6E). However, after transferring terminally exhausted cells (Slamf6⁻Tim-3⁺), only Tim-3⁺ cells were recovered (Fig. 4.6E). Similar results were obtained after *in vitro* stimulation of both subsets (Fig. 4.6F-G).

To test if this differentiation was associated with expected functional changes, we assessed progenitor exhausted cells that remained Slamf6⁺Tim-3⁻ or become Slamf6⁻Tim-3⁺ after *in vitro* stimulation. Progenitor exhausted cells that acquired the phenotype of terminally exhausted cells showed increased IFN-γ (82% vs. 61%) and granzyme B production (63% vs. 23%; Fig. 4.6H). Conversely, newly formed Slamf6⁻Tim-3⁺ had decreased IFN-γ and TNF co-production (20% vs. 35%; Fig. 4.6H), suggesting that *in vitro* TCR stimulation was sufficient to induce phenotypic and functional differentiation of progenitor exhausted cells.

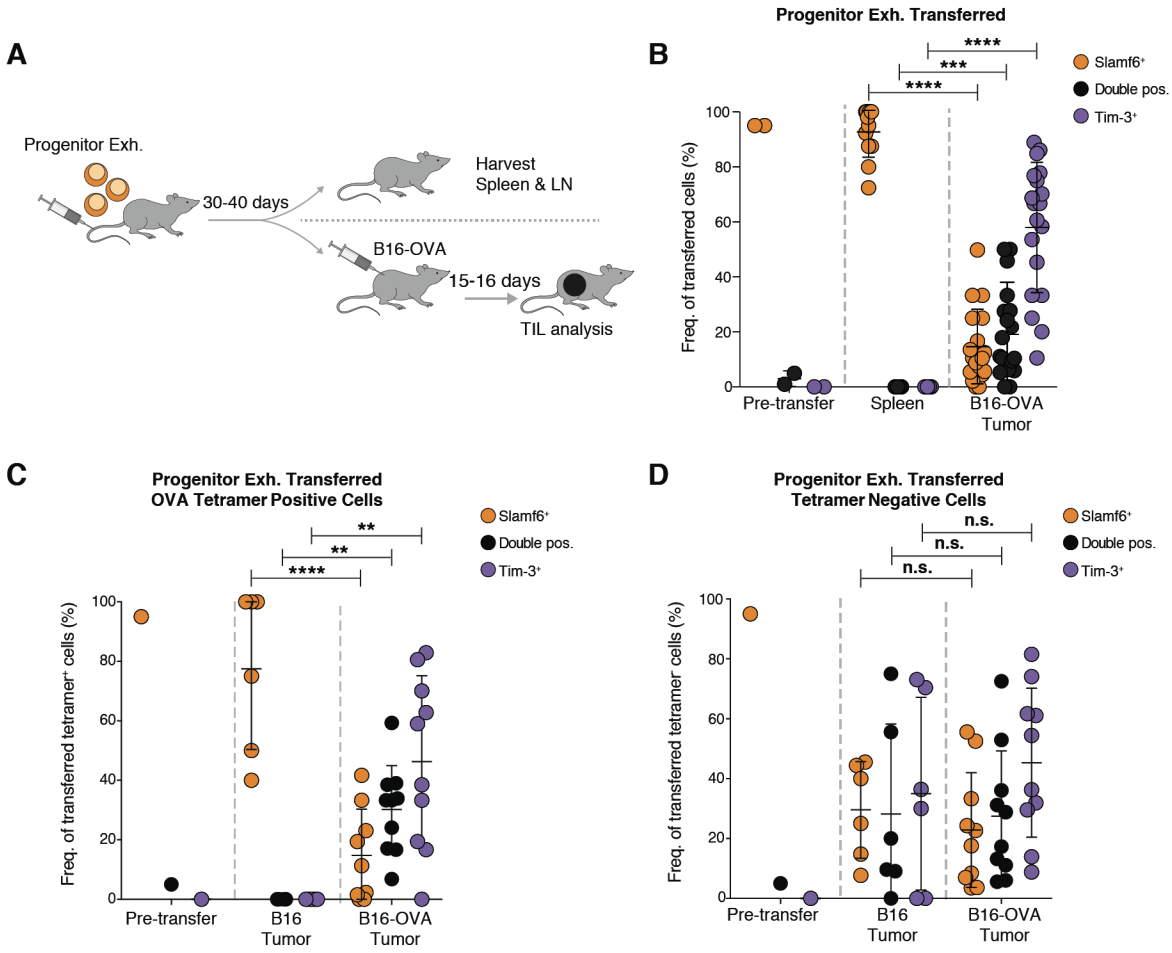


Figure 4.7. Differentiation of progenitor exhausted CD8⁺ T cells requires antigen-specific TCR signaling. (A) Schema of experimental design for *in vivo* persistence and tumor assays. **(B)** Phenotype of transferred progenitor exhausted cells harvested from spleen or tumors. **(C-D)** Phenotype of progenitor exhausted cells transferred into mice with B16 or B16-OVA tumors, gated on transferred tetramer⁺ **(C)** or tetramer⁻ **(D)** cells from the recipient tumors.

To ask if TCR stimulation was required for differentiation *in vivo*, we transferred progenitor exhausted cells into congenically-marked mice without tumors (Fig. 4.7A). When recovered from the spleens of recipient mice 30-40 days later, transferred cells maintained their progenitor exhausted phenotype (Fig. 4.7B). However, when the mice were implanted with B16-OVA tumors 30-40 days later, transferred progenitor exhausted cells had acquired a terminally exhausted phenotype in the TME (Fig. 4.7B).

To isolate the contribution of antigen encounter versus other factors in the TME, we transferred progenitor exhausted cells from B16-OVA tumors into host mice bearing either B16-

OVA tumors or B16 tumors lacking OVA antigen. While tetramer$^+$ progenitor exhausted cells (that recognize OVA antigen) readily differentiated into Tim-3$^+$ cells in B16-OVA tumors, they maintained the progenitor exhausted phenotype in B16 tumors with no source of OVA antigen (Fig. 4.7C). In contrast, tetramer$^-$ progenitor exhausted cells (that do not recognize OVA antigen) in the same TME differentiated into terminally exhausted cells, likely in response to shared antigens between B16 and B16-OVA tumors (Fig. 4.7D). Thus, progenitor exhausted T cells gave rise to terminally exhausted cells through a process that required TCR stimulation.

Progenitor exhausted cells can persist in the absence of antigen and mediate long term tumor control in vivo

We next asked whether progenitor and terminally exhausted CD8$^+$ T cells had differential ability to persist in the tumor microenvironment. We analyzed the relative frequency of the two populations in tumors following *in vivo* transfer (Fig. 4.8A). We recovered approximately 100-fold more transferred progenitor exhausted cells and recovered progenitor exhausted, but not terminally exhausted, cells in tumor draining lymph nodes (Fig. 4.8A). These results are consistent with the increased proliferative potential and decreased apoptosis of progenitor exhausted CD8$^+$ TILs. Importantly, despite expressing molecules for homing to secondary lymphoid organs (*Sell*, *Ccr7*), transferred progenitor exhausted cells trafficked to the TME.

To determine if antigen stimulation was required for differential persistence, we transferred each cell population into naive congenically-marked mice and assayed cell recovery 30-40 days later (Fig. 4.8B). Significantly more transferred progenitor exhausted cells were recovered from secondary lymphoid organs (89-fold in spleen, 7-fold in pooled lymph nodes; Fig. 4.8C-D), consistent with their higher expression of central memory-associated transcripts such as *Il7r* and *Satb1*. We then implanted B16-OVA tumors 30-40 days after cell transfer, and recovered significantly more transferred progenitor exhausted cells in the tumor compared with secondary

lymphoid organs (approx. 100-fold enrichment; Fig. 4.8E), suggesting improved trafficking or proliferation in the TME.

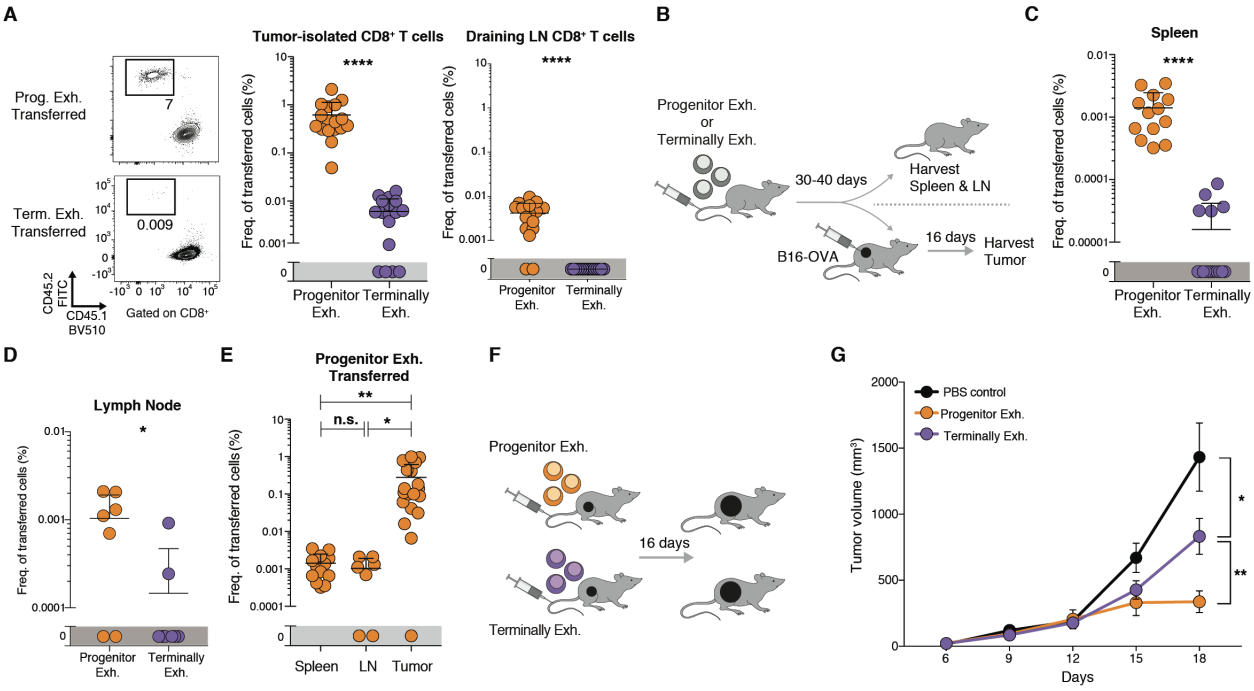


Figure 4.8. Progenitor exhausted CD8+ T cells persist in the absence of antigen and mediate long term tumor control *in vivo*. (A) Frequency of transferred (CD45.2+) progenitor exh. or terminally exh. cells isolated from the tumors (left) or draining lymph node (right) of recipient mice. **(B)** Schema of experimental design for *in vivo* persistence and tumor challenge assay. **(C)** Frequency of transferred progenitor exh. or terminally exh. cells in spleens of recipient mice. **(D)** Frequency of transferred progenitor or terminally exhausted cells in lymph nodes from *in vivo* persistence assay mice without tumor implantation. **(E)** Frequency of transferred progenitor exhausted cells in spleens, lymph nodes, or tumors of recipient mice. **(F)** Schema of experimental design for *in vivo* transfer assay. **(G)** Growth curves of B16-OVA tumors after transfer of progenitor exh. cells, terminally exh. cells, or PBS control injection on day two.

Given the differences in functionality and persistence, we reasoned that progenitor exhausted TILs would have superior ability to control tumors upon transfer (Fig. 4.8F). Tumor growth was slower after transferring either population than in control-treated mice, suggesting both populations could mediate some degree of anti-tumor immunity. However, tumor control was

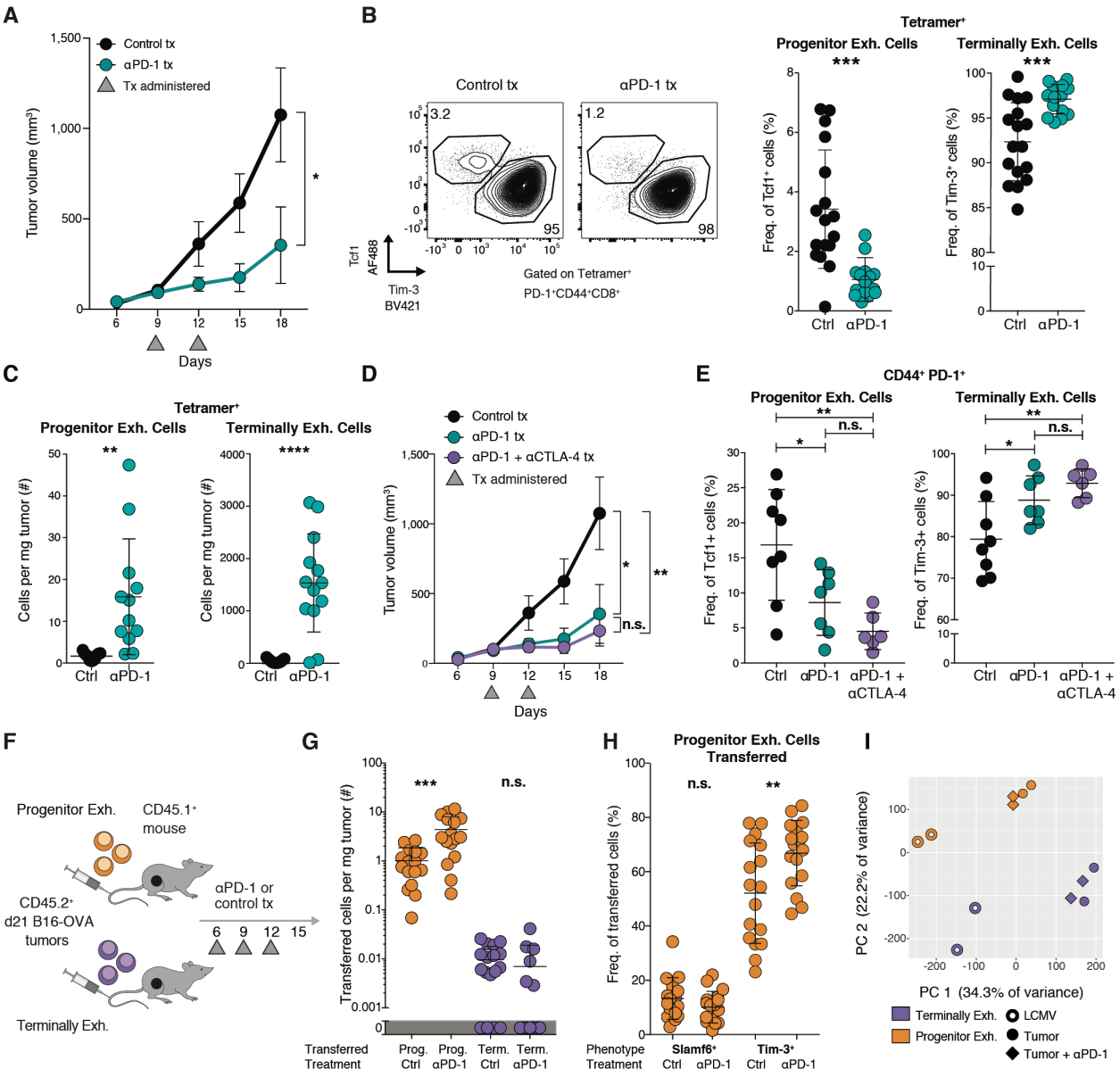


Figure 4.9. Anti-PD-1 treatment increases progenitor exhausted cell numbers and differentiation to terminally exhausted cells. (A) Growth curves of B16-OVA tumors treated with 100μg anti-PD-1 or isotype control antibodies on days 9 and 12. **(B)** Frequency of progenitor exhausted and terminally exhausted CD8⁺ T cells from isotype control or anti-PD-1 treated B16-OVA tumors pre-gated on tetramer⁺ cells. **(C)** Cell number/mg tumor of progenitor exhausted and terminally exhausted CD8⁺ T cells from isotype control or anti-PD-1 treated B16-OVA tumors, gated on tetramer⁺ cells. **(D)** Growth curves of B16-OVA tumors treated with 100μg anti-PD-1 +/- 100μg anti-CTLA-4 or isotype control antibodies on days 9 and 12. **(E)** Frequency of progenitor exhausted and terminally exhausted cells. **(F)** Schema of *in vivo* transfer with anti-PD-1 assay. **(G)** Cell numbers/mg tumor of transferred (CD45.2⁺) progenitor exhausted or terminally exhausted CD8⁺ T cells in tumors from isotype control or anti-PD-1 treated mice. **(H)** Phenotype of transferred (CD45.2⁺) progenitor exhausted cells isolated from isotype control or anti-PD-1 treated recipient mice. **(I)** Principal component analysis of replicate samples from ATAC-seq analysis of progenitor exhausted and terminally exhausted CD8⁺ T cells sorted from LCMV-infected mice or B16-OVA tumors treated with isotype control or anti-PD-1 antibodies, as indicated.

significantly greater after transfer of progenitor exhausted cells (Fig. 4.8G), likely due to improved proliferative capacity, and ability to differentiate into cytotoxic terminally exhausted CD8$^+$ T cells.

Progenitor exhausted CD8$^+$ T cells respond to PD-1 blockade

To determine how anti-PD-1 therapy affects exhausted TIL subpopulations, we treated B16-OVA tumor-bearing mice with PD-1 blocking antibody. As expected, checkpoint blockade improved tumor control and increased tumor CD8$^+$ T cell infiltration (Fig. 4.9A)[182]. We recovered increased numbers of both subpopulations after PD-1 therapy, but observed greater relative frequency of terminally exhausted CD8$^+$ T cells (Fig. 4.9B-C). Similar results were obtained with combination therapy (anti-PD-1 + anti-CTLA-4), although no additive therapeutic effect was observed (Fig. 4.9D-E).

To assess the relative effects of anti-PD-1 therapy on each population, we transferred progenitor or terminally exhausted cells into tumor-bearing mice that received anti-PD-1 or control treatment (Fig. 4.9F). Transferred progenitor exhausted cells in the TME significantly increased in number (4.4-fold) following PD-1 blockade while terminally exhausted cell numbers did not (Fig. 4.9G). Treatment with anti-PD-1 resulted in a significant increase in the conversion of progenitor exhausted cells to a terminally exhausted phenotype (67% vs 52%; Fig. 4.9H).

To assess if anti-PD-1 therapy altered the differentiation state of exhausted TILs, we performed ATAC-seq and RNA-seq on CD8$^+$ TILs treated with anti-PD-1 or control antibodies. We observed minimal change in the epigenetic profiles of progenitor or terminally exhausted cells (less than 2.6% of all genes or regions, FDR < 0.05; Fig. 4.9I).[150] Thus, anti-PD-1 treatment increased progenitor exhausted cell numbers and promoted their differentiation to terminally exhausted cells, without fundamentally changing the epigenetic state of either population in the tumor (Fig. 4.9I).

Finally, we asked if we could identify progenitor exhausted CD8⁺ T cells in patients with melanoma. We performed quantitative multiplex immunofluorescence of pre-treatment biopsies from 25 patients with metastatic melanoma treated with nivolumab (anti-PD-1) and ipilimumab (anti-CTLA-4) (Fig. 4.10A). TCF1⁺PD-1⁺CD8⁺ T cells, consistent with the progenitor exhausted

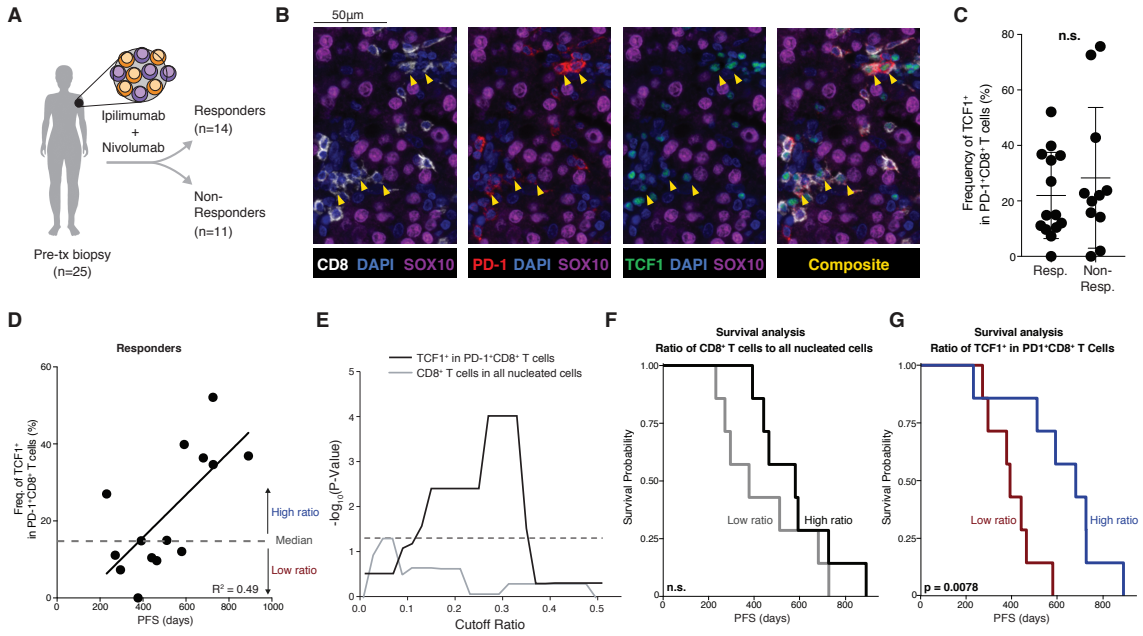


Figure 4.10. Increased fraction of progenitor exhausted CD8⁺ T cells is associated with duration of response to checkpoint blockade in patients with advanced melanoma. (A) Schema of biopsy samples obtained from patients with Stage III-IV melanoma. **(B)** Multiplex immunofluorescence image of representative progenitor exhausted cells (indicated with yellow arrowheads), identified as TCF1⁺PD-1⁺CD8⁺SOX10⁻ cells. **(C)** Frequency of TCF1⁺ cells in PD-1⁺CD8⁺ cells in patients with durable clinical benefit (responders, n = 14) or no clinical benefit (non-responders, n = 11). **(D)** Frequency of progenitor exhausted cells in all activated/exhausted cells plotted against progression-free survival (days) in patients with durable clinical benefit (responders, n = 14). Linear regression line shown. **(E)** Graph plotting the significance value from survival analysis for different cutoff ratios of TCF1⁺ in PD-1⁺CD8⁺ T cells (black line) or CD8⁺ T cells in all nucleated cells (grey line), from 0 to max ratio in responders (n = 14). Dotted line at p = 0.05. **(F-G)** Kaplan-Meier curves of progression-free survival in responders (n = 14) by high vs. low percentage of total CD8⁺ T cells in all nucleated cells **(F)** (cutoff at median 7.6%) or by percentage of progenitor exhausted cells (TCF1⁺) in all activated/exhausted PD-1⁺CD8⁺ T cells **(G)** (cutoff at median 14.9%).

phenotype, could be readily identified in almost all biopsies, and their percentage of the total CD8⁺ population varied widely (Fig. 4.10B).

No significant difference in the frequency of TCF1⁺PD-1⁺CD8⁺ T cells was seen between patients who achieved durable clinical benefit to immunotherapy (responders) and those who did

not (non-responders) (Fig. 4.10C). Among responders, the duration of response correlated with the frequency of TCF1$^+$PD-1$^+$CD8$^+$ T cells (Fig. 4.10D), but not in non-responders. Increased frequency of TCF1$^+$PD-1$^+$CD8$^+$ T cells was significantly associated with prolonged progression-free survival (PFS) (PFS hazard ratio [95% CI]: 0.43 [0.19, 0.77], p=0.002;) (Fig. 4.10E-G). Among responders, patients with higher total CD8$^+$ T cell infiltration did not have a longer PFS in this cohort (Fig. 4.10F). In contrast, patients with a higher than median frequency of TCF1$^+$ in PD-1$^+$CD8$^+$ T cells experienced significantly longer PFS therapy (median PFS of 681 vs. 441 days; Fig. 4.10G). Therefore, a larger fraction of progenitor exhausted CD8$^+$ T cells is associated with anti-PD-1 efficacy in patients with melanoma.

Discussion

The basis for T cell dysfunction in cancer is not well understood, nor is the mechanism by which anti-PD-1 therapy reinvigorates T cell function. Here, we define the heterogeneity within exhausted T cells from chronic viral infection, and use this to better understand the heterogeneity of exhausted CD8$^+$ TILs. We found that CD8$^+$ T cells from mouse transplantable tumors share phenotypic, transcriptional, epigenetic, and functional properties with populations of exhausted CD8$^+$ T cells from a chronic viral infection model. As in chronic viral infection, we found two major subsets of exhausted T cells in the tumor microenvironment: a progenitor population with greater polyfunctionality and the ability to persist in the absence of antigen, as well as a terminally exhausted population with superior cytotoxicity but reduced long-term survival. The progenitor population gave rise to terminally exhausted CD8$^+$ T cells, had enhanced tumor control, and retained responsiveness to PD-1 blockade. Cells phenotypically similar to progenitor exhausted CD8$^+$ T cells were found in human melanoma where they were associated with long-term responses to checkpoint blockade therapy. Our study has three important implications for understanding the role of exhausted T cells in tumor immunity.

First, despite differences between chronic viral infection and cancer that result in disease-specific epigenetic imprinting, both disease states elicit largely similar states of exhausted CD8+ T cells. T cell exhaustion therefore represents a fundamental adaptation to conditions of chronic antigen stimulation and inflammation. Previous studies have found that CD8+ TILs appear exhausted[50, 55, 148], however, recent studies suggest that dysfunctional CD8+ TILs are distinct from exhausted cells in chronic viral infection[56, 57]. Our study helps resolve this contradiction by establishing both common features of T cell exhaustion and disease specific features that reflect an additional imprint of the unique microenvironment. Critically, we identified a shared epigenetic program of exhaustion that is independent of disease-specific milieu. Further analysis of this epigenetic program may help highlight the most important regulators of T cell exhaustion. In addition to shared regions, exhausted TILs also demonstrate unique epigenetic changes that may reflect the distinct microenvironment of cancer, including those involved in metabolism[183] and cytokine signaling which may fine-tune the underlying program of T cell exhaustion.

Second, we have identified subpopulations of exhausted CD8+ TILs with important and complementary functional specialization. Effective T cell mediated immunity requires both cells with robust anti-tumor functionality and cells to sustain a durable response. We show that terminally exhausted cells are the primary cytotoxic CD8+ T cells in the TME but are short lived[184], whereas progenitor exhausted cells are poorly cytolytic but can persist long-term. This suggests that a balance of both progenitor exhausted and terminally exhausted cell types may be required for effective tumor control, as in chronic viral infection[172]. It may seem counterintuitive that populations of exhausted CD8+ T cells are capable of potent anti-tumor properties, given previous studies showing that exhausted cells are impaired in functional attributes relative to memory T cells[1, 116]. However, our findings are consistent with observations that exhausted CD8+ T cells still possess effector functions in chronic viral infection[14, 172]. Furthermore, single-cell analysis of

exhausted CD8+ T cells demonstrates significant heterogeneity within Tim-3+ cells, which may explain contradictory results in the literature about the functionality of these cells.

Finally, these results may have important implications for cancer immunotherapy. Transfer experiments in the mouse model show that anti-PD-1 therapy acts on progenitor exhausted, but not terminally exhausted, CD8+ T cells. Based on these data, we propose that anti-PD-1 therapy induces the proliferation and differentiation of progenitor exhausted cells in the TME, leading to an increase in cytotoxic, but short-lived, terminally exhausted cells. Consistent with this, in patients with advanced melanoma, the relative frequency of progenitor exhausted CD8+ T cells correlates with improved duration of response to checkpoint blockade therapy. Interestingly, unlike other studies that identify these populations in human tumors[185] and demonstrate their predictive value for checkpoint blockade response[186, 187], we did not find a difference in the percentage of progenitor exhausted cells between responders and non-responders. This may be due to the limited cohort size or other unmeasured but potentially important parameters, such as tumor mutational burden, resistance mutations (i.e. B2m loss[188]), and PD-L1 expression, which may also affect response. Nevertheless, these data suggest the ultimate outcome of checkpoint blockade therapy may depend on the representation of more durable progenitor exhausted CD8+ T cells within the pool of exhausted cells.

In this study, we define the population of TILs – progenitor exhausted CD8+ T cells – that mediate superior tumor control and can respond to PD-1 blockade. This suggests that efforts to increase their frequency may represent an important therapeutic strategy. Moreover, given the intense interest in understanding the biomarkers that predict response to checkpoint blockade, our findings suggest that evaluating the specific state of exhaustion in CD8+ TILs, not just their numbers, may be an important predictor of immunotherapy response.

Materials and methods

Mice, cell lines, and TIL isolation

Female C57BL/6J mice and CD45.1$^+$ congenic mice (strain B6.SJL-*Ptprc*^{a}*Pepc*^{b}/BoyJ) were purchased from The Jackson Laboratory. B16.F10 cells and GVAX (B16 cells secreting GM-CSF) were a gift from G. Dranoff. D4M.3A cells were a gift from Dr. David Fisher[181]. Cells underwent intermittent mycoplasma testing using the LookOut Mycoplasma PCR detection kit (Sigma). Lentiviral transduction was used to express ovalbumin under control of the PGK promoter in all three cell lines. B2m-null B16-OVA cells were generated by CRISPR/Cas9-mediated deletion of B2m by transient transfection with PX459 (Addgene), a plasmid expressing Cas9 and a guide targeting B2m (sequence: CACCGACAAGCACCAGAAAGACCA). Cells were selected in puromycin and B2m deletion confirmed by flow cytometry.

Mice were subcutaneously implanted with 3 x 10^5 B16-OVA or 3 x 10^5 D4M.3A-OVA cells in 1x HBSS (Life Technologies). When needed, mice were vaccinated with an equal number of irradiated GVAX-OVA cells (3500 Gy). Tumors were measured starting at day 6 every 3 days. 100μg anti-PD-1 (clone 29F.1A12, BioXcell) or 100μg isotype control (Rat IgG2a, BioXCell) and 100μg anti-CTLA-4 (clone 9D9, BioXCell) or 100μg isotype control (Mouse IgG2b, BioXCell) were administered via intraperitoneal (IP) injection on days 9 and 12. On the indicated days post cancer cell injection, tumors were dissected from the surrounding fascia, mechanically minced, and treated with collagenase P (2mg/mL, Sigma) and DNAse I (50μg/mL, Sigma) for 10 minutes at 37°C. Tumor-infiltrating leukocytes were enriched using an Optiprep (Sigma) density gradient followed by CD45$^+$ or CD8$^+$ MACS positive selection (Miltenyi). When necessary, cells were sorted on a FACS Aria II (BD Biosciences) to obtain greater than 95% purity. Spleen and lymph nodes were dissected from euthanized mice, mechanically minced, and filtered to single-cell suspension. RBC lysis (ACK lysis buffer, Quality Biological) was performed on all spleen samples, followed by CD8+ MACS positive selection (Miltenyi).

From B16-OVA tumors the following gating strategies were used: progenitor exhausted cells (Live CD45$^+$CD8$^+$PD-1$^+$CD44$^+$Slamf6$^+$Tim-3$^-$); terminally exhausted cells (Live CD45$^+$CD8$^+$PD-1$^+$CD44$^+$Slamf6$^-$Tim-3$^+$), further gated on SIINFEKL-tetramer$^+$ or tetramer$^-$ populations as indicated. From LCMV-infected spleens the following gating strategies were used: progenitor exhausted cells (GP33-tetramer$^+$ Live CD45$^+$CD8$^+$CD44$^+$Slamf6$^+$Tim-3$^-$); terminally exhausted cells (GP33-tetramer$^+$ Live CD45$^+$CD8$^+$CD44$^+$Slamf6$^-$Tim-3$^+$). All *in vitro* T cell assays were performed using complete RPMI-10: RPMI-1640 (Gibco), 10% FCS (Gemini Bio-Products), 1% HEPES (Gibco), 0.5% penicillin/streptomycin (Life Technologies), and 0.1% β-mercaptoethanol (Gibco). All tumor cell lines were grown in complete DMEM-10: DMEM (Gibco), 10% FCS (Gemini Bio-Products), and 0.5% penicillin/streptomycin (Life Technologies). All animal procedures were performed in accordance with ethical regulations and pre-approved by the Dana-Farber Cancer Institute Institutional Animal Care and Use Committee.

Flow cytometry

Cells were blocked with anti-mouse CD16/32 antibody (BioLegend) and surface stained with indicated antibodies for 20 min at 4°C. Dead cells were excluded using Live/Dead (1:1,000, ThermoFisher Scientific) added concurrently with surface antibodies. When needed, cells were fixed with the Foxp3/Transcription Factor Staining Buffer Set (eBiosciences) for all stains except IL-2 as per manufacturer's instructions, blocked again with 5% mouse and rat serum + anti-mouse CD16/32 antibody, then stained with intracellular antibodies. For IL-2 staining, cells were fixed overnight with the BD Cytofix/Cytoperm Fixation and Permeabilization Solution (Fisher Scientific) as per manufacturer's instructions, blocked with 5% mouse and rat serum + anti-mouse CD16/32 antibody, then stained with intracellular antibodies. Annexin-V (Fisher Scientific) staining was performed after cell surface staining per the manufacturer's instructions. For BrdU experiments, mice were administered 1mg BrdU (BD Pharmingen) via IP injection at the indicated times prior

to tumor harvest. BrdU staining was performed after cell surface staining as per BrdU kit protocol. Spherotech AccuCount Fluorescent particles were added for cell quantification before analysis on an LSR Fortessa (BD Biosciences). Data was collected using FACSDiva (v.8.0.1, BD Pharmingen). Analysis was performed using FlowJo software (v10.4.1, TreeStar) using single-color compensation controls and fluorescence-minus-one thresholds to set gate margins.

LCMV viral infection

Mice were infected with LCMV Clone 13 (4 x 10^6 plaque-forming units (pfu) by intravenous injection) or LCMV Armstrong (2 x 10^5 pfu IP) as previously described[116]. Viral titers were assessed as previously described[189]. Briefly, diluted serum from infected animals was plated on Vero cells. The cells were covered with an agarose layer and allowed to form plaques over 96 hours. Live cells were stained with neutral red and plaques counted 14 hours later. All counts were normalized to serum volume.

***In vivo* transfer assay**

7-10 week old female C57BL/6J ($CD45.2^+$) mice were subcutaneously implanted with 3 x 10^5 B16-OVA cells on day 0. On day 3-5, they were vaccinated once with 3 x 10^5 GVAX cells. Progenitor exhausted or terminally exhausted TILs were sorted from day 19-21 tumors (approximately 1000-2000mm^3) as described above. After sorting, cells were centrifuged at 350 r.c.f. and resuspended in PBS. 50,000 progenitor or terminally exhausted cells were transferred via retroorbital IV injection into 7-10 week old female C57BL/6 ($CD45.2^+$) or $CD45.1^+$ congenic mice who had been subcutaneously implanted with 3 x 10^5 B16-OVA or 3 x 10^5 B16.F10 cells two days prior. Tumors were measured at day 6 and every 3 days afterwards. TILs were isolated on day 17-18 for analysis as previously described.

In vivo persistence and tumor challenge assays

Progenitor exhausted or terminally exhausted TILs were isolated from day 19-21 tumors as per the *in vivo* transfer assay above and 50,000 cells of each cell type were IV injected into two cohorts of female CD45.1$^+$ mice without tumors. After 30-40 days, the first cohort of mice was sacrificed to analyze secondary lymphoid organs. In the second cohort, after 30-40 days mice were subcutaneously implanted with 3 x 10^5 B16-OVA cells. On day 15-16 post tumor implantation, TILs were isolated as previously described to determine transferred cell numbers and phenotypes.

In vivo transfer with anti-PD-1 assay

Progenitor exhausted or terminally exhausted TILs were isolated from day 19-21 tumors as per the *in vivo* transfer assay above and 50,000 cells of each cell type were IV injected into female CD45.1$^+$ mice who had been subcutaneously implanted with 1 x 10^6 B16-OVA cells two days prior. Mice were treated with 100μg isotype control or anti-PD-1 antibodies on days 6, 9 and 12. Tumors were harvested on day 15 or 16 for analysis.

In vitro cytotoxicity, cytokine production, CFSE proliferation, and conversion

To compare the cytotoxicity of both subpopulations, we plated tetramer-positive progenitor exhausted or terminally exhausted CD8$^+$ T cells with a 1:1 mixture of target cells (B16-OVA) and control cells (B2m-null B16-OVA in which B2m has been deleted using CRISPR/Cas9, making them resistant to cell mediated cytotoxicity) (Fig. 4.5H-J). This competitive cytotoxicity assay allowed us to measure direct cytotoxicity while controlling for cytokine-mediated effects on tumor cell viability. Specifically, *in vitro* killing assay was performed by plating 5,000 B16-OVA (target) and 5,000 B2m-null B16-OVA (non-target) cells into 96 well flat-bottom plates for 24 hours with IFN-γ (100ng/mL, Cell Signaling Technology) to upregulate MHC-I, washing the cells with PBS,

then adding the indicated numbers of naive CD8$^+$ T splenocytes, sorted tetramer$^+$ progenitor exhausted cells, or tetramer$^+$ terminally exhausted cells to each well. After 40 hours, cells were trypsinized from the wells and stained for CD45, Slamf6, Tim-3, live/dead, and H-2K^b to determine the ratio of the two tumor cell populations and phenotype of the T cells. The ratio of target to non-target cells was normalized to the ratio of the populations in wells in which no T cells were added.

Evaluation of *in vitro* cytokine production was performed by sorting tetramer$^+$ CD8$^+$ TILs from day 19-21 B16-OVA tumors and plating 100,000 CD8$^+$ T cells with 100,000 irradiated splenic dendritic cells (isolated by CD11c$^+$ MACS positive selection and irradiated with 3000 cGy) with SIINFEKL peptide (1μM, Invivogen) and brefeldin A 3.0 μg/ml for 6 hours. Alternatively, we isolated CD8$^+$ TILs from day 19-21 B16-OVA tumors using CD8$^+$ MACS positive selection (Miltenyi) and plated 2 x 10^5 cells in 96 well plates with PMA 50ng/mL + ionomycin 1μg/mL + brefeldin A 3.0 μg/ml for 6 hours. The cells were stained for surface antigens, then fixed and stained for intracellular cytokines as described above.

In vitro CFSE proliferation was performed by sorting progenitor or terminally exhausted T cells from day 19-21 B16-OVA tumors or MACS-enriching naive CD8$^+$ splenocytes and labeling with 0.5μM CFSE for 8 minutes at 37°C. Cells were washed twice with RPMI-10, then counted. 50,000 cells per well were plated in 96-well U-bottom plates coated with 1μg/mL anti-CD3 (Fisher Scientific) and 1μg/mL anti-CD28 (Fisher Scientific) in RPMI-10 with recombinant human IL-2 100U/ml (DFCI supply center). Cells were harvested after 4 days and stained against CD8$^+$ and Live/dead and analyzed as previously described.

In vitro conversion was performed by sorting progenitor or terminally exhausted CD8$^+$ T cells from day 19-21 B16-OVA tumors and plating 50,000 cells per well in 96-well U-bottom plates coated with 1μg/mL anti-CD3 (Fisher Scientific) and 1μg/mL anti-CD28 (Fisher Scientific) in RPMI-10 without IL-2. After 36 hours in culture brefeldin A 3.0 μg/ml was added to the cultures

for 6 hours, then the cells were stained for surface antigens, fixed and stained for intracellular antigens as described above.

TCR sequencing

Tetramer negative progenitor exhausted or terminally exhausted cells were sorted from two separate pools of day 20 B16-OVA tumors as previously described to generate independent replicates. Genomic DNA was isolated using QIAamp DNA Blood Mini Kit (Qiagen), eluted in TE buffer, and sent to Adaptive Biotechnologies for sequencing. Analysis was performed on genomic TCRβ sequences using the ImmunoSEQ Analyzer platform (v3.0).

Bulk RNA-seq library preparation and analysis

Tetramer positive progenitor exhausted or terminally exhausted cells were sorted from spleens of day 30 LCMV Cl13 infected mice or day 22 B16-OVA tumors in pools of 400 cells into a microplate containing 20μL of RLT buffer (Qiagen) with 1% v/v beta-mercaptoethanol in each well. Immediately following sorting, the plates were sealed, vortexed briefly, spun at 400 xg for 1 min, and flash-frozen on dry ice for storage at -80C until library preparation. Cellular lysates were converted to cDNA in an adapted SmartSeq2 protocol as previously described[190].

Libraries were sequenced on a NextSeq500 instrument by 37bp paired-end reads. After demultiplexing, low-quality reads were trimmed with Trimmomatic (v0.33) using the following parameters: LEADING: 15, TRAILING: 15, SLIDINGWINDOW: 4:15, and MINLEN: 16. Trimmed reads were aligned to the mm10 mouse genome using Bowtie2 (v2.2.4). HTSeq (v0.6.1p1) was used to map aligned reads to genes and generate a gene count matrix. Technical replicates were averaged for each biologically independent sample. Gene counts were normalized by library size and differential expression analysis was performed using DESeq2 (v1.18.1). Following differential expression analysis between phenotypic groups, a ranking metric was calculated for each gene

as R = -$\log_{10}(q)$, where q is the FDR-adjusted P-value. Preranked GSEA[191] (v3.0) was performed using the C2, C5, and C7 gene-sets in the MSigDB database. In order to compare our data with other RNA-seq datasets from the literature, the top 150 differentially expressed genes (ranked by q value) were determined between the two indicated states for each sample generated as previously described or identified from the literature. A hypergeometric overlap test was performed to determine the overlap of each gene set with all others.

Single-cell RNA-seq library preparation and analysis

The following cells were sorted for single-cell RNA-seq: GP33-Tetramer$^+$ Live CD8$^+$PD-1$^+$CD44$^+$ cells from spleens of day 28 LCMV Cl13 infected mice; SIINFEKL-Tetramer$^+$ Live CD45$^+$CD8$^+$ cells from day 20 B16-OVA tumors and Live PD-1$^+$CD44$^+$CD45$^+$CD8$^+$ cells from day 10 B16-OVA tumors. Cells were counted and loaded onto the Chromium Controller (10x Genomics) for a target recovery of 5,000 single cells. Samples were processed per the manufacturer's protocol and sequenced on an Illumina NextSeq500 sequencer using a 75bp kit with paired-end reads. Sample demultiplexing, barcode processing, alignment, filtering, UMI counting, and aggregation of sequencing runs were performed using the Cell Ranger analysis pipeline (v1.2). Downstream analyses were performed in R using the Seurat package[192] (v2.1.0).

For each cell, two quality control metrics were calculated: (1) the total number of genes detected and (2) the proportion of UMIs contributed by mitochondrially encoded transcripts. Cells in which fewer than 200 genes were detected and in which mitochondrially encoded transcripts constituted greater than 10% of the total library were excluded from downstream analysis. Genes detected in fewer than three cells across the dataset were also excluded, yielding an expression matrix of 9,194 cells by 13,642 genes (LCMV), 11,212 cells by 14,496 genes (day 10 + 20 tumor), or 4,313 cells by 13,880 genes (day 20 tumor). Each gene expression measurement was normalized by total expression within the corresponding cell and multiplied by a scaling factor of 10,000. Mean and dispersion values were calculated for each gene across all cells; 1,653 genes

(LCMV), 1,234 genes (day 10 + 20 tumor), or 914 genes (day 20 tumor) classified as highly variable. Highly variable genes were used for principal components analysis (PCA). Principal components were determined to be significant ($P < 0.01$) using the jackstraw method and tSNE was performed on these significant PCs using default parameters for 1,000 iterations for visualization in two dimensions. Unsupervised clustering was performed using a shared nearest neighbor modularity optimization-based algorithm[193]. Differential expression analysis was performed between each cluster and all other cells using a Wilcoxon rank sum test. Single-cell signature scoring using FastProject[194] (v0.9.2) was performed with a curated version of the C7 Immune Signatures database from MSigDB. Significance of signature enrichment within single cell datasets of one cluster relative to other clusters was determined using a Kolmogorov–Smirnov test. FastProject signature scoring of $CD8^+$ T cells from tumors was performed in the scope of transcriptional signatures derived from the subpopulations we identified in LCMV or from signatures derived from the literature. Tumor cells were plotted on a two-dimensional axis based on their scores for the terminally exhausted and progenitor exhausted signatures on the x and y axes, respectively.

ATAC-seq library preparation and analysis

5,000-50,000 tetramer positive progenitor exhausted or terminally exhausted cells per replicate were sorted from spleens of day 30 LCMV Cl13 infected mice or day 22 B16-OVA tumors into PBS with 10% FBS. Pelleted cells were incubated in 5-50μl of reaction mix (containing 2x TD, Tn5 enzyme, 2% digitonin in nuclease-free water) as previously described[98]. The reaction was performed at 37°C for 30 minutes with agitation at 300 RPM. DNA was purified using a QIAgen MinElute Reaction Cleanup kit. Post-PCR bead cleanup was done using Agencourt AMPure XP bead cleanup (Beckman Coulter/Agencourt) and library quality was verified using Tapestation

analysis. Samples were sequenced on an Illumina NextSeq500 sequencer using paired-end 37bp reads.

Quality trimming and primer removal within raw fastq files were done with Trimmomatic (v0.33) using the following parameters: LEADING:15 TRAILING:15 SLIDINGWINDOW:4:15 MINLEN:36. Trimmed reads were aligned to mm9 with Bowtie2 (v2.2.4) using a maximum insert size of 1000. Aligned bams were sorted, duplicates marked, and reads mapping to the blacklist region removed[97]. Peak-calling using MACS (v2.1.1) was performed on merged bam files (Samtools v1.3) from biological replicates using a *q*-value threshold of 0.001. Consensus peaks from all biological conditions were merged to create a single peak universe. Cut sites were extracted from each biological replicate and the number of cuts within each peak region was quantified to generate a raw counts matrix. DESeq2 (v1.18.1) was used to normalize the counts matrix and perform differential accessibility analysis between all relevant comparisons. Tracks were visualized using Integrative Genomics Viewer (v2.3.77, Broad Institute). Gene to peak associations were determined using the GREAT software package (v3.0.0, http://bejerano.stanford.edu/great/public/html/) with default settings. K-means clustering was applied using GENE-E (v3.0.215, Broad Institute) to differential ChAR signal intensity across cell states. GENE-E was also used for heatmap visualization and similarity matrix calculations (Pearson). Principal component analysis was performed using R (v3.3.1, R Core Team). Gene Ontology (GO) term enrichment was performed for each biological condition using GREAT, with default settings and binomial enrichment. Motif enrichment analysis was performed using HOMER (v3.0) with default settings.

Human multiplex immunofluorescence and survival analysis

Through the Center for Immuno-Oncology, IRB-approved consent was obtained from patients with advanced melanoma to collect and analyze tumor samples as companion to the combination

treatment of Ipilimumab and Nivolumab they received. All human studies were performed in accordance with ethical regulations and pre-approved by the Dana-Farber Cancer Institute IRB (2016P002770). Formalin-fixed, paraffin embedded whole tissues from tumors were obtained from Department of Pathology, Brigham and Women's Hospital. Hematoxylin & eosin stained tissue sections and the diagnostic reports were reviewed by expert pathologists (S.J.R. and G.K.G.). Tissue sections of 4 μM thickness were obtained for each sample and stained with primary antibodies sequentially and paired with unique fluorochromes followed by DAPI staining per published protocol[195]. In brief, tissue sections were baked for 3 hours at 60°C before loading on BOND RX fully automated stainers (Leica Biosystems) for approximately 9 hours. Slides were deparaffinized (BOND DeWax Solution, Leica Biosystems) and rehydrated with sequential washes in graded ethanol to deionized water, followed by antigen retrieval in BOND Epitope Retrieval Solution 1 (ER1, Leica Biosystems) at pH 6 for 10 minutes at 98°C. Next, slides were serially stained with primary antibodies for 40 minutes. Anti-rabbit Polymeric Horseradish Peroxidase (Poly-HRP, BOND Polymer Refine Detection Kit, Leica Biosystems) was applied as a secondary label for 10 minutes. Signal for antibody complexes was visualized by their corresponding Opal Fluorophore Reagents (PerkinElmer) by incubating the slides for 5 minutes. Slides were air dried, mounted with Prolong Diamond Anti-fade mounting medium (#P36965, Life Technologies) and stored in a light-proof box at 4° C prior to imaging. 3-5 images per sample were obtained using the Mantra multispectral imaging platform (Vectra 3, PerkinElmer) at 20X resolution. Areas without tumor or with residual normal tissue (i.e. normal lymph node) were excluded. For each region, tiled fields of view (FOVs) were acquired at 20X resolution as multispectral images. Each FOV is spectrally separated and analyzed using Inform 2.3 software (PerkinElmer), a supervised machine learning algorithm which assigns phenotypes to all cells in the image, according to a combination of immunofluorescence characteristics associated with

nuclei (DAPI signal). Thresholds for "positive" staining and the accuracy of phenotypic algorithms were confirmed by the pathologist (S.J.R.) for each case.

Patients were characterized as having either a durable clinical benefit or no clinical benefit as defined[196]. Durable clinical benefit was defined as at least 6 months of freedom from disease or stable/decreased tumor burden from the first radiological can following treatment. Increased tumor volume or a clinical benefit lasting less than 6 months from the first post treatment radiological scan was defined as no durable clinical benefit. Progression free survival (PFS) was calculated from the date of treatment until radiological evidence of progression or unequivocal clinical progression as determined by the clinician, leading to treatment discontinuation/switch or death, whichever occurred first. Overall survival (OS) was calculated from the date of treatment until date of death or censure.

Statistical analysis

All mouse experiments were randomized prior to treatment without investigator blinding, and sample sizes of 5-10 animals per experimental arm were chosen to ensure adequate power. Paired two-sided t-tests were run on comparisons within experimental animals, and all other experimental data were analyzed using unpaired two-sided Student's t-tests in Graphpad Prism 7. Rout outlier tests were run with default parameters in Prism on all mouse experimental data. Statistical analysis of differential gene expression and differential chromatin accessibility tests was done using DESeq2, and FDR correction was performed using the Benjamini-Hochberg method in R (v3.3.1). Significance of GO term enrichments and motif enrichments were calculated with binomial tests and hypergeometric tests. Survival analysis was performed using the Cox proportional hazards model and likelihood ratio tests using the Survminor (v0.4.1) and Survival (v2.43.3) packages in R. All significant variables from the univariable analysis were included in the multivariable analysis. P-values and q-values < 0.05 were considered to indicate a significant

difference. Asterisks used to indicate significance correspond with: n.s. $p > 0.05$, * $p \leq 0.05$, ** $p \leq 0.01$, *** $p \leq 0.001$, **** $p \leq 0.0001$.

Data Availability

All sequencing data from this study have been deposited in the National Center for Biotechnology Information Gene Expression Omnibus (GEO) and are accessible through the GEO Series accession number GSE122713.

Chapter 5. Conclusions

The development of T cell exhaustion is a defining feature of chronic viral infections and cancer. In this thesis, we have sought to understand the regulatory "switches" that control the development of functional versus exhausted $CD8^+$ T cells. Using novel techniques to define changes in chromatin accessibility, we show that exhaustion is a distinct and stable state of T cell differentiation, maintained by a unique epigenetic landscape in both chronic viral infection and cancer. We identify state-specific enhancers that regulate key molecules such as PD-1, highlighting that exhausted $CD8^+$ T cells have fundamentally different "wiring" that is central to their dysfunction. Critically, we observe that checkpoint blockade immunotherapy as well as direct-acting antiviral therapy do not fundamentally reverse exhaustion-associated epigenetic changes. Exhaustion is therefore a conserved, stable epigenetic state that becomes fixed and persists independent of chronic antigen stimulation.

In particular, this work has three major findings with therapeutic implications. First, we show that the development of T cell exhaustion involves the establishment of a distinct epigenetic program. Indeed, changes in chromatin accessibility during chronic infection were far more extensive than the relative changes in gene expression, suggesting that redundant epigenetic mechanisms may mediate "phenotypic robustness" of the exhausted state[197]. Marked differences in enhancer availability relative to acute infection that were evident by day 8 post-infection, clearly preceding functional defects. This suggests that the most successful strategies to address T cell exhaustion must prevent the early establishment of this exhaustion program.

The field is now interested in new CRISPR-Cas9 based genome and epigenome editing technologies for targeted manipulation of T cells[198, 199]. Our work could provide a roadmap for rational engineering to prevent $CD8^+$ T cell exhaustion. We provide proof-of-concept here by targeting an exhaustion-specific enhancer near PD-1 and selectively reducing, but not ablating, the aberrant up-regulation of PD-1 *in vitro*.

We are currently characterizing mice with a germ-line deletion of this region to understand the role of this enhancer *in vivo*. In preliminary experiments, we observe 2-3-fold enrichment of PD-1 enhancer-null cells over control cells in chronic LCMV infection. Critically, cells in the hematopoietic system at baseline have demonstrated no major differences, potentially avoiding deleterious side effects seen with PD-1 gene KO experiments[30, 31, 32, 200]. Therefore, editing exhaustion-specific enhancers may provide a more "tunable" and state-specific approach to modulate T cell function than deleting coding regions of genes.

Second, we show that the epigenetic state of exhaustion in $CD8^+$ T cells is largely irreversible, even after cure of infection or checkpoint blockade therapy. In particular, we describe epigenetic "scars" of exhaustion that are retained more than a year after curative therapy. A possibility remains that epigenetic recovery simply occurs on a longer time-scale. Therefore, further study is required to assess maintenance of this scarring and to resolve whether observed differences could be driven by underlying changes in population dynamics. Nevertheless, these findings are consistent with studies showing limited $CD8^+$ T cell reactivity to HIV antigens after successful anti-retroviral therapy (ART)[201].

Many have attributed the striking anti-tumor efficacy PD-1 blockade in part to reversal of T cell dysfunction in the TME[148]. While transient improvements have been observed in $CD8^+$ T cell frequency and effector function, an ongoing collaboration with John Wherry's group first revealed the epigenetic inflexibility of T cells in chronic LCMV post-PD-1 checkpoint blockade[150]. Here, we extend these findings to $CD8^+$ T cells in the tumor microenvironment. Therapeutic efforts to reverse exhaustion, therefore, needs to focus on initiating global epigenetic changes. One possible approach could rely on the action of chromatin modifying drugs such as histone deacetylase (HDAC) inhibitors, histone acetyl transferase (HAT) inhibitors and DNA methyl-transferase (DNMT) inhibitors. Indeed, changes in DNA methylation have also been recently defined within exhausted T cells, with loss of Dnmt3a restoring some functionality[202]. Many of these drug classes are already being tested in clinical settings to reverse HIV latency[203], as well

as to modulate expression of tumor-suppressors and oncogenes[204]. We propose that these trials could be leveraged to investigate the ability of epigenome modifying compounds to reprogram $CD8^+$ T cell exhaustion.

Third, we identify subsets of functionally specialized $CD8^+$ exhausted TILs and define their role in mediating long-term tumor control. Exhausted $CD8^+$ TILs can be broadly separated into two transcriptionally, epigenetically and functionally distinct states: progenitor exhausted and terminally exhausted. Our data suggests that a balance of both populations is important for effective immunity in the tumor microenvironment. Therefore, we suggest that the development of rational immunotherapy combinations to "tune" the balance of progenitor and terminally exhausted cells in tumors may improve immune responses in the tumor microenvironment.

In addition to extending our understanding of the heterogeneity and functionality of exhausted $CD8^+$ TILs, our work has important implications for understanding the regulation of T cell exhaustion. Here, we resolve a long-standing controversy in the field about how T cell dysfunction in the tumor relates to canonical T cell exhaustion. By comparing chronic viral infection and cancer, we show that exhausted T cells adopt a similar epigenetic profile in response to chronic antigen, regardless of the disease state. Therefore, T cell exhaustion may have evolved as a host strategy to preserve specific aspects of T cell effector function while reducing bystander host tissue damage.

Despite its initial description as a mechanism for limiting virus-induced immunopathology, this property has not always been appreciated in the subsequent literature. Misconceptions about the extent to which exhausted T cells can mediate effector function, and the contexts in which they arise are not uncommon. Furthermore, the degeneracy of exhaustion-associated cell surface markers may contribute to this confusion, and cloud future avenues of research. By mapping chromatin accessibility changes in several contexts of T cell exhaustion, we establish a core epigenetic signature that can act as a precise biomarker of the exhausted state.

Defining this core program may also allow identification of transcription factors that act as a “master regulator” of the exhausted state. While TFs such as T-bet[68, 172], Eomes[172], NFAT[69], Blimp-1[67], and Batf[65] have been implicated in T cell exhaustion, all of these also have important roles in other aspects of T cell differentiation and function. Through analysis of differential enhancer activity near epigenetic scars, our data prioritizes transcription factors such as Tox and Hif1a as key candidate regulators that may govern the exhausted state. Therefore, these transcription factors could represent novel therapeutic targets for improving T cell immunity to cancers and increasing the efficacy of adoptive T cell therapy.

Overall, our work dissecting the epigenetic determinants of T cell exhaustion demonstrates that it is a fundamental adaptation in response to chronic antigen exposure. We also reveal state-specific mechanisms of gene regulation and offer strategies for rational engineering to prevent or reverse T cell exhaustion.

Bibliography

1. Moskophidis, D., Lechner, F., Pircher, H. & Zinkernagel, R.M. Virus persistence in acutely infected immunocompetent mice by exhaustion of antiviral cytotoxic effector T cells. *Nature* **362**, 758-761 (1993).

2. Altman, J.D. *et al.* Phenotypic analysis of antigen-specific T lymphocytes. *Science* **274**, 94-96 (1996).

3. Gallimore, A. *et al.* Induction and exhaustion of lymphocytic choriomeningitis virus-specific cytotoxic T lymphocytes visualized using soluble tetrameric major histocompatibility complex class I-peptide complexes. *J Exp Med* **187**, 1383-1393 (1998).

4. Zajac, A.J. *et al.* Viral immune evasion due to persistence of activated T cells without effector function. *J Exp Med* **188**, 2205-2213 (1998).

5. Zhou, X., Ramachandran, S., Mann, M. & Popkin, D.L. Role of lymphocytic choriomeningitis virus (LCMV) in understanding viral immunology: past, present and future. *Viruses* **4**, 2650-2669 (2012).

6. Salvato, M., Borrow, P., Shimomaye, E. & Oldstone, M.B. Molecular basis of viral persistence: a single amino acid change in the glycoprotein of lymphocytic choriomeningitis virus is associated with suppression of the antiviral cytotoxic T-lymphocyte response and establishment of persistence. *J Virol* **65**, 1863-1869 (1991).

7. Pircher, H., Burki, K., Lang, R., Hengartner, H. & Zinkernagel, R.M. Tolerance induction in double specific T-cell receptor transgenic mice varies with antigen. *Nature* **342**, 559-561 (1989).

8. Matloubian, M., Concepcion, R.J. & Ahmed, R. CD4+ T cells are required to sustain CD8+ cytotoxic T-cell responses during chronic viral infection. *J Virol* **68**, 8056-8063 (1994).

9. Wherry, E.J., Blattman, J.N., Murali-Krishna, K., van der Most, R. & Ahmed, R. Viral persistence alters CD8 T-cell immunodominance and tissue distribution and results in distinct stages of functional impairment. *J Virol* **77**, 4911-4927 (2003).

10. Shin, H., Blackburn, S.D., Blattman, J.N. & Wherry, E.J. Viral antigen and extensive division maintain virus-specific CD8 T cells during chronic infection. *J Exp Med* **204**, 941-949 (2007).

11. Angelosanto, J.M., Blackburn, S.D., Crawford, A. & Wherry, E.J. Progressive loss of memory T cell potential and commitment to exhaustion during chronic viral infection. *J Virol* **86**, 8161-8170 (2012).

12. Kaech, S.M. *et al.* Selective expression of the interleukin 7 receptor identifies effector CD8 T cells that give rise to long-lived memory cells. *Nat Immunol* **4**, 1191-1198 (2003).

13. Joshi, N.S. *et al.* Inflammation directs memory precursor and short-lived effector CD8(+) T cell fates via the graded expression of T-bet transcription factor. *Immunity* **27**, 281-295 (2007).

14. Schmitz, J.E. *et al.* Control of viremia in simian immunodeficiency virus infection by CD8+ lymphocytes. *Science* **283**, 857-860 (1999).

15. Appay, V. *et al.* HIV-specific CD8(+) T cells produce antiviral cytokines but are impaired in cytolytic function. *J Exp Med* **192**, 63-75 (2000).

16. Goepfert, P.A. *et al.* A significant number of human immunodeficiency virus epitope-specific cytotoxic T lymphocytes detected by tetramer binding do not produce gamma interferon. *J Virol* **74**, 10249-10255 (2000).

17. Kostense, S. *et al.* Persistent numbers of tetramer+ CD8(+) T cells, but loss of interferon-gamma+ HIV-specific T cells during progression to AIDS. *Blood* **99**, 2505-2511 (2002).

18. Lichterfeld, M. *et al.* Loss of HIV-1-specific CD8+ T cell proliferation after acute HIV-1 infection and restoration by vaccine-induced HIV-1-specific CD4+ T cells. *J Exp Med* **200**, 701-712 (2004).

19. Migueles, S.A. *et al.* HIV-specific CD8+ T cell proliferation is coupled to perforin expression and is maintained in nonprogressors. *Nat Immunol* **3**, 1061-1068 (2002).

20. Zhang, D. *et al.* Most antiviral CD8 T cells during chronic viral infection do not express high levels of perforin and are not directly cytotoxic. *Blood* **101**, 226-235 (2003).

21. Gruener, N.H. *et al.* Sustained dysfunction of antiviral CD8+ T lymphocytes after infection with hepatitis C virus. *J Virol* **75**, 5550-5558 (2001).

22. Wedemeyer, H. *et al.* Impaired effector function of hepatitis C virus-specific CD8+ T cells in chronic hepatitis C virus infection. *J Immunol* **169**, 3447-3458 (2002).

23. Barber, D.L. *et al.* Restoring function in exhausted CD8 T cells during chronic viral infection. *Nature* **439**, 682-687 (2006).

24. Freeman, G.J. *et al.* Engagement of the PD-1 immunoinhibitory receptor by a novel B7 family member leads to negative regulation of lymphocyte activation. *J Exp Med* **192**, 1027-1034 (2000).

25. Latchman, Y. *et al.* PD-L2 is a second ligand for PD-1 and inhibits T cell activation. *Nat Immunol* **2**, 261-268 (2001).

26. Latchman, Y.E. *et al.* PD-L1-deficient mice show that PD-L1 on T cells, antigen-presenting cells, and host tissues negatively regulates T cells. *Proc Natl Acad Sci U S A* **101**, 10691-10696 (2004).

27. Ishida, Y., Agata, Y., Shibahara, K. & Honjo, T. Induced expression of PD-1, a novel member of the immunoglobulin gene superfamily, upon programmed cell death. *EMBO J* **11**, 3887-3895 (1992).

28. Shinohara, T., Taniwaki, M., Ishida, Y., Kawaichi, M. & Honjo, T. Structure and chromosomal localization of the human PD-1 gene (PDCD1). *Genomics* **23**, 704-706 (1994).

29. Nishimura, H., Minato, N., Nakano, T. & Honjo, T. Immunological studies on PD-1 deficient mice: implication of PD-1 as a negative regulator for B cell responses. *Int Immunol* **10**, 1563-1572 (1998).

30. Nishimura, H., Nose, M., Hiai, H., Minato, N. & Honjo, T. Development of lupus-like autoimmune diseases by disruption of the PD-1 gene encoding an ITIM motif-carrying immunoreceptor. *Immunity* **11**, 141-151 (1999).

31. Nishimura, H. *et al.* Autoimmune dilated cardiomyopathy in PD-1 receptor-deficient mice. *Science* **291**, 319-322 (2001).

32. Keir, M.E., Freeman, G.J. & Sharpe, A.H. PD-1 regulates self-reactive CD8+ T cell responses to antigen in lymph nodes and tissues. *J Immunol* **179**, 5064-5070 (2007).

33. Petrovas, C. *et al.* SIV-specific CD8+ T cells express high levels of PD1 and cytokines but have impaired proliferative capacity in acute and chronic SIVmac251 infection. *Blood* **110**, 928-936 (2007).

34. Trautmann, L. *et al.* Upregulation of PD-1 expression on HIV-specific CD8+ T cells leads to reversible immune dysfunction. *Nat Med* **12**, 1198-1202 (2006).

35. Day, C.L. *et al.* PD-1 expression on HIV-specific T cells is associated with T-cell exhaustion and disease progression. *Nature* **443**, 350-354 (2006).

36. Petrovas, C. *et al.* PD-1 is a regulator of virus-specific CD8+ T cell survival in HIV infection. *J Exp Med* **203**, 2281-2292 (2006).

37. Urbani, S. *et al.* PD-1 expression in acute hepatitis C virus (HCV) infection is associated with HCV-specific CD8 exhaustion. *J Virol* **80**, 11398-11403 (2006).

38. Radziewicz, H. *et al.* Liver-infiltrating lymphocytes in chronic human hepatitis C virus infection display an exhausted phenotype with high levels of PD-1 and low levels of CD127 expression. *J Virol* **81**, 2545-2553 (2007).

39. Boni, C. *et al.* Characterization of hepatitis B virus (HBV)-specific T-cell dysfunction in chronic HBV infection. *J Virol* **81**, 4215-4225 (2007).

40. Golden-Mason, L. *et al.* Upregulation of PD-1 expression on circulating and intrahepatic hepatitis C virus-specific CD8+ T cells associated with reversible immune dysfunction. *J Virol* **81**, 9249-9258 (2007).

41. Nakamoto, N. *et al.* Functional restoration of HCV-specific CD8 T cells by PD-1 blockade is defined by PD-1 expression and compartmentalization. *Gastroenterology* **134**, 1927-1937, 1937 e1921-1922 (2008).

42. Fisicaro, P. *et al.* Antiviral intrahepatic T-cell responses can be restored by blocking programmed death-1 pathway in chronic hepatitis B. *Gastroenterology* **138**, 682-693, 693 e681-684 (2010).

43. Velu, V. *et al.* Enhancing SIV-specific immunity in vivo by PD-1 blockade. *Nature* **458**, 206-210 (2009).

44. Topalian, S.L. *et al.* Safety, activity, and immune correlates of anti-PD-1 antibody in cancer. *N Engl J Med* **366**, 2443-2454 (2012).

45. Ribas, A. & Wolchok, J.D. Cancer immunotherapy using checkpoint blockade. *Science* **359**, 1350-1355 (2018).

46. Dong, H. *et al.* Tumor-associated B7-H1 promotes T-cell apoptosis: a potential mechanism of immune evasion. *Nat Med* **8**, 793-800 (2002).

47. Iwai, Y., Terawaki, S. & Honjo, T. PD-1 blockade inhibits hematogenous spread of poorly immunogenic tumor cells by enhanced recruitment of effector T cells. *Int Immunol* **17**, 133-144 (2005).

48. Hirano, F. *et al.* Blockade of B7-H1 and PD-1 by monoclonal antibodies potentiates cancer therapeutic immunity. *Cancer Res* **65**, 1089-1096 (2005).

49. Zippelius, A. *et al.* Effector function of human tumor-specific CD8 T cells in melanoma lesions: a state of local functional tolerance. *Cancer Res* **64**, 2865-2873 (2004).

50. Ahmadzadeh, M. *et al.* Tumor antigen-specific CD8 T cells infiltrating the tumor express high levels of PD-1 and are functionally impaired. *Blood* **114**, 1537-1544 (2009).

51. Mumprecht, S., Schurch, C., Schwaller, J., Solenthaler, M. & Ochsenbein, A.F. Programmed death 1 signaling on chronic myeloid leukemia-specific T cells results in T-cell exhaustion and disease progression. *Blood* **114**, 1528-1536 (2009).

52. Long, A.H. *et al.* 4-1BB costimulation ameliorates T cell exhaustion induced by tonic signaling of chimeric antigen receptors. *Nat Med* **21**, 581-590 (2015).

53. Cherkassky, L. *et al.* Human CAR T cells with cell-intrinsic PD-1 checkpoint blockade resist tumor-mediated inhibition. *J Clin Invest* **126**, 3130-3144 (2016).

54. Gros, A. *et al.* PD-1 identifies the patient-specific CD8(+) tumor-reactive repertoire infiltrating human tumors. *J Clin Invest* **124**, 2246-2259 (2014).

55. Baitsch, L. *et al.* Exhaustion of tumor-specific CD8(+) T cells in metastases from melanoma patients. *J Clin Invest* **121**, 2350-2360 (2011).

56. Schietinger, A. *et al.* Tumor-Specific T Cell Dysfunction Is a Dynamic Antigen-Driven Differentiation Program Initiated Early during Tumorigenesis. *Immunity* **45**, 389-401 (2016).

57. Singer, M. *et al.* A Distinct Gene Module for Dysfunction Uncoupled from Activation in Tumor-Infiltrating T Cells. *Cell* **166**, 1500-1511 e1509 (2016).

58. Blank, C. *et al.* Absence of programmed death receptor 1 alters thymic development and enhances generation of CD4/CD8 double-negative TCR-transgenic T cells. *J Immunol* **171**, 4574-4581 (2003).

59. Agata, Y. *et al.* Expression of the PD-1 antigen on the surface of stimulated mouse T and B lymphocytes. *Int Immunol* **8**, 765-772 (1996).

60. Brown, J.A. *et al.* Blockade of programmed death-1 ligands on dendritic cells enhances T cell activation and cytokine production. *J Immunol* **170**, 1257-1266 (2003).

61. Iwai, Y., Terawaki, S., Ikegawa, M., Okazaki, T. & Honjo, T. PD-1 inhibits antiviral immunity at the effector phase in the liver. *J Exp Med* **198**, 39-50 (2003).

62. Wherry, E.J. *et al.* Molecular signature of CD8+ T cell exhaustion during chronic viral infection. *Immunity* **27**, 670-684 (2007).

63. Blackburn, S.D. *et al.* Coregulation of CD8+ T cell exhaustion by multiple inhibitory receptors during chronic viral infection. *Nat Immunol* **10**, 29-37 (2009).

64. Doering, T.A. *et al.* Network analysis reveals centrally connected genes and pathways involved in CD8+ T cell exhaustion versus memory. *Immunity* **37**, 1130-1144 (2012).

65. Quigley, M. *et al.* Transcriptional analysis of HIV-specific CD8+ T cells shows that PD-1 inhibits T cell function by upregulating BATF. *Nat Med* **16**, 1147-1151 (2010).

66. Wolski, D. *et al.* Early Transcriptional Divergence Marks Virus-Specific Primary Human CD8(+) T Cells in Chronic versus Acute Infection. *Immunity* **47**, 648-663 e648 (2017).

67. Shin, H. *et al.* A role for the transcriptional repressor Blimp-1 in CD8(+) T cell exhaustion during chronic viral infection. *Immunity* **31**, 309-320 (2009).

68. Kao, C. *et al.* Transcription factor T-bet represses expression of the inhibitory receptor PD-1 and sustains virus-specific CD8+ T cell responses during chronic infection. *Nat Immunol* **12**, 663-671 (2011).

69. Martinez, G.J. *et al.* The transcription factor NFAT promotes exhaustion of activated CD8(+) T cells. *Immunity* **42**, 265-278 (2015).

70. Moffett, H.F. *et al.* The microRNA miR-31 inhibits CD8(+) T cell function in chronic viral infection. *Nat Immunol* **18**, 791-799 (2017).

71. Goldberg, A.D., Allis, C.D. & Bernstein, E. Epigenetics: a landscape takes shape. *Cell* **128**, 635-638 (2007).

72. Allis, C.D. & Jenuwein, T. The molecular hallmarks of epigenetic control. *Nat Rev Genet* **17**, 487-500 (2016).

73. Klemm, S.L., Shipony, Z. & Greenleaf, W.J. Chromatin accessibility and the regulatory epigenome. *Nat Rev Genet* (2019).

74. Waddington, C.H. *The strategy of the genes; a discussion of some aspects of theoretical biology*. Allen & Unwin: London,, 1957.

75. Benoist, C. & Chambon, P. In vivo sequence requirements of the SV40 early promotor region. *Nature* **290**, 304-310 (1981).

76. Banerji, J., Rusconi, S. & Schaffner, W. Expression of a beta-globin gene is enhanced by remote SV40 DNA sequences. *Cell* **27**, 299-308 (1981).

77. Banerji, J., Olson, L. & Schaffner, W. A lymphocyte-specific cellular enhancer is located downstream of the joining region in immunoglobulin heavy chain genes. *Cell* **33**, 729-740 (1983).

78. Gillies, S.D., Morrison, S.L., Oi, V.T. & Tonegawa, S. A tissue-specific transcription enhancer element is located in the major intron of a rearranged immunoglobulin heavy chain gene. *Cell* **33**, 717-728 (1983).

79. Xi, H. *et al.* Identification and characterization of cell type-specific and ubiquitous chromatin regulatory structures in the human genome. *PLoS Genet* **3**, e136 (2007).

80. Felsenfeld, G., Boyes, J., Chung, J., Clark, D. & Studitsky, V. Chromatin structure and gene expression. *Proc Natl Acad Sci U S A* **93**, 9384-9388 (1996).

81. Okano, M., Bell, D.W., Haber, D.A. & Li, E. DNA methyltransferases Dnmt3a and Dnmt3b are essential for de novo methylation and mammalian development. *Cell* **99**, 247-257 (1999).

82. Bird, A. DNA methylation patterns and epigenetic memory. *Genes Dev* **16**, 6-21 (2002).

83. Mikkelsen, T.S. *et al.* Genome-wide maps of chromatin state in pluripotent and lineage-committed cells. *Nature* **448**, 553-560 (2007).

84. Ernst, J. *et al.* Mapping and analysis of chromatin state dynamics in nine human cell types. *Nature* **473**, 43-49 (2011).

85. Heintzman, N.D. *et al.* Distinct and predictive chromatin signatures of transcriptional promoters and enhancers in the human genome. *Nat Genet* **39**, 311-318 (2007).

86. Creyghton, M.P. *et al.* Histone H3K27ac separates active from poised enhancers and predicts developmental state. *Proc Natl Acad Sci U S A* **107**, 21931-21936 (2010).

87. Boyer, L.A. *et al.* Polycomb complexes repress developmental regulators in murine embryonic stem cells. *Nature* **441**, 349-353 (2006).

88. Jenuwein, T. & Allis, C.D. Translating the histone code. *Science* **293**, 1074-1080 (2001).

89. Lee, C.K., Shibata, Y., Rao, B., Strahl, B.D. & Lieb, J.D. Evidence for nucleosome depletion at active regulatory regions genome-wide. *Nat Genet* **36**, 900-905 (2004).

90. Kaplan, N. *et al.* The DNA-encoded nucleosome organization of a eukaryotic genome. *Nature* **458**, 362-366 (2009).

91. Wu, C. The 5' ends of Drosophila heat shock genes in chromatin are hypersensitive to DNase I. *Nature* **286**, 854-860 (1980).

92. Elgin, S.C. The formation and function of DNase I hypersensitive sites in the process of gene activation. *J Biol Chem* **263**, 19259-19262 (1988).

93. Crawford, G.E. *et al.* DNase-chip: a high-resolution method to identify DNase I hypersensitive sites using tiled microarrays. *Nat Methods* **3**, 503-509 (2006).

94. Sabo, P.J. *et al.* Genome-scale mapping of DNase I sensitivity in vivo using tiling DNA microarrays. *Nat Methods* **3**, 511-518 (2006).

95. Boyle, A.P. *et al.* High-resolution mapping and characterization of open chromatin across the genome. *Cell* **132**, 311-322 (2008).

96. Thurman, R.E. *et al.* The accessible chromatin landscape of the human genome. *Nature* **489**, 75-82 (2012).

97. Buenrostro, J.D., Giresi, P.G., Zaba, L.C., Chang, H.Y. & Greenleaf, W.J. Transposition of native chromatin for fast and sensitive epigenomic profiling of open chromatin, DNA-binding proteins and nucleosome position. *Nat Methods* **10**, 1213-1218 (2013).

98. Corces, M.R. *et al.* Lineage-specific and single-cell chromatin accessibility charts human hematopoiesis and leukemia evolution. *Nat Genet* **48**, 1193-1203 (2016).

99. Buenrostro, J.D. *et al.* Single-cell chromatin accessibility reveals principles of regulatory variation. *Nature* **523**, 486-490 (2015).

100. Corces, M.R. *et al.* The chromatin accessibility landscape of primary human cancers. *Science* **362** (2018).

101. Lara-Astiaso, D. *et al.* Immunogenetics. Chromatin state dynamics during blood formation. *Science* **345**, 943-949 (2014).

102. Buenrostro, J.D. *et al.* Integrated Single-Cell Analysis Maps the Continuous Regulatory Landscape of Human Hematopoietic Differentiation. *Cell* **173**, 1535-1548 e1516 (2018).

103. John, S. *et al.* Chromatin accessibility pre-determines glucocorticoid receptor binding patterns. *Nat Genet* **43**, 264-268 (2011).

104. Barozzi, I. *et al.* Coregulation of transcription factor binding and nucleosome occupancy through DNA features of mammalian enhancers. *Mol Cell* **54**, 844-857 (2014).

105. Farh, K.K. *et al.* Genetic and epigenetic fine mapping of causal autoimmune disease variants. *Nature* **518**, 337-343 (2015).

106. Canver, M.C. *et al.* BCL11A enhancer dissection by Cas9-mediated in situ saturating mutagenesis. *Nature* **527**, 192-197 (2015).

107. Smith, E.C. *et al.* Strict in vivo specificity of the Bcl11a erythroid enhancer. *Blood* **128**, 2338-2342 (2016).

108. Vahedi, G. *et al.* STATs shape the active enhancer landscape of T cell populations. *Cell* **151**, 981-993 (2012).

109. Russ, B.E. *et al.* Distinct epigenetic signatures delineate transcriptional programs during virus-specific CD8(+) T cell differentiation. *Immunity* **41**, 853-865 (2014).

110. Utzschneider, D.T. *et al.* T cells maintain an exhausted phenotype after antigen withdrawal and population reexpansion. *Nat Immunol* **14**, 603-610 (2013).

111. Youngblood, B. *et al.* Chronic virus infection enforces demethylation of the locus that encodes PD-1 in antigen-specific CD8(+) T cells. *Immunity* **35**, 400-412 (2011).

112. Youngblood, B. *et al.* Cutting edge: Prolonged exposure to HIV reinforces a poised epigenetic program for PD-1 expression in virus-specific CD8 T cells. *J Immunol* **191**, 540-544 (2013).

113. Hashimoto, M. *et al.* CD8 T Cell Exhaustion in Chronic Infection and Cancer: Opportunities for Interventions. *Annu Rev Med* **69**, 301-318 (2018).

114. Moguche, A.O. *et al.* Antigen Availability Shapes T Cell Differentiation and Function during Tuberculosis. *Cell Host Microbe* **21**, 695-706 e695 (2017).

115. McKinney, E.F., Lee, J.C., Jayne, D.R., Lyons, P.A. & Smith, K.G. T-cell exhaustion, co-stimulation and clinical outcome in autoimmunity and infection. *Nature* **523**, 612-616 (2015).

116. Zajac, A.J. *et al.* Viral Immune Evasion Due to Persistence of Activated T Cells Without Effector Function. *The Journal of Experimental Medicine* **188**, 2205-2213 (1998).

117. Barber, D.L. *et al.* Restoring function in exhausted CD8 T cells during chronic viral infection. *Nature* **439**, 682-687 (2006).

118. Porter, D.L., Levine, B.L., Kalos, M., Bagg, A. & June, C.H. Chimeric antigen receptor-modified T cells in chronic lymphoid leukemia. *N Engl J Med* **365**, 725-733 (2011).

119. Gallimore, A. *et al.* Induction and Exhaustion of Lymphocytic Choriomeningitis Virus–specific Cytotoxic T Lymphocytes Visualized Using Soluble Tetrameric Major Histocompatibility Complex Class I–Peptide Complexes. *The Journal of Experimental Medicine* **187**, 1383-1393 (1998).

120. Kaech, S.M. & Cui, W. Transcriptional control of effector and memory CD8+ T cell differentiation. *Nat Rev Immunol* **12**, 749-761 (2012).

121. Austin, J.W., Lu, P., Majumder, P., Ahmed, R. & Boss, J.M. STAT3, STAT4, NFATc1, and CTCF regulate PD-1 through multiple novel regulatory regions in murine T cells. *J Immunol* **192**, 4876-4886 (2014).

122. Vierstra, J. *et al.* Mouse regulatory DNA landscapes reveal global principles of cis-regulatory evolution. *Science* **346**, 1007-1012 (2014).

123. Raimondi, G., Shufesky, W.J., Tokita, D., Morelli, A.E. & Thomson, A.W. Regulated compartmentalization of programmed cell death-1 discriminates CD4+CD25+ resting regulatory T cells from activated T cells. *J Immunol* **176**, 2808-2816 (2006).

124. Shalem, O. *et al.* Genome-scale CRISPR-Cas9 knockout screening in human cells. *Science (New York, N.Y.)* **343**, 84-87 (2014).

125. Vierstra, J. *et al.* Functional footprinting of regulatory DNA. *Nat Methods* **12**, 927-930 (2015).

126. Gjoneska, E. *et al.* Conserved epigenomic signals in mice and humans reveal immune basis of Alzheimer/'s disease. *Nature* **518**, 365-369 (2015).

127. Villar, D. *et al.* Enhancer evolution across 20 mammalian species. *Cell* **160**, 554-566 (2015).

128. Stelekati, E. *et al.* Bystander chronic infection negatively impacts development of CD8(+) T cell memory. *Immunity* **40**, 801-813 (2014).

129. Rutebemberwa, A. *et al.* High-programmed death-1 levels on hepatitis C virus-specific T cells during acute infection are associated with viral persistence and require preservation of cognate antigen during chronic infection. *J Immunol* **181**, 8215-8225 (2008).

130. Kasprowicz, V. *et al.* High level of PD-1 expression on hepatitis C virus (HCV)-specific CD8+ and CD4+ T cells during acute HCV infection, irrespective of clinical outcome. *J Virol* **82**, 3154-3160 (2008).

131. Gupta, P.K. *et al.* CD39 Expression Identifies Terminally Exhausted CD8+ T Cells. *PLoS Pathog* **11**, e1005177 (2015).

132. Stromnes, I.M. *et al.* T Cells Engineered against a Native Antigen Can Surmount Immunologic and Physical Barriers to Treat Pancreatic Ductal Adenocarcinoma. *Cancer Cell* **28**, 638-652 (2015).

133. Hendel, A. *et al.* Chemically modified guide RNAs enhance CRISPR-Cas genome editing in human primary cells. *Nat Biotechnol* **33**, 985-989 (2015).

134. Schumann, K. *et al.* Generation of knock-in primary human T cells using Cas9 ribonucleoproteins. *Proc Natl Acad Sci U S A* **112**, 10437-10442 (2015).

135. Kurachi, M. *et al.* The transcription factor BATF operates as an essential differentiation checkpoint in early effector CD8+ T cells. *Nat Immunol* **15**, 373-383 (2014).

136. Odorizzi, P.M., Pauken, K.E., Paley, M.A., Sharpe, A. & Wherry, E.J. Genetic absence of PD-1 promotes accumulation of terminally differentiated exhausted CD8+ T cells. *The Journal of experimental medicine* (2015).

137. Langmead, B., Trapnell, C., Pop, M. & Salzberg, S.L. Ultrafast and memory-efficient alignment of short DNA sequences to the human genome. *Genome biology* **10** (2009).

138. Flicek, P. *et al.* Ensembl 2011. *Nucleic acids research* **39**, 6 (2011).

139. Griffith, O.L. *et al.* ORegAnno: an open-access community-driven resource for regulatory annotation. *Nucleic acids research* **36**, 13 (2008).

140. Pruitt, K.D., Tatusova, T. & Maglott, D.R. NCBI reference sequences (RefSeq): a curated non-redundant sequence database of genomes, transcripts and proteins. *Nucleic acids research* **35**, 5 (2007).

141. Chen, X. *et al.* Integration of external signaling pathways with the core transcriptional network in embryonic stem cells. *Cell* **133**, 1106-1117 (2008).

142. Hume, M.A., Barrera, L.A., Gisselbrecht, S.S. & Bulyk, M.L. UniPROBE, update 2015: new tools and content for the online database of protein-binding microarray data on protein-DNA interactions. *Nucleic acids research* **43**, 22 (2015).

143. Mathelier, A. *et al.* JASPAR 2014: an extensively expanded and updated open-access database of transcription factor binding profiles. *Nucleic acids research* **42**, 7 (2014).

144. Grant, C.E., Bailey, T.L. & Noble, W.S. FIMO: scanning for occurrences of a given motif. *Bioinformatics (Oxford, England)* **27**, 1017-1018 (2011).

145. Sen, D.R. *et al.* The epigenetic landscape of T cell exhaustion. *Science* **354**, 1165-1169 (2016).

146. Micallef, J.M., Kaldor, J.M. & Dore, G.J. Spontaneous viral clearance following acute hepatitis C infection: a systematic review of longitudinal studies. *J Viral Hepat* **13**, 34-41 (2006).

147. Bengsch, B. *et al.* Coexpression of PD-1, 2B4, CD160 and KLRG1 on exhausted HCV-specific CD8+ T cells is linked to antigen recognition and T cell differentiation. *PLoS Pathog* **6**, e1000947 (2010).

148. Sakuishi, K. *et al.* Targeting Tim-3 and PD-1 pathways to reverse T cell exhaustion and restore anti-tumor immunity. *J Exp Med* **207**, 2187-2194 (2010).

149. Wei, S.C. *et al.* Distinct Cellular Mechanisms Underlie Anti-CTLA-4 and Anti-PD-1 Checkpoint Blockade. *Cell* **170**, 1120-1133 e1117 (2017).

150. Pauken, K.E. *et al.* Epigenetic stability of exhausted T cells limits durability of reinvigoration by PD-1 blockade. *Science* **354**, 1160-1165 (2016).

151. Feld, J.J. *et al.* Treatment of HCV with ABT-450/r-ombitasvir and dasabuvir with ribavirin. *N Engl J Med* **370**, 1594-1603 (2014).

152. Ferenci, P. *et al.* ABT-450/r-ombitasvir and dasabuvir with or without ribavirin for HCV. *N Engl J Med* **370**, 1983-1992 (2014).

153. Baumert, T.F., Berg, T., Lim, J.K. & Nelson, D.R. Status of Direct-Acting Antiviral Therapy for Hepatitis C Virus Infection and Remaining Challenges. *Gastroenterology* **156**, 431-445 (2019).

154. Wieland, D. *et al.* TCF1(+) hepatitis C virus-specific CD8(+) T cells are maintained after cessation of chronic antigen stimulation. *Nat Commun* **8**, 15050 (2017).

155. Cox, A.L. *et al.* Cellular immune selection with hepatitis C virus persistence in humans. *J Exp Med* **201**, 1741-1752 (2005).

156. van der Ree, M.H. *et al.* Immune responses in DAA treated chronic hepatitis C patients with and without prior RG-101 dosing. *Antiviral Res* **146**, 139-145 (2017).

157. Chipumuro, E. *et al.* CDK7 inhibition suppresses super-enhancer-linked oncogenic transcription in MYCN-driven cancer. *Cell* **159**, 1126-1139 (2014).

158. Adam, R.C. *et al.* Pioneer factors govern super-enhancer dynamics in stem cell plasticity and lineage choice. *Nature* **521**, 366-370 (2015).

159. Vahedi, G. *et al.* Super-enhancers delineate disease-associated regulatory nodes in T cells. *Nature* **520**, 558-562 (2015).

160. Heyn, H. *et al.* Epigenomic analysis detects aberrant super-enhancer DNA methylation in human cancer. *Genome Biol* **17**, 11 (2016).

161. Suzuki, H.I., Young, R.A. & Sharp, P.A. Super-Enhancer-Mediated RNA Processing Revealed by Integrative MicroRNA Network Analysis. *Cell* **168**, 1000-1014 e1015 (2017).

162. Alatrakchi, N. *et al.* Hepatitis C virus (HCV)-specific CD8+ cells produce transforming growth factor beta that can suppress HCV-specific T-cell responses. *J Virol* **81**, 5882-5892 (2007).

163. Brooks, D.G. *et al.* Interleukin-10 determines viral clearance or persistence in vivo. *Nat Med* **12**, 1301-1309 (2006).

164. Ejrnaes, M. *et al.* Resolution of a chronic viral infection after interleukin-10 receptor blockade. *J Exp Med* **203**, 2461-2472 (2006).

165. Tinoco, R., Alcalde, V., Yang, Y., Sauer, K. & Zuniga, E.I. Cell-intrinsic transforming growth factor-beta signaling mediates virus-specific CD8+ T cell deletion and viral persistence in vivo. *Immunity* **31**, 145-157 (2009).

166. Cheng, L. *et al.* Blocking type I interferon signaling enhances T cell recovery and reduces HIV-1 reservoirs. *J Clin Invest* **127**, 269-279 (2017).

167. Whyte, W.A. *et al.* Master transcription factors and mediator establish super-enhancers at key cell identity genes. *Cell* **153**, 307-319 (2013).

168. Hnisz, D. *et al.* Super-enhancers in the control of cell identity and disease. *Cell* **155**, 934-947 (2013).

169. Thommen, D.S. & Schumacher, T.N. T Cell Dysfunction in Cancer. *Cancer Cell* **33**, 547-562 (2018).

170. Wherry, E.J. T cell exhaustion. *Nat Immunol* **12**, 492-499 (2011).

171. Mognol, G.P. *et al.* Exhaustion-associated regulatory regions in CD8(+) tumor-infiltrating T cells. *Proc Natl Acad Sci U S A* **114**, E2776-E2785 (2017).

172. Paley, M.A. *et al.* Progenitor and terminal subsets of CD8+ T cells cooperate to contain chronic viral infection. *Science* **338**, 1220-1225 (2012).

173. Utzschneider, D.T. *et al.* T Cell Factor 1-Expressing Memory-like CD8(+) T Cells Sustain the Immune Response to Chronic Viral Infections. *Immunity* **45**, 415-427 (2016).

174. Im, S.J. *et al.* Defining CD8+ T cells that provide the proliferative burst after PD-1 therapy. *Nature* **537**, 417-421 (2016).

175. He, R. *et al.* Follicular CXCR5- expressing CD8(+) T cells curtail chronic viral infection. *Nature* **537**, 412-428 (2016).

176. Leong, Y.A. *et al.* CXCR5(+) follicular cytotoxic T cells control viral infection in B cell follicles. *Nat Immunol* **17**, 1187-1196 (2016).

177. Wu, T. *et al.* The TCF1-Bcl6 axis counteracts type I interferon to repress exhaustion and maintain T cell stemness. *Sci Immunol* **1** (2016).

178. Blackburn, S.D., Shin, H., Freeman, G.J. & Wherry, E.J. Selective expansion of a subset of exhausted CD8 T cells by alphaPD-L1 blockade. *Proc Natl Acad Sci U S A* **105**, 15016-15021 (2008).

179. Philip, M. *et al.* Chromatin states define tumour-specific T cell dysfunction and reprogramming. *Nature* **545**, 452-456 (2017).

180. Fidler, I.J. Biological behavior of malignant melanoma cells correlated to their survival in vivo. *Cancer Res.* **35**, 218-224 (1975).

181. Jenkins, M.H. *et al.* Multiple murine BRaf(V600E) melanoma cell lines with sensitivity to PLX4032. *Pigment Cell Melanoma Res* **27**, 495-501 (2014).

182. Tumeh, P.C. *et al.* PD-1 blockade induces responses by inhibiting adaptive immune resistance. *Nature* **515**, 568-571 (2014).

183. Ho, P.C. *et al.* Phosphoenolpyruvate Is a Metabolic Checkpoint of Anti-tumor T Cell Responses. *Cell* **162**, 1217-1228 (2015).

184. Horton, B.L., Williams, J.B., Cabanov, A., Spranger, S. & Gajewski, T.F. Intratumoral CD8(+) T-cell Apoptosis Is a Major Component of T-cell Dysfunction and Impedes Antitumor Immunity. *Cancer Immunol Res* **6**, 14-24 (2018).

185. Brummelman, J. *et al.* High-dimensional single cell analysis identifies stem-like cytotoxic CD8(+) T cells infiltrating human tumors. *J Exp Med* **215**, 2520-2535 (2018).

186. Sade-Feldman, M. *et al.* Defining T Cell States Associated with Response to Checkpoint Immunotherapy in Melanoma. *Cell* **175**, 998-1013 e1020 (2018).

187. Thommen, D.S. *et al.* A transcriptionally and functionally distinct PD-1(+) CD8(+) T cell pool with predictive potential in non-small-cell lung cancer treated with PD-1 blockade. *Nat Med* **24**, 994-1004 (2018).

188. Sade-Feldman, M. *et al.* Resistance to checkpoint blockade therapy through inactivation of antigen presentation. *Nat Commun* **8**, 1136 (2017).

189. Welsh, R.M. & Seedhom, M.O. Lymphocytic choriomeningitis virus (LCMV): propagation, quantitation, and storage. *Curr Protoc Microbiol* **Chapter 15**, Unit 15A 11 (2008).

190. Yates, K., Bi, K., Haining, W.N., Cantor, H. & Kim, H.J. Comparative transcriptome analysis reveals distinct genetic modules associated with Helios expression in intratumoral regulatory T cells. *Proc Natl Acad Sci U S A* **115**, 2162-2167 (2018).

191. Subramanian, A. *et al.* Gene set enrichment analysis: a knowledge-based approach for interpreting genome-wide expression profiles. *Proc Natl Acad Sci U S A* **102**, 15545-15550 (2005).

192. Satija, R., Farrell, J.A., Gennert, D., Schier, A.F. & Regev, A. Spatial reconstruction of single-cell gene expression data. *Nat Biotechnol* **33**, 495-502 (2015).

193. Waltman, L. & van Eck, N.J. A smart local moving algorithm for large-scale modularity-based community detection. *The European Physical Journal B* **86**, 471 (2013).

194. DeTomaso, D. & Yosef, N. FastProject: a tool for low-dimensional analysis of single-cell RNA-Seq data. *BMC Bioinformatics* **17**, 315 (2016).

195. Carey, C.D. *et al.* Topological analysis reveals a PD-L1-associated microenvironmental niche for Reed-Sternberg cells in Hodgkin lymphoma. *Blood* **130**, 2420-2430 (2017).

196. Snyder, A. *et al.* Genetic basis for clinical response to CTLA-4 blockade in melanoma. *N Engl J Med* **371**, 2189-2199 (2014).

197. Osterwalder, M. *et al.* Enhancer redundancy provides phenotypic robustness in mammalian development. *Nature* **554**, 239-243 (2018).

198. Rupp, L.J. *et al.* CRISPR/Cas9-mediated PD-1 disruption enhances anti-tumor efficacy of human chimeric antigen receptor T cells. *Sci Rep* **7**, 737 (2017).

199. Roth, T.L. *et al.* Reprogramming human T cell function and specificity with non-viral genome targeting. *Nature* **559**, 405-409 (2018).

200. Odorizzi, P.M., Pauken, K.E., Paley, M.A., Sharpe, A. & Wherry, E.J. Genetic absence of PD-1 promotes accumulation of terminally differentiated exhausted CD8+ T cells. *J Exp Med* **212**, 1125-1137 (2015).

201. Rutishauser, R.L. *et al.* Early and Delayed Antiretroviral Therapy Results in Comparable Reductions in CD8(+) T Cell Exhaustion Marker Expression. *AIDS Res Hum Retroviruses* **33**, 658-667 (2017).

202. Ghoneim, H.E. *et al.* De Novo Epigenetic Programs Inhibit PD-1 Blockade-Mediated T Cell Rejuvenation. *Cell* **170**, 142-157 e119 (2017).

203. Spivak, A.M. & Planelles, V. HIV-1 Eradication: Early Trials (and Tribulations). *Trends Mol Med* **22**, 10-27 (2016).

204. Jones, P.A., Issa, J.P. & Baylin, S. Targeting the cancer epigenome for therapy. *Nat Rev Genet* **17**, 630-641 (2016).

Publications

First author

Sen DR*, Kaminski J*, Barnitz RA, Kurachi M, Gerdemann U, Yates KB, Tsao HW, Godec J, LaFleur MW, Brown FD, Tonnerre P, Chung RT, Tully DC, Allen TM, Frahm N, Lauer GM, Wherry EJ, Yosef N, Haining WN. *The epigenetic landscape of T cell exhaustion.* **Science.** 2016 Dec 2;354(6316):1165-1169. *these authors contributed equally

Paper was highlighted as the cover article in the Dec 2016 issue of Science.

Miller BC*, **Sen DR***, Al Abosy R, Bi K, Lafleur MW, Yates KB, Felt K, Naik GS, Manos M, Gjini E, Virkud YV, Brown FD, Hodi FS, Rodig SJ, Sharpe AH, Haining WN. *Functionally specialized subsets of exhausted CD8⁺ T cells mediate tumor control and differentially respond to checkpoint blockade.* **Nature Immunology.** 2019; 20:326–336. *these authors contributed equally

Sen DR, Yates KB, Gerdemann U, Tonnerre P, Wolski D, Martin GE, Al Abosy R, Comstock DE, Weiss SA, Frater J, Lauer GM, Haining WN. *Epigenetic scarring of exhausted CD8⁺ T cells in chronic Hepatitis C infection after curative therapy.* **Manuscript in preparation**

Co-author

Brown FD, **Sen DR**, Godec J, LaFleur MW, Lukacs-Kornek V, Schildberg FA, Kim HJ, Yates KB, Ricoult SJH, Bi K, Trombley JD, Kapoor VN, Castiglioni A, Stanley IA, Cremasco V, Danial NN, Manning BD, Sharpe AH, Haining WN, Turley SJ. *Fibroblastic reticular cells enhance T cell metabolism and survival via epigenetic remodeling*. **Nature Immunology.** (under review)

Mani V, Bromley SK, Carrizosa E, Warner RD, Hamze MM, **Sen DR**, Chasse AY, Äijö T, Jeffrey KL, Marangoni F, Lacy-Hulbert A, Mempel TR. *Conditioning of naïve CD8⁺ T cells for tissue-resident memory formation.* **Science** (under review)

Ishizuka JJ*, Manguso RT*, Cheruiyot CK, Bi K, Panda A, Iracheta-Vellve A, Miller BC, Du PP, Yates KB, Dubrot J, Buchumenski I, Comstock DE, Brown FD, Ayer A, Kohnle IC, Pope HW, Zimmer MD, **Sen DR**, Lane-Reticker SK, Robitschek EJ, Griffin GK, Collins NB, Long AH, Doench JG, Kozono D, Levanon EY, Haining WN. *Loss of ADAR1 in tumours overcomes resistance to immune checkpoint blockade*. **Nature**. 2019 Jan;565(7737):43-48. doi: 10.1038/s41586-018-0768-9. Epub 2018 Dec 17.

Cañadas I, Thummalapalli R, Kim JW, Kitajima S, Jenkins RW, Christensen CL, Campisi M, Kuang Y, Zhang Y, Gjini E, Zhang G, Tian T, **Sen DR**, Miao D, Imamura Y, Thai T, Piel B, Terai H, Aref AR, Hagan T, Koyama S, Watanabe M, Baba H, Adeni AE, Lydon CA, Tamayo P, Wei Z, Herlyn M, Barbie TU, Uppaluri R, Sholl LM, Sicinska E, Sands J, Rodig S, Wong KK, Paweletz CP, Watanabe H, Barbie DA. *Tumor innate immunity primed by specific interferon-stimulated endogenous retroviruses.* **Nature Medicine.** Nat Med. 2018 Jul 23. doi: 10.1038/s41591-018-0116-5.

Tong P, Granato A, Zuo T, Chaudhary N, Zuiani A, Han SS, Donthula R, Shrestha A, **Sen DR**, Magee JM, Gallagher MP, Van Der Poel CE, Carroll MC, Wesemann DR. *IgH isotype-specific B cell receptor expression influences B cell fate.* **PNAS.** 2017 Oct 3;114(40):E8411-E8420.

Pauken KE, Sammons MA, Odorizzi PM, Manne S, Godec J, Khan O, Drake AM, Chen Z, **Sen DR**, Kurachi M, Barnitz RA, Bartman C, Bengsch B, Huang AC, Schenkel JM, Vahedi G, Haining WN, Berger SL, Wherry EJ. *Epigenetic stability of exhausted T cells limits durability of reinvigoration by PD-1 blockade.* **Science.** 2016 Dec 2;354(6316):1160-1165.

This paper is in the top 0.1% of articles in Immunology by number of citations, according to Web of Science.

Sage PT, Ron-Harel N, Juneja VR, **Sen DR**, Maleri S, Sungnak W, Kuchroo VK, Haining WN, Chevrier N, Haigis M, Sharpe AH. *Suppression by TFR cells leads to durable and selective inhibition of B cell effector function.* **Nat Immunol.** 2016 Dec;17(12):1436-1446. doi: 10.1038/ni.3578.